1966

Fast flux measurement by a single multi-threshold foil

Kenneth Lawrence Cage

Department:

FAST FLUX MEASUREMENT BY A SINGLE MULTI-THRESHOLD FOIL

by

Kenneth Lawrence Cage

A

THESIS

submitted to the faculty of the

UNIVERSITY OF MISSOURI AT ROLLA

in partial fulfillment of the requirements for the

Degree of

Master of Science in Nuclear Engineering

Rolla, Missouri

1966

Approved by

J. R. Edwards (Advisor)

S. Pagano

John T. Park

A. H. Culp, Jr.

ABSTRACT

The purpose of this investigation is to determine the fast neutron spectrum by use of a single multi-threshold foil. The foils and the elements which constituted the foils were selected by the following criteria: availability of adequate cross-section data, energy dependence of the given reaction, gamma radiation emitted during decay and the half-life of the daughter. The two foils selected were an In-Fe-P pellet, and ALCOA 2509 (Al-Ni). The gamma spectrum of each constitute was stripped from the composite spectra using a least-squares fit. The activation results were utilized to calculate the fast flux using the weighted orthonormal method. An extensive error analysis was performed on calculated results.

ACKNOWLEDGEMENT

The author wishes to express his appreciation to Dr. Doyle Ray Edwards, Director of the University of Missouri at Rolla Nuclear Reactor for his assistance and encouragement throughout this project.

He also is grateful to Mr. Alva Elliott, Reactor Supervisor, and the entire staff for their assistance and suggestions during the course of this work.

This project has been performed under the auspices of National Science Foundation Grant GP-3050.

TABLE OF CONTENTS

TABLE OF CONTENTS (Continued)

TABLE OF CONTENTS (Concluded)

LIST OF FIGURES

LIST OF FIGURES (Continued)

LIST OF FIGURES (Concluded)

LIST OF TABLES

I. INTRODUCTION

The purpose of this thesis is to develop an experimental, analytical, and calculational method of obtaining fast neutron spectral information from a single multi-threshold metallic foil. A few of the common needs for measuring neutron environment are instrument calibration, reactor experiment monitoring, shield survey experimentation, and radiation damage analysis.

The neutron environment may be determined by semi-conductor spectrometers, photographic emulsions, fission counter, proton recoil methods, and nuclear reactions. The routine needs for measuring neutron fluxes and spectra are best met by threshold foils. Threshold foils are inexpensive, simple to use, and insensitive to gamma radiation. Such detectors have been used for nearly 20 years. However, the use has been hindered by the lack of sufficient reliable cross-section data and standardization of techniques. A single multi-threshold foil is an attempt to bring reliability and standardization to neutron flux spectra measurements. If the neutron flux is measured at different energies simultaneously, several sources of error may be eliminated.

This thesis reports a study of selecting multiple threshold detectors, exposing detectors to an unknown flux and counting the gamma-ray energy spectrum, relating the gamma spectrum to detector activation, and relating detector activation to the unknown flux.

II. LITERATURE REVIEW

A. General

The neutron flux may be defined as the product of neutron density and neutron speed. Neutron velocity (or energy) is the usual means of classification. A convenient breakdown is as follows (13):

Thermal Neutrons - - - Energies below .5 ev

Epithermal Neutrons - - 0.5 ev to 10 Kev

Fast Neutrons - - - - - 10 Kev to 200 Mev

The thermal neutron distribution is usually Maxwellian or a hardened Maxwellian. The actual energy limits depend on the average temperature of the slowing down media. The epithermal (or slowing down region) neutron flux distribution varies with a 1/E dependence. The fast or fission spectra ranges from 15 Mev to .01 Mev. The most common empirical relationship to describe the fission spectrum is the Watt spectrum.

$$N(E) = e^{-E} \text{ Sinh } (2E)^{1/2}$$

This formula is consistent with a model in which the neutrons are emitted from the highly-excited fission fragments after they have separated. The actual fast flux spectrum is not that of Watt's spectrum, since the lower portion is usually more attenuated more than the upper end of the spectra. This effect is due to very high energy neutrons (15 Mev) having several scattering collisions, but retaining enough energy (1.0 Mev) to remain fast neutrons. Neutrons passing through a substance may undergo various processes, depending on the energy of the incident neutron and the substance. The cross-section is defined as the

area associated with a nucleus for particle reaction. The cross-sections for reactions may be written as $\sigma(n,x)$. The first symbol in parentheses is the incident particle or radiation, and the second the emitted particle or radiation. After the neutron interacts with the material the nuclei is evelated to an excited or unstable state. These nuclei undergo particle or photon emission until they reach a stable form. The particular mode of decay for a nucleus is its decay scheme. The incident gamma activity of a given material would be proportional to the number of nuclei, the incident neutron flux, and the cross-section.

A foil may be defined as a discrete quantity of material, solid, liquid or gas, which can be irradiated and measured for its induced activity. A threshold foil has a particular response to a given flux at a specific neutron energy characteristic of that material. In this work the author will limit his foil selection to solid metallic foils, or semi-metallic powders. Metallic foils are inexpensive, easily obtainable and require little preparation for insertion in a swimming pool reactor core. Semi-metallic foils may be metallic powders and other elements on a homogenous powder. However, these must be placed in water tight containers for irradiation.

The fundamental problem in prior fast neutron spectrum measurements is that much of the fast neutron energy spectrum effective in radiation damage to solids lies below the threshold reactions in materials. Careful attention was focused on reactions in the Kev range to combat this problem.

Neutron fluxes in many present day reactors enable experimenters to attain appreciable activation of materials even when only trace

amounts of these materials are present. This characteristic of nuclear radiation has opened up many possibilities not previously available to the analytical chemist. The first systematic presentation of radioactivation analysts as a method was made in 1947 by Clark (3).

B. Threshold Detectors

Atomic species which undergo nuclear reactions of neutron capture in higher energy regions (above .1 Mev) and for which the capture cross-section is small below a certain threshold energy and considerably larger above this energy are called threshold detectors. Ideally, threshold detectors have zero sensitivity below the threshold energy and constant sensitivity above the threshold energy. In practical situations, the cross-sections of the threshold detector nuclei increase with energy after the threshold energy has been reached, and at higher neutron energies, the cross section valve is not constant.

The concept of "effective threshold energy" was introduced by D. J. Hughes (10). It was assumed the cross-section rises smoothly from zero at the actual threshold energy (calculated from reaction energies) to a constant value. The rise may be determined by theoretical considerations, or by observed cross-section dependence with energy. The effective cross-section is calculated such that the same total reaction yield would be obtained if the cross-section rose discontinuously from zero to its constant value at effective threshold energy.

The product of the cross-section and the neutron distribution (fission spectrum) as a function of energy is known as the response function of reaction yield. T. Passell and R. Heath have published response functions for the fission reaction with uranium-238, the (n,p)

reactions of phosphorus-31, iron-56, and sulfur-32, and the (n,α) reaction of Aluminum (3) then utilized the cross-section data tabulated by R. J. Howeraton. Moteff, Beever, and McDoule successfully used a Cu-Mn-Co Alloy for slow neutron measurements in 1959. This was one of the first applications of a multi-foil detector. J. C. Ringle and R. A. Rydin investigated single-threshold detectors over a energy range of 0 to 30 Mev. Passell and Heath investigated the properties of nickel as a fast flux monitor.

A detailed study by W. W. Gerken presents a summary of multiple threshold detectors, the neutron energy effects measured, counting techniques and corrections employed. Irradiation conditions were reported to enable future experiments to select detector materials (1963). The construction of a multi-threshold foil was investigated by M. Holkenbrink. An Indium, Iron, Phosphorus Powder Foil was fabricated for preliminary measurements of fast flux (7).

The author selected seven multi-threshold detectors for further study and analysis. The entire selection criteria of elements and multi-threshold detectors is reviewed in section III.

C. Cross-Sections

The threshold concept depends primarily upon the accuracy of the tabulated cross-section data. There is considerable variation found in literature of cross-section data as a function of energy. Considerable experimentation is under way to improve and extend the data available on the cross section of elements. Cross-sections for threshold detectors are generally published as the average cross section over the fission spectrum.

The importance of cross-sections to threshold detectors for flux determinations has been realized by several investigators. They have attempted to standardize and compare cross-section values to those measured by various laboratories. The first tabulation of threshold data was by D. J. Hughes in 1953 (10). R. Rochlim made a considerable number of cross-section measurements in the Brookhaven National Laboratory Graphite Reactor in 1959 (3). In 1961, C. E. Mellish presented a tabulation of published values for a number of threshold reactions. In an attempt to standardize cross-section measurements between laboratories, Mellish normalized the cross-section measurement to 60 millibarns for the $S^{32}(n,p)P^{32}$ reaction. This value appears to be much more accurate than the value of 30 millibarns found by Hughes, Spatz, and Goldstein in 1946 (15). The normalization by Mellish indicates substantially better agreement between laboratories than had been previously realized. Hughes updated his cross-section measurements with the Brookhaven National Laboratory Report 325 (11). The first supplement was issued in 1960, changing 80 cross-section curves. A second supplement was issued in May 1964 by Magurno in an attempt to include new measurements of neutron cross-sections.

The author utilized the latest cross-section data available, 2nd supplement, Brookhaven Report 325, by Magurno; where applicable, supplemented by D.J. Hughes and Howeraton. An attempt was made to select mean values over the entire energy range. The estimated cross-section accuracy of the reactions used in this work is presented in Table 2.1.

Table 2.1

Estimated Accuracy of Reaction
Cross-Section Data

No	Reaction	Reference	Energy Range (Mev)	Estimated Uncertainty
1	$Al^{27}(n,\alpha)Na^{24}$	1	5-20	+ 10%
		13	6.7-14.2	± 10 - 15%
2	$Al^{27}(n,p)Mg^{27}$	10,11	14-14.1	± 7 - 15%
		13	2.5-7.5	+ 15%
3	$Ag^{107}(n,2n)Ag^{106}$	10,11	9.6-14.5	± 10%
4	$Au^{197}(n,\alpha)Au^{198}$	10,11	Epithermal	± 10%
5	$Ni^{58}(n,p)Co^{58}$	1	0.5-15.0	± 10%
6	$In^{115}(n,n')In^{115m}$	10,11	0.35-5.3	± 10%
7	$P^{31}(n,p)Si^{31}$	13	1.6-14.1	± 5 - 10%
8	$Fe^{56}(n,p)Mn^{56}$	10,10	3.4-14.1	± 10 - 15%
9	$Zn^{64}(n,p)Cu^{64}$	25	2.-3.6	± 10%

1 - Rydin, R. J.

25 - Howoraton

13 - Magurno

10,11 - Hughes

D. Counting Technique

Scintillation counting is one of the oldest detection techniques. The visually detected scintillations of energetic alpha-particles were first noted by Sir William Crookes in 1903. The visual scintillation counter became obsolete in the 1930's, and the next 20 years were characterized by the rapid growth and development of electronic counting techniques. Gas filled ionization chambers as the ionization detector, the proportional counter, and the Geiger-Muller counter are well developed operating methods. With the development of sensitive photo multiplier tubes, the scintillation counter regained its former prominent place in nuclear physics research. Curran and Baker in 1944 first used the current generated by a photomultiplier with a zinc sulfide screen for the measurement of the intensity of alpha omitting sources (17).

Since the gamma spectra is the most predominant and simplest to detect, it was selected to be utilized. A single 1 3/4" x 2" sodium iodine, thallium activated crystal was selected for gamma ray detection. Gamma rays interact in a NaI(Ti) crystal in essentially three ways: the photoelectric effect, the Compton effect, and pair production. The absorption coefficients for three basic processes, along with the total absorption coefficient for NaI are shown in Figure 2.1. Below about .1 Mev, the photoelectric process is dominant. From 0.1 to 0.4 Mev the photoelectric and Compton processes are both important; from about 0.4 to 2 Mev the Compton process alone is dominant. From about 2 to 7 Mev both the Compton process and pair production are significant. And above about 7 Mev the pair production process alone becomes predominant. The gamma rays we observe have energies that range from 0.1 to 2 Mev; thus the photoelectric and Compton processes are our main consideration.

After the rays interact and deposit energy in the NaI(Ti) crystal, this energy is released as a light pulse or scintillation. The light pulses emitted by the scintillation crystal are proportional to the energy deposited in the crystal by the gamma ray. These pulses are collected and stored in a pulse height analyzer and are displayed as the number of pulses of a given height versus channel number.

From the gamma-ray pulse height spectrum the energy of the gamma ray source and the half life of the spectra can be found. The pulse height at which the photopeak reaches its maximum height corresponds to the energy of the incident gamma ray. The intrinsic variables that affect the gamma-ray spectrum are: 1) the decay schemes of the various nuclides, and 2) the interaction processes of radiation with matter.

E. Gamma Spectra Analysis

Various methods have been developed to analyze gamma spectra. Spectrum stripping is the oldest and probably the simplest method of spectrum analysis. The pulse height spectra resulting from different monoenergetic gamma rays interacting in the counting crystal is determined experimentally; these are response functions. A library of response functions is developed, covering the energy range of the unknown spectrum. A response function of the same energy is adjusted in intensity so that it matches the photopeak of the highest energy. This response function is then subtracted from the unknown spectrum. This corresponds to removing from the unknown spectrum the entire contribution of the highest gamma ray. The next highest photopeak is then handled by the same technique, until the resultant spectrum is zero at all energies (2).

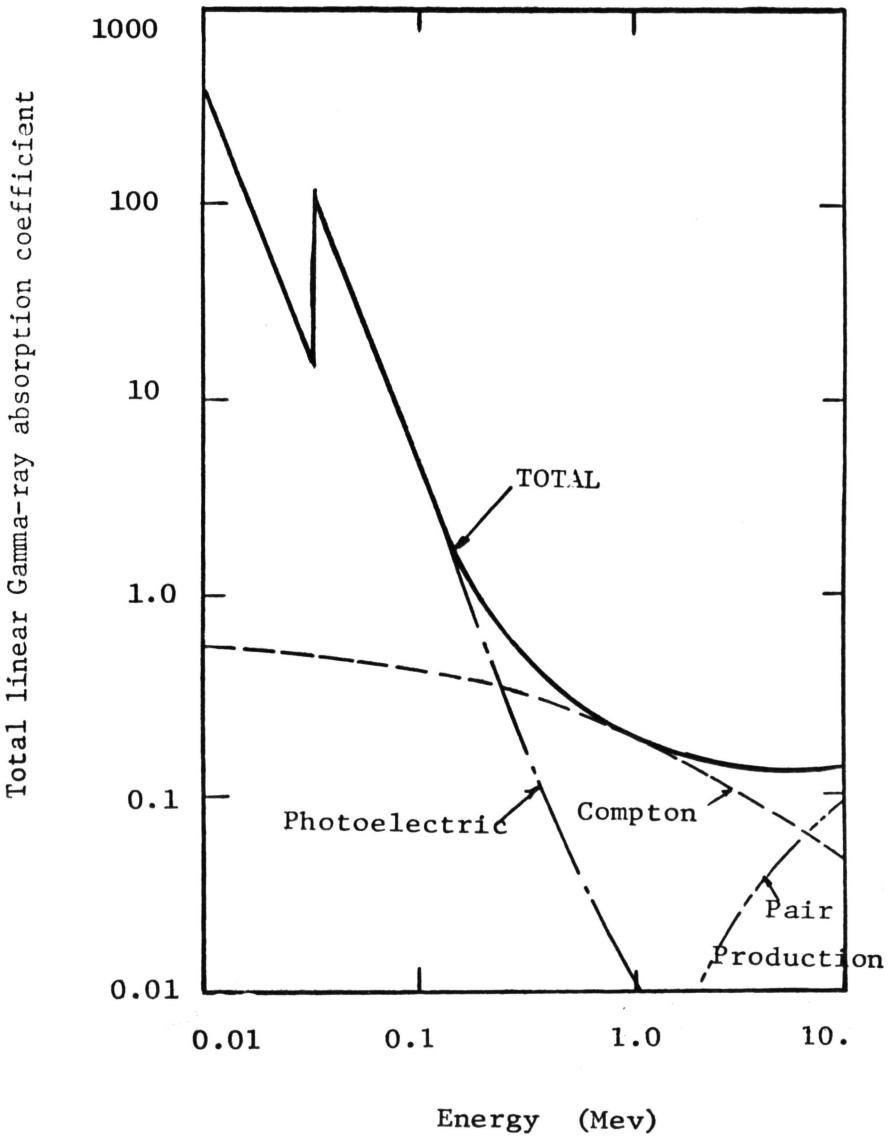

Figure 2.1 Total linear Gamma-ray absorption coefficient vs Energy for NaI.

Matrix inversion, or spectrum unfolding is similar to the stripping method but is more sophisticated and more accurate. A theoretical approach relies on a minimum of experimental information; the probabilities are derived for all possible interactions of the incident gamma rays using Monte Carlo calculations (3).

The best method of analyzing a complex spectrum appears to be the least-squares analysis. The response functions are fitted to the unknown spectrum by the least-squares technique. The method by Heath is general in scope, capable of accurate photopeak area calculations, and corrects for gain shift.

Ringle used a modified spectrum-stripping technique for gamma analysis. The Compton distributions from each ray are removed by subtraction of experimentally determined Compton distributions. The photopeak areas are found by a non-linear least-squares technique and the photopeaks are removed from the spectrum. The experimental Compton distributions were obtained from various monoenergetic sources. Corrections were made for detector efficiency, source self-absorption, background in the crystal, and dead time in the pulse height analyzer.

In this work the author uses a method of resolving the composite gamma ray spectra of several nuclides by a least squares technique. Dr. D. R. Edwards, Director of the University of Missouri at Rolla Reactor, modified a computer program, PPA, by Murphy for an IBM 1620 Model II computer. The experimental data is fitted with a Gaussian distribution function, containing a linear bias term through the use of the iterative least-squares technique (26).

F. Flux Measurements

Numerous investigators have presented successful measurements of fast neutron spectra. J. B. Trice made a series of thermal, epithermal, and fast neutron measurements in the Materials Testing Reactor (3). An attempt was made to establish a correlation between neutron-energy distribution and radiation damage (8). However, the measurements resulted in crude neutron spectra, due to inaccurate cross-section data. Trice compared the results of measurements made between several reactors and indicated good results. P. Leger and B. Sautiez measured the neutron spectrum in the Melusine reactor at Saelay, France, in 1959 using phosphorus, sulphur, magnesium, and aluminum as detector materials (9).

J. A. Grundl and A. Usner made measurements of the fast neutron spectra of several fast reactors. They represent spectral differences by comparing the ratios of the activities of threshold detector reactions. The fast neutron spectrum in the Oak Ridge Research Reactor (ORR) was measured by P. Dragoumis in 1960 (3). These measurements evaluated the effects of gas atoms in the ORR Reactor. Hurst developed a technique for measuring neutron spectra by calibrating a series of threshold detectors with activities thresholds at successively increasing energies, up to 3 Mev (21).

Early work with nickel resulted in considerable disagreement and uncertainty between laboratories (21). Cobalt-58 obtained from the (n,p) reaction of nickel-58 may be detected free from interference by all other activities produced by neutrons on nickel. However, interference due to cobalt-60 from thermal capture in cobalt impurity can be troublesome for long irradiations. It was noted the cobalt-58 has a thermal burnout of one percent for thermal fluxes greater than 10^{15}. R. G. Jung, et. al.,

at Battelle Memorial Institute has developed a method for determining effective threshold energies and cross sections (3). The effective threshold energy is determined by irradiating materials at different distances from a fission source in water. As the effective relaxation distance of each energy group in water is different, the effective threshold energy of a material can be determined. J. R. Ringle at Lawrence Radiation Laboratory developed a technique for measuring neutron spectra in the energy range of 2 to 30 Mev (2). The threshold foils were used as energy dependent neutron detectors with the restriction the residual nucleus must emit a gamma ray. Computer programs were developed to analyze the gamma spectra, calculate the cross sections, and generate the neutron spectrum.

The effective threshold method is one of the oldest and most widely used of analytic methods (5). The expression, for the activation of a threshold foil is replaced by an equivalent expression which assumes that the actual cross-section curve as a function of energy can be replaced by a step function which starts at an effective threshold energy.

The polynomial method assumes the spectral shape to be composed of an arbitrary weighting function times a polynomial in energy. The difficulty with this procedure is that the resulting set of linear equations is poorly conditioned which leads to oscillations and even negative values for the flux (4).

The Dierckx Method is based on the fact that the spectral shape of reactor spectrum is a decreasing exponential function of energy. Also an assumption is made that the initial part of the cross section curve for each detector contributes essentially all of the activation since the fast neutron spectrum decreases rapidly with energy. The energy spectrum

is broken up into (n - 1) energy bands corresponding to n detectors with two detectors in the upper band and one in each of the others. The flux in each band is assumed to have the following shape corresponding to the first assumption. It is noted that this method is limited to reactor type spectra (5).

J. J. Baum developed the Italian Iterative Method. This method is essentially a combination of the effective threshold method and the Dierckx method and offers a solution to the problem of curve fitting with the effective threshold method (15).

The weighted, orthonormal method (or cross-section expansion) assumes the flux to be given by a weighting function times an expansion of known functions of energy which are required to form an orthonormal set (33). The weighted orthonormal polynomial method is a combination of the orthonormal and polynomial methods. In this method the flux is expanded in a series of polynomials which are defined to be orthonormal. J. C. Ringle and R. A. Rydin received good results utilizing this method.

Ringle developed a method where the cross-sections and flux are expanded in a series of legendre polynomials. He also used a method of expanding the flux in a series of orthonormal trigonometric sine and cosine functions. D. Di Cola and A. Rota summarized various flux expansion methods and developed the method of least-squares series expansion methods. This method holds a good deal of promise; however, this procedure involves a statistical study based on the Monte Carlo method.

The previous listed methods for spectra evaluation were compared by various authors. Generally, the flux was assumed to be a 1) straight line, 2) step function, 3) sloping line, and 4) various combinations

of the preceding three assumptions. Each spectra evaluation was compared against these flux assumptions.

The weighted orthonormal method was found to be as good as, if not better than, any foil method presently available. A primary advantage of the method is its ability to fit arbitrary spectra, while other methods are restricted to spectra with certain distinch features. This author selected the above method for flux calculations. The program FUSE-3 by Rydin was modified to fit the IBM-1620 Model II computer (1). The least-squares expansion method is being further investigated by Dr. D. R. Edwards for flux determination from multi-threshold foils. This work is in conjunction with the National Science Foundation Grant for Fast Flux Determination from a Single Multi-Threshold Foil.

III. FOIL SELECTION

A. Desirable Criteria

Threshold reactions with neutrons are observed for a number of different processes. In general, we choose from the inelastic scattering reactions and any charged particle reaction. The usefulness of these reactions can be determined from the following criteria.

1. Threshold. The effective threshold of the material would have to be from .1 Mev to 15 Mev and sensitive to fast neutrons only. There exist reactions which occur at thermal or epithermal energies that introduce unwanted complications and activities.
2. Cross Section. The reaction cross section as a function of energy must be recently tabulated for 0 to 15 Mev. The energy dependence of the cross section should indicate a sharp increase at energies just above the effective threshold energy, preferably similar to a step function.
3. Gamma Spectra. The daughter should decay to produce a prominant gamma peak which is easily identified between 0 and 2 Mev. It should be formed in sufficient quantity to allow for reasonable detection statistics. The prominant peak will be used to gain knowledge of the activation of the material but will yield an observation point used in spectrum stripping of the materials in the multi-threshold foil.
4. Half-Life. The half-life of the daughter nucleus should be on the order of hours to days. A half-life of this order will omit enough radiation for good detection in reasonable activation times.
5. Miscellaneous. The cost of the material used, and a purity necessary to yield clear data with little interference, should be reasonably low. The material should be obtained in a form that allows easy transport and core placement.

Although salts, liquids, and other states are observed to exhibit threshold reactions this survey was focused on metallic foils. The metallic foils are small, inexpensive, and easily irradiated. Also many alloys are manufactured from desirable metallic elements which exhibit the above criteria. Since the UMRR does not, at present, have a pneumatic tube for irradiation of samples, foils were exposed to the water environment or placed in water tight containers. An exception to the metallic foils was the In-P-Fe powder foil developed by M. Holkenbrink at the University of Missouri at Rolla. This foil and one of its constituents were irradiated in a water-tight container.

In selecting a single multi-threshold foil other factors to consider are: 1) the compilation of other nuclear reactions that might interfere with detection of the radiations from the desired reactions, and 2) the probability of interference from the reactions as cross-section for each reaction, abundance of target material, half-life and energies of radiation from the product nuclear.

B. Selection of Elements

The periodic chart of elements was examined, considering the state and desirable criteria listed in the preceding section. The chart of the nuclides was studied to further eliminate elements with conflicting radioactivity. The previous work by various authors and their recommendations for future work was considered in selecting various elements.

The various authors indicated the Ni^{56} (n,p) and Fe^{56} (n,p) reaction should be included in a multi-threshold foil (3, 12). The Al^{27} (n,p) and (n,α) reactions were selected using the authors suggestions (1, 2, 12, 20).

There was considerable difficulty in selecting a low energy detector (< 1 Mev). An isotope of silver was considered

eliminated as the emitted radiation is weak and has poor detection statistics. The Ni^{62} (n, α) reaction was considered but dismissed for the above reason. The remaining detector in the low energy range was indium. It has a low threshold energy of .4 Mev; however, it has interferring radiation from other nuclear reactions and poor alloying quantities. The cross section data is incomplete past 5.5 Mev for the (n,n') reaction. Since indium was readily available in pure form, it held the most promise as the low-energy detector.

Phosphorus was selected as it has only one isotope, and has one predominate nuclear reaction. Silver has several reactions which covers a range of low to high threshold reactions. Copper and zinc were considered for future study due to the number of isotopes, reactions and alloying characteristics. Gold is alloyed easily with indium; hence, data is presented to account for the alloys gamma spectrum.

This composite selection of elements varies from phosphorus with one isotope to zinc, and copper with five isotopes. The range of the elements varies from indium at .4 Mev to copper at 11.4 Mev. The gold is not considered as a threshold detector and will only be treated for information purposes.

A summary of the elements and the desired reactions is presented in Table 3.1. They are listed in the order increasing magnitude of threshold energy. It should be noted the wide variety and assortment of values the authors have for the threshold parameters. The authors selected the most recent values as displayed in Table 3.3.

The gamma spectra of each element was recorded using the counting technique described in Section 4. All samples were irradiated at a power level of 10 Kw for the time period shown in Table 3.2. The foil

Table 3.1

Threshold Reactions of Elements for Fast Flux Monitoring

Element and Nuclear Reaction	Effective Threshold (Mev)	Effective Cross Section (Mb)	Reference	γ Radiation (Mev)	Half Life
$Au^{197}(n,\gamma)Au^{198}$	None	204	5,19	.412	2.6 d
	None	——	18,19	.412	2.6 d
$In^{115}(n,n')In^{115m}$	1.2	300	22	.335	4.5 h
	1.3	290	1	.335	4.5 h
	.45	——	18,19	.335	4.5 h
$P^{31}(n,p)Si^{31}$	2.4	276	3	None	2.6 h
	2.71	110	8	——	2.6 h
	0.7	——	2,18	1.26	2.6 h
	2.5	75	31	1.26	2.62 h
$Ni^{58}(n,p)Co^{58}$	2.9	455	3	.81	72 d
	3.09	550	1	.805	71.3 d
	*-.04	——	2	——	71 d
	4.1	——	18,19	.80	71.3 d
	2.6	600	22	.810	72 d
$Al^{27}(n,p)Mg^{27}$	4.6	44	3	.83,1.01	9.5 m
	5.46	80	1	.83,1.01	9.5 m
	4.67	56	8	——	9.4 m
	1.8	56	2	——	9.5 m
	4.6	——	18,19	.83,1.01	9.5 m
$Zn^{64}(n,p)Cu^{64}$	4.7	486	3	1.34	12.8 h
	*-0.2	——	2,19	1.34	12.8 h
	4.0	——	11	——	——
	3.3	250	22	1.51	12.5 h
$Fe^{56}(n,p)Mg^{56}$	8.1	85	3	0.84	2.58 h
	6.42	50	1	0.845	2.58 h
	6.33	52.4	8	——	2.58 h
	2.9	——	2	——	2.6 h
	2.94	——	18,19	.84	2.6 h
	6.7	80	22	.845	2.6 h

* Theoretical effective threshold energy

Table 3.1 (Continued)

Element and Nuclear Reaction	Effective Threshold (Mev)	Effective Cross Section	Reference	γ Radiation (Mev)	Half Life
$Al^{27}(n,\alpha)Na^{24}$	8.1	107	3	1.38	15 h
	7.52	70	1	1.36	15 h
	7.25	59	8	——	14.9 h
	3.1	——	2	——	15 h
	8.1	——	18,19	1.38	15 h
	7.2	100	36	——	15 h
$Ag^{107}(n,2n)Ag^{106}$	9.6	——	18,19	None	24.3 m
$Cu^{65}(n,2n)Cu^{64}$	11.4	1000	30	.511	12.6 h

Table 3.2

Foil Elements Weights and Times

Material	*Incapuslation		Weight (GM)	**Irradiation Time	Time to Counting	Counting Time
Aluminum 1	Plastic	Cd	.0647	30 m	161 m	10 m
Aluminum 2	Stringer	Cover	.0639	60 m	36,149 m	10 m
Copper 1	Plastic	Cd	.1279	30 m	190 m	10 m
Copper 2	Stringer	Cover	.1362	30 m	46 m, 5.1 h	10 m
Gold 1	Plastic	Cd	.1078	30 m	25.57 h	10 m
Gold 2	Stringer	Cover	.1077	30 m	3301 h	10 m
Indium 1	Plastic	Cd	.2415	30 m	11.8,75.6 h	10 m
Indium 2	Stringer	Cover	.2411	30 m	8.7,9.1 h	10 m
Iron 1	Plastic	Cd	.1301	30 m	219 m	10 m
Iron 2	Stringer	Cover	.1300	30 m	139 m	10 m
Nickel 1	Plastic	Cd	.1527	30 m	193 m, 72.3 h	10 m
Nickel 2	Stringer	Cover	.1500	60 m	81 m, 37.4 h	10 m
Phosphorus 1	Water Tight	Cd	.5762	60 m	400 m, 12.9 h	10 m
Phosphorus 2	Container	Cover	.8119	30 m	119 m	10 m
Silver 1	Plastic	Cd	.1729	30 m	9.38 h	10 m
Silver 2	Stringer	Cover	.1713	30 m	3.05 h	10 m
Zinc 1	Plastic	Cd	.9147	30 m	9138 h	10 m
Zinc 2	Stringer	Cover	.8793	30 m	3.56 h	10 m

* Core Position D-2, UMRR

** 10 KW Power Level

weights and times are shown in Table 3.2. An attempt was made to identify the gamma photopeaks, particularly the desired reactions and the individual curves of the products. A complete listing of each element reaction plus the results of the irradiation runs and other parameters are displayed in Appendix B.1.

C. Selection of Multi-Threshold Foils

A literature search was conducted for alloys containing combinations of the elements listed in Table 3.2. A thorough listing of desired alloys was obtained by using the Design Materials Handbook. The catalog had an excellent listing of ferrous and non-ferrous alloys and the percentage by weight of each element in the alloy.

Further literature study eliminated any speculation concerning some alloys as detectors. Inconel was considered; however, complete discrimination between gamma radiations was not possible. Duranickel had a very small percentage of aluminum (4.5%) that excessive power levels would be necessary for good statistical results. Also, activities from other reactions force considerable delay time before the activity can be measured.

Alcoa 2509 has the same elements as duranickel, but the percentage breakdown permits the detection of three threshold reactions. Although this alloy does not have a low threshold reaction (1.0 Mev), it does combine two desirable elements in a multi-threshold detector. In agreement with Gerkan, Alcoa 2509 was selected as one multi-threshold detector.

A copper, nickel, zinc alloy was selected as it covered the desirable energy spectra from 2.9 to 11.4 Mev and contained three separate elements. Correspondence with the industrial concerns located a suitable indium alloy. Since such an alloy material would contain a low energy threshold reaction, an indium, silver, copper alloy and an indium, gold, copper alloy were

Table 3.3

Multi-Threshold Foils Eliminated as Threshold Detectors

Material	% Elements	Remarks
CDA Alloy 735	70.5-73.5% Cu, 16.9-19.5% Ni, 7.15-12.15% Zn, 10% Pb, 0.25% Fe and 0.50% Mn	The $Cu^{63}(n,\gamma)$ and Zn (n,p) reaction provide the same daughter Cu^{64}. (Figure 3.1)
*Duranickel	94% Ni, 4.5% Al, 0.55% Si, .50% Ti, .25% Mn, .15% Si, .05% Cu and 0.005% S	A practical threshold detector for power levels above 10 Kw and long irradiation times
*Inconel	76.0% Ni, 7.20% Fe, 15.8% Cr, 0.20% Mn, 0.20% Si, 0.10% Cu, 0.001 S	The $Ni^{58}(n,p)$ and $Fe^{56}(n,p)$ reactions at .81 Mev prohibit complete discrimination of gamma spectrum
Incuro-60	60% Au, 38% Cu, and 2% Indium	The $Au^{197}(n,\gamma)$ resonance reaction dominates the $Cu^{63}(n,2n)$ and $In^{115}(n,n')$ reaction. The gamma photopeaks overlapp at .412, .51 and .335 Mev respectively (Figure 3.2)
Incosil-10	63% Ag, 21% Cu, and 10% In	The $Cu^{63}(n,2n)$ reaction covers the weak $Ag^{107}(n,2n)$ reactions gamma photopeak at .51 Mev. (Figure 3.3)

*Data from Gerkan

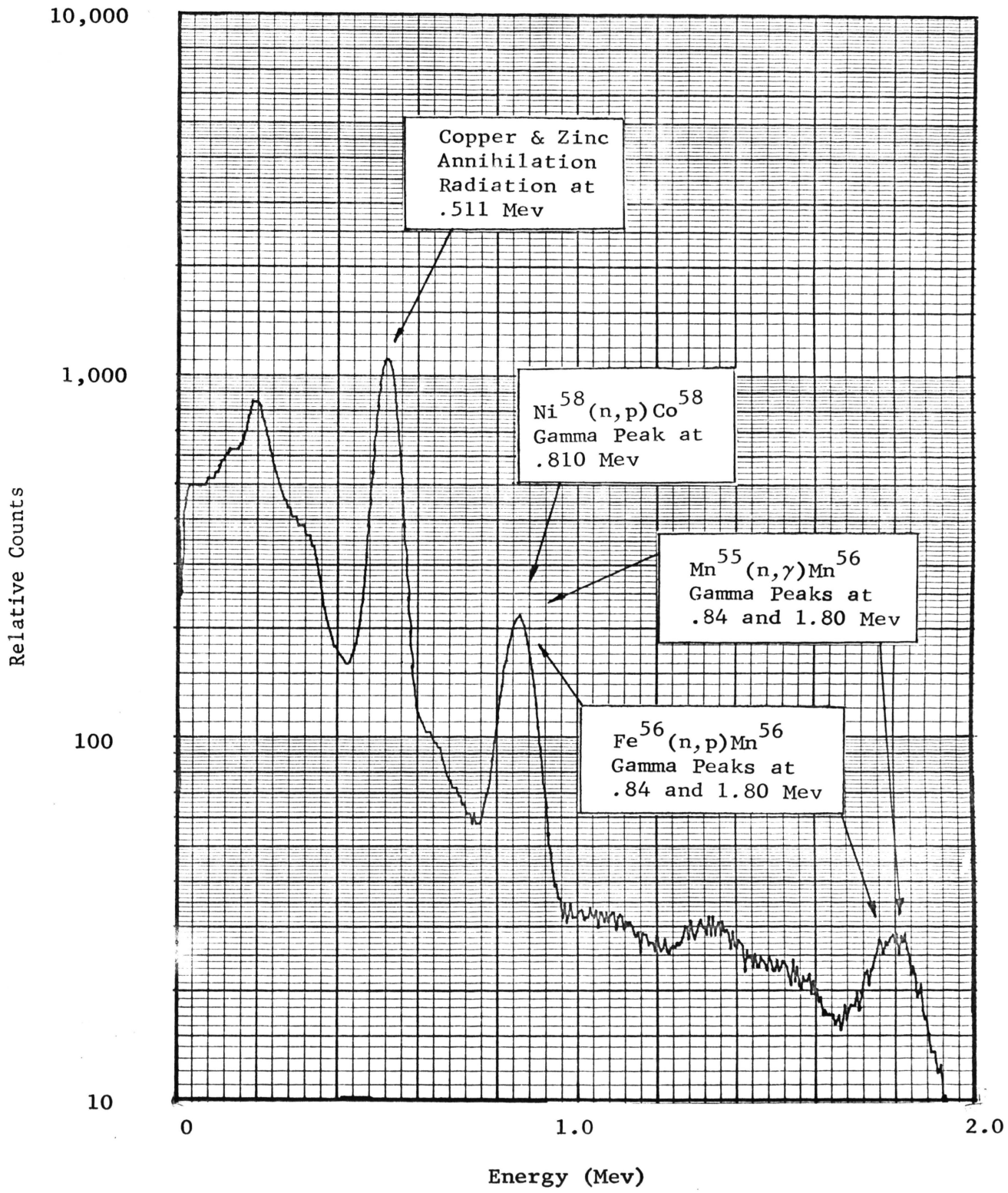

Figure 3.1 CDA Alloy 735 Gamma Spectrum 2.00 hours after Irradiation Relative Counts versus Energy

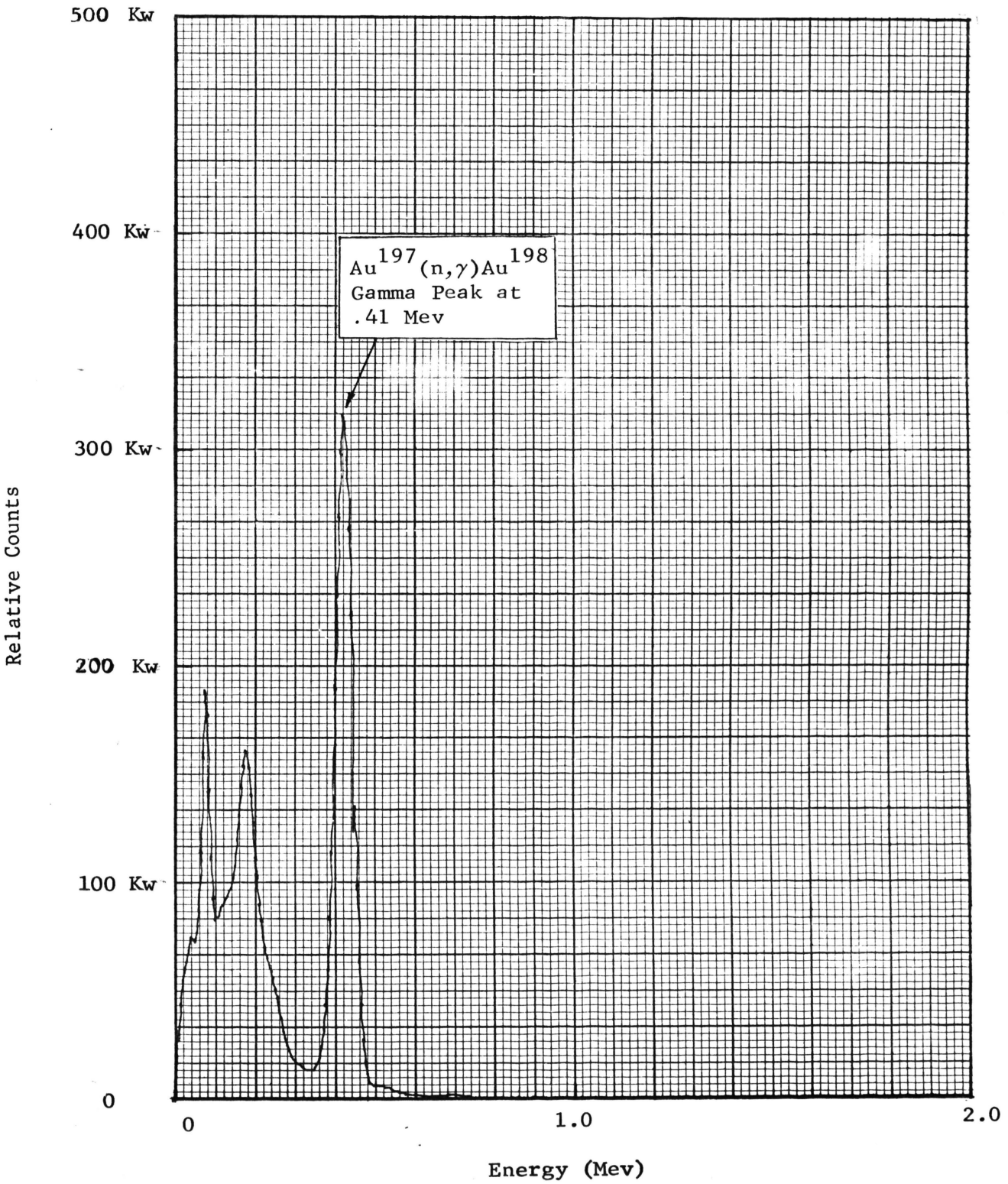

Figure 3.2 INCORO-60 Gamma Spectrum 17.28 hours after Irradiation Relative Counts versus Energy

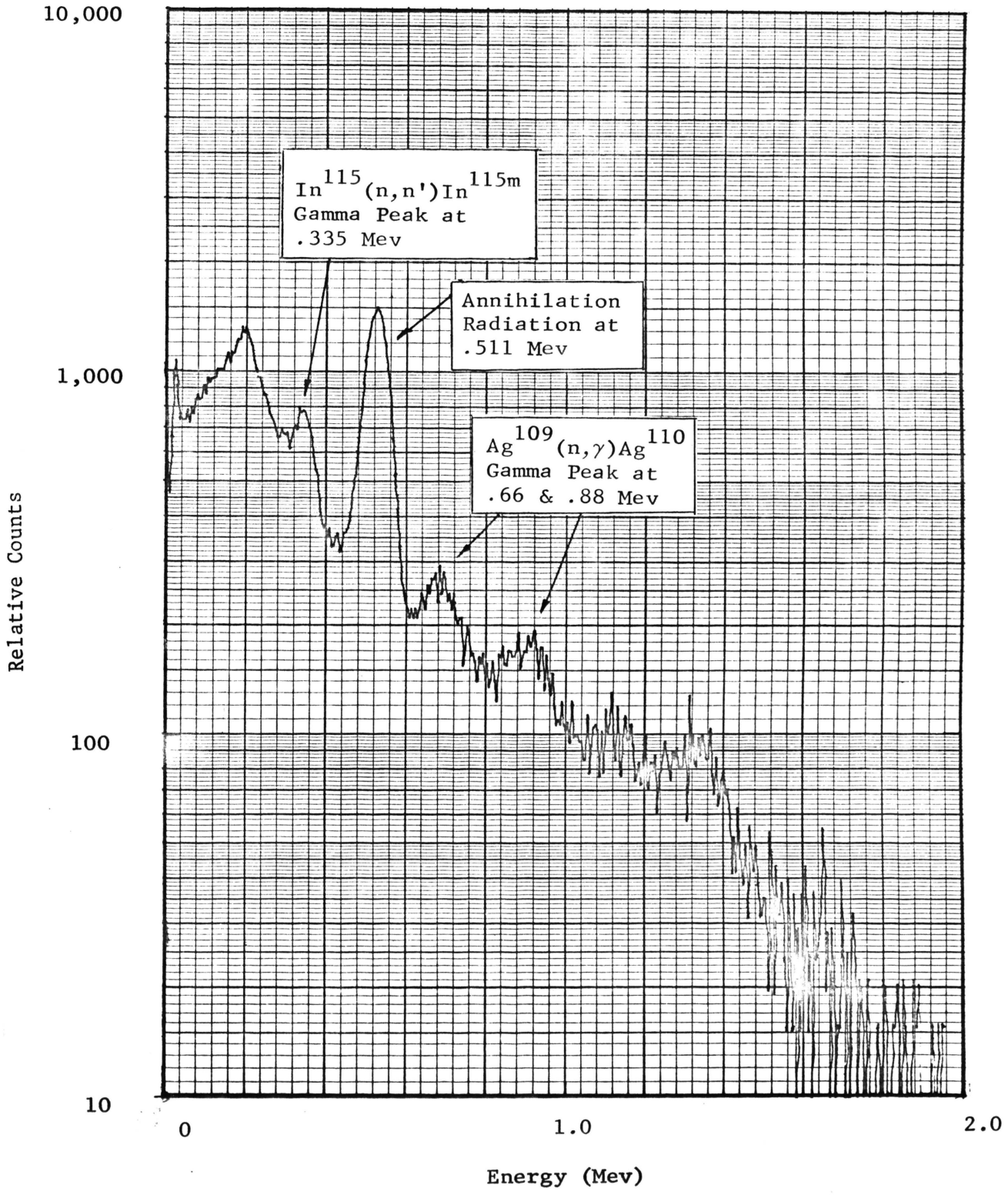

Figure 3.3 IncoSIL-10 Gamma Spectrum 16.75 hours after Irradiation Relative Counts versus Energy

procured. In order to meet ideal criteria for a multi-threshold foil, attention was focused on the tailored pressed disk foil constructed by M. Holkenbrink. This indium-phosphorus-iron was readily obtainable as this work was done at the University of Missouri at Rolla.

C.1 Gamma Spectra of Multi-Threshold Foils

Further study of desired reactions and constituent elements eliminated all but two foils, Alcoa 2509 and In-P-Fe. A summary of the multi-foils that were not further considered is presented in Table 3.5. The gamma spectra of these alloys are shown in Figures 3.1 to 3.3. The reactions of each foil selected for further study are shown in Table 3.4. Table 3.5 displays the composition of the two multi-threshold alloys, their weights and times.

C.1.a Alcoa 2509

It was possible to determine three threshold energy fluxes using Alcoa 2509. The reactions involved were Ni^{58} (n,p) Co^{58} for fluxes of energy greater than 2.9 Mev, Al^{27} (n,p) Mg^{27} for fluxes greater than 4.6 Mev, and Al^{27} (n,) Na^{24} for fluxes of energy greater than 8.1 Mev. (Figure 3.4). The half-lives of the above products are 72 days, 9.5 minutes and 15 hours respectively. The products and half-lives and energies of the gammas emitted were sufficiently different to enable good discrimination of the products of each reaction. The gamma radiation from both the Co^{58} and Mg^{27} is about 0.82 Mev. In order to separate the components of each, it was necessary to determine the decay curves. The Mg^{27} half-life of 9.5 minutes and the Co^{58} half-life of 72 days would normally permit rapid discrimination, since the Mg would decay completely in less than an hour. However, Co^{58} has a 9.5 hour isomer which necessitates the separation of three decay components. Complete separation of

Table 3.4

Threshold Reactions of Multi-Threshold Foils for Fast Flux Monitoring

Foil % Element Composition	Nuclear Reaction	Effective Threshold (Mev)	Effective Cross Section (mb)	Gamma Photopeak (Mev)	t 1/2
Alcoa 2509					
Ni (10.10)	$Ni^{58}(n,p)Co^{58}$	2.9	455.0	0.81	72 d
Al (89.57)	$Al^{27}(n,p)Mg^{27}$	4.6	107.0	1.38	9.5 m
	$Al^{27}(n,\alpha)Na^{24}$	8.1	44.5	.83,1.01	150 h
In-P-Fe					
*In (1)	$In^{115}(n,n')In^{115}$	.45	290.0	0.335	4.5 h
*P (55.2)	$P^{31}(n,p)S^{31}$	2.4	97.7	1.260	2.62 h
*Fe (43.8)	$Fe^{56}(n,p)Mn^{56}$	6.42	50.0	0.845	2.55 h

*Approximate percentages by weight

Table 3.5

Multi-Threshold Foils, Weights and Times

Material	*Incapsulation	Weight (Gm)	**Irradiation Time	Time to Counting	Counting Time
Alcoa 2509-1	Plastic Stringer	.6086	60 min	28m, 133m 62.05 h	10 min
Alcoa 2509-2	(Cd covers)	.6414	60 min	169 min	10 min
In-P-Fe 1	Water Tight Cd	3.5011	30 min	10 hours	10 min
In-P-Fe 2	Container Covers	3.7659	60 min	14.8, 15.4 16.4, 23.2 hours	10 min

Percentage Composition of Elements by Weight

Alcoa 2509 - 82.57% Al, 10.0% Ni, 0.22% Fe, 0.08% Si and 0.03% Ga

In-P-Fe - 43 - 44 % P, 54 - 56 % Fe, 1 - 5% In

* Core position D-2, UMRR

**10 Kw power level

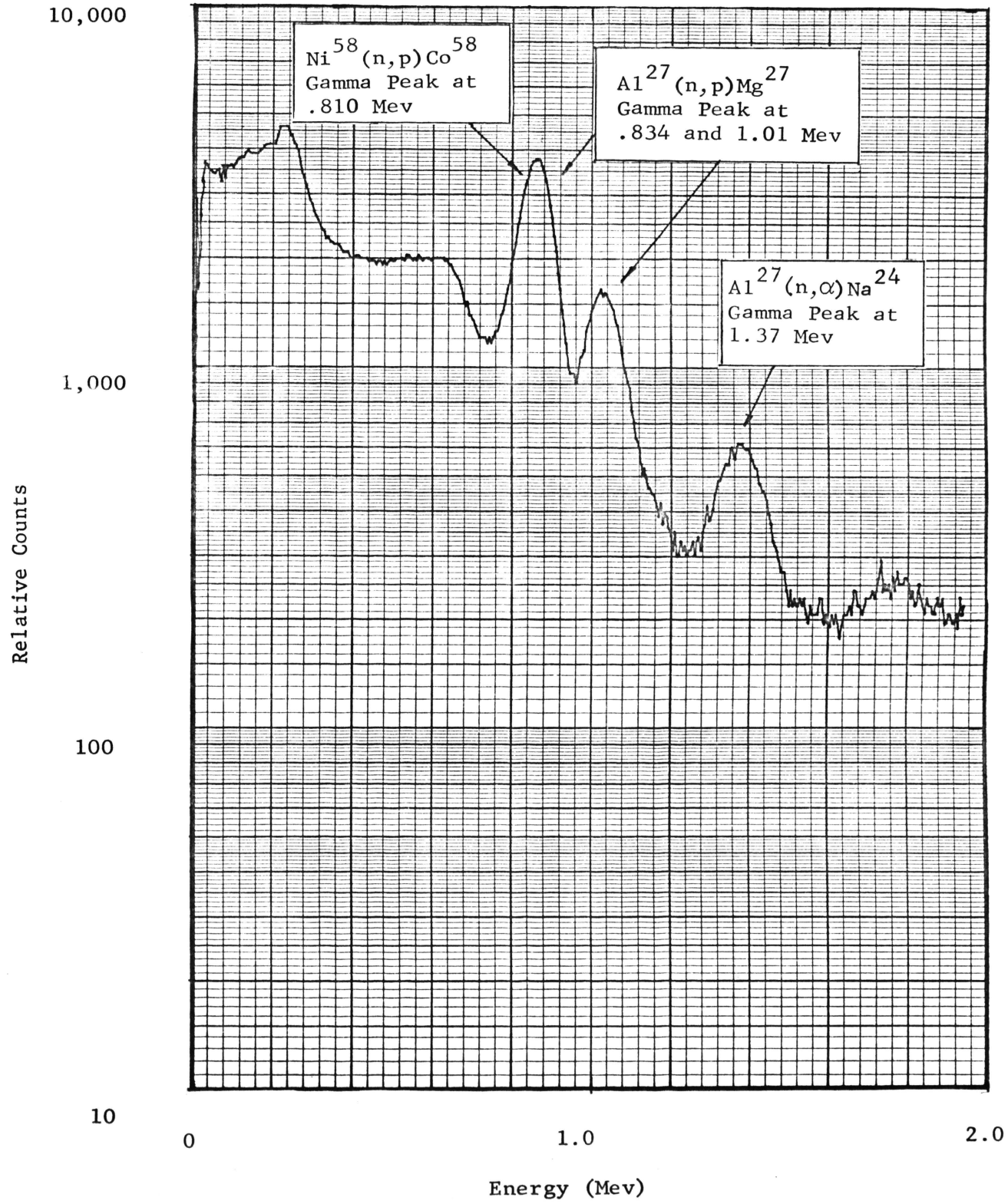

Figure 3.4 Alcoa 2509 Gamma Spectrum 28 minutes after Irradiation
Relative Counts versus Energy

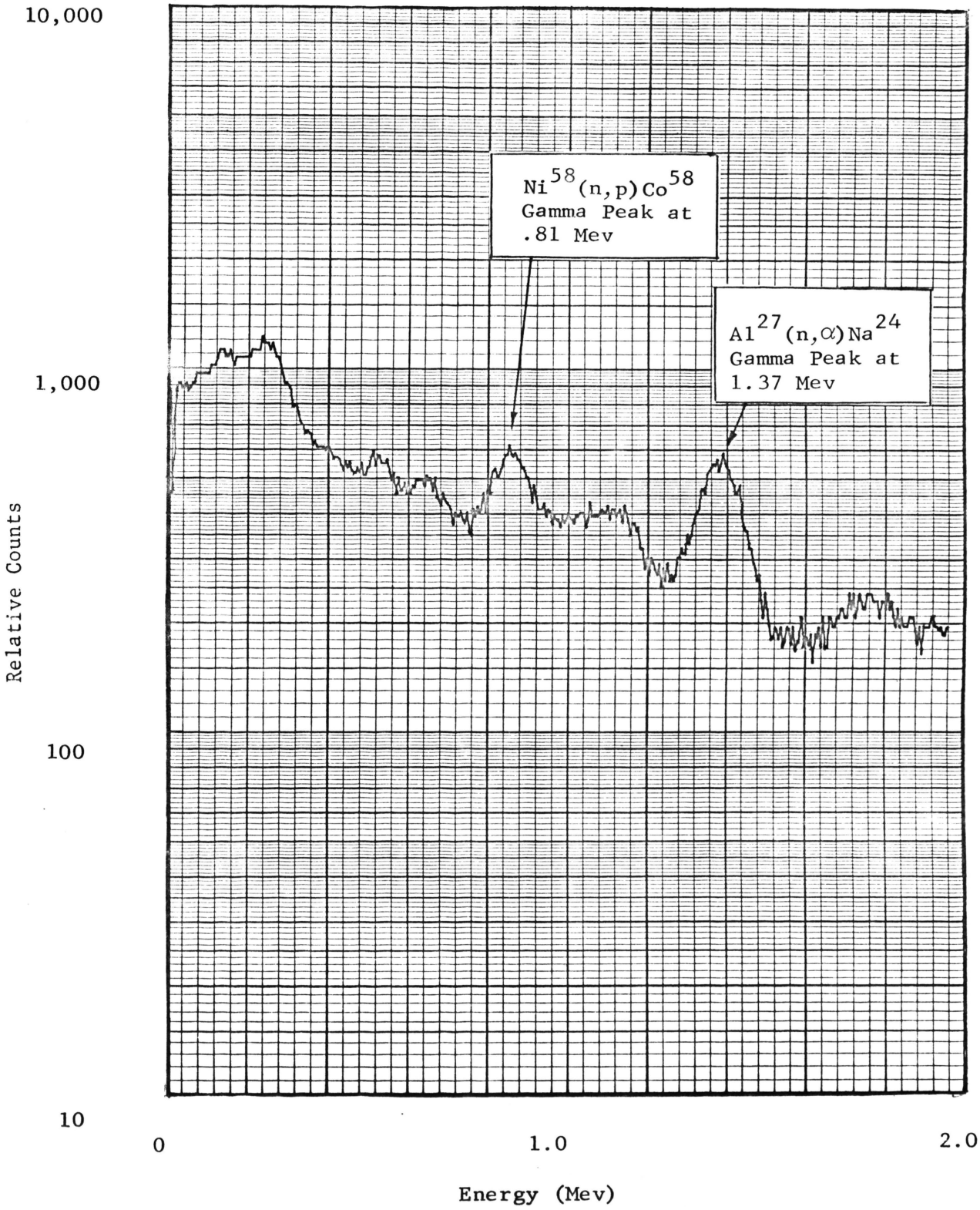

Figure 3.5 Alcoa 2509 Gamma Spectrum 133 minutes after Irradiation
Relative Counts versus Energy

the decay products required measurements up to 60 hours after irradiation as shown in Figure 3.5. This allows the complete decay of the 9.5 hour Co^{58} isomer and the slight amount of 14.1 hour gallium-72 impurity.

In addition, the decay of Ni^{65} yielding a gamma at 1.49 Mev with a half-life of 2.56 hours requires that the Na^{24} measurement at 1.38 Mev be made several hours later to allow the Ni^{65} to decay (3).

C.1.b Indium-Phosphorus-Iron Pressed Disk

The reactions of interest are the In^{115} (n,n'), P^{31} (n,p) and the Fe^{56} (n,p). The gamma photopeaks or the reactions are .335, 1.26 and 0.84 Mev respectively. The gamma spectrum of the foil is displayed in Figure 3.6. The indium is clearly the dominant reaction at 10 hours after irradiation. In particular, notice the heights of the In^{146m} photopeaks, especially the approximately equal heights at the photopeaks at .62, 1.065, and 1.274 Mev. At 15.95 hours after irradiation, the $In^{.116m}$ has decayed sufficiently to show the desired In^{115} (n,n') reaction with the gamma peak at .35 Mev. There is a difference in height between the peaks at .62 Mev, and 1.06 and 1.26 Mev at this time interval. The Fe^{56} (n,p) reaction has passed the rapidly decaying In^{116m}. Finally at 17.26 hours the phosphorus (n,p) reaction becomes more predominant over the In^{116m} reaction as shown in Figure 3.7. 30.00 hours later all traces of the In^{116m} have disappeared. The gamma photopeaks of In^{115}(n,n'), Fe^{56}(n,p) and P^{31}(n,p) are visible in Figure 3.7. However, at this counting, counting statistics will be accurate due to the low activity. The long half-life of In^{114m} is displayed in Figure B.7. This spectra will be subtracted from the spectrum at 17.26 hours to take into accoutn background radiation and the In^{114m} activity.

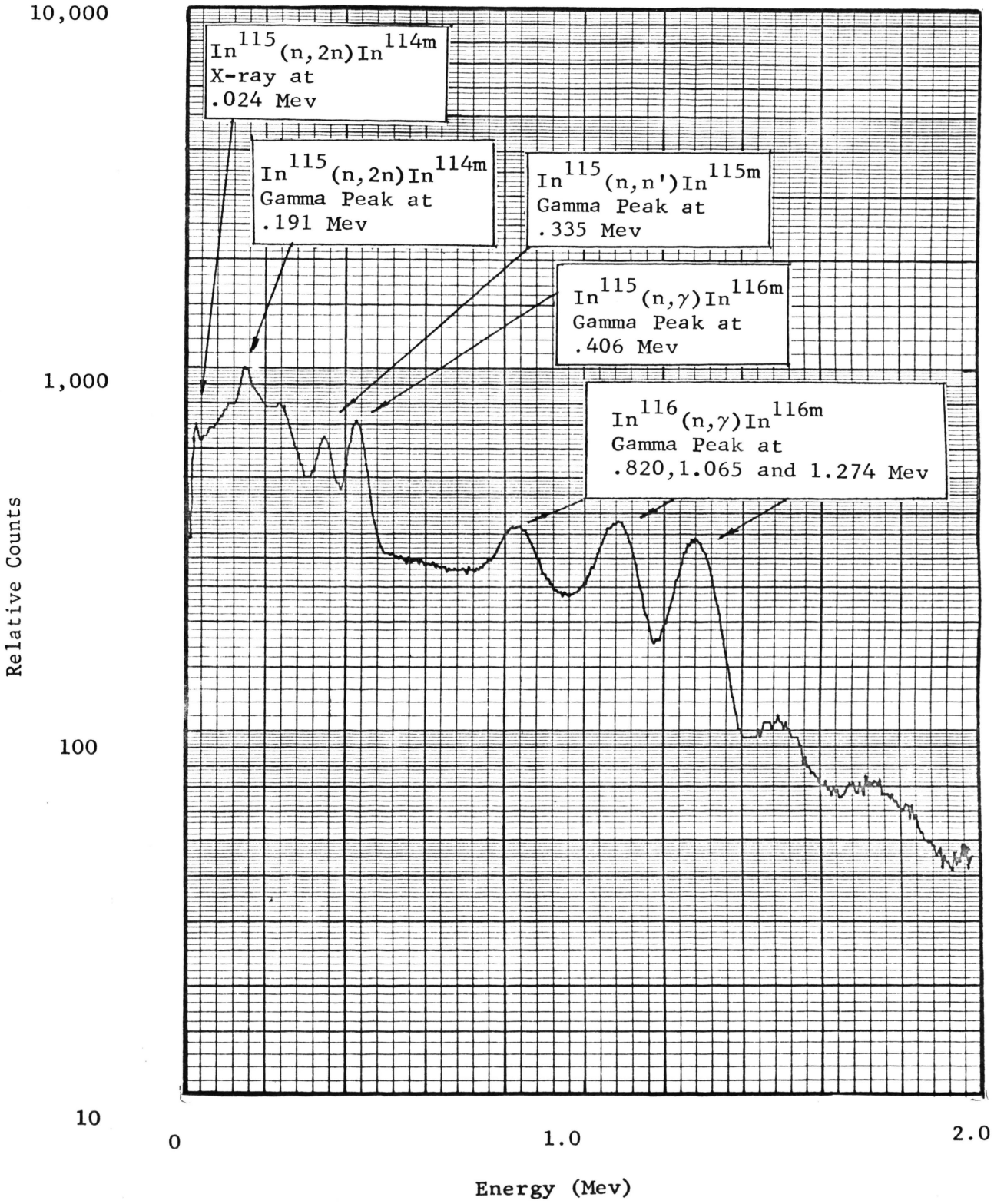

Figure 3.6 In-P-Fe Gamma Spectrum 10 hours after Irradiation
Relative Counts versus Energy

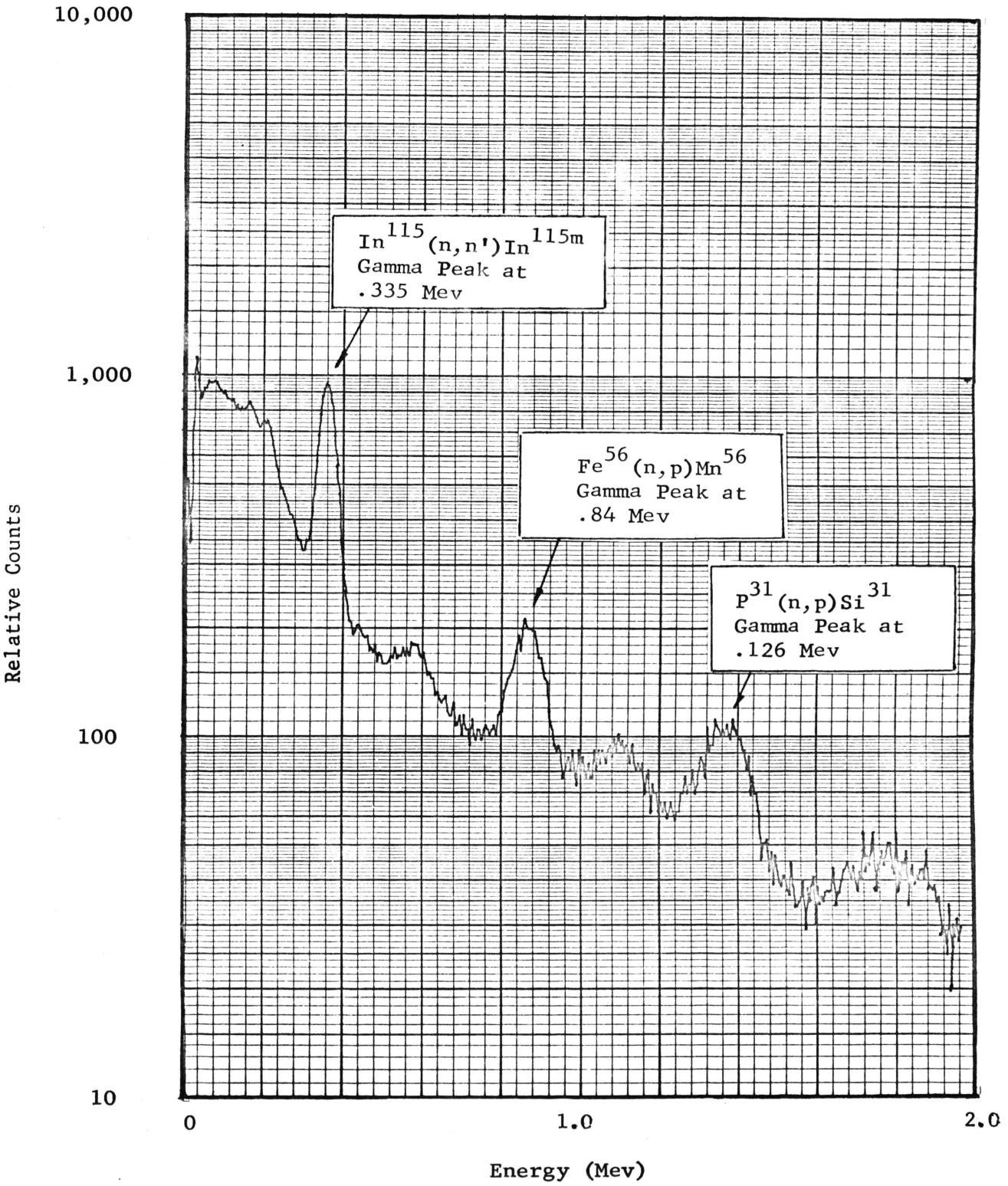

Figure 3.7 In-P-Fe Gamma Spectrum 17.26 hours after Irradiation Relative Counts versus Energy

The indium domination of gamma spectra was not expected. Using the standard activity correction formula, the percentage of indium was found to be higher than stated by the vendor. Apparently, the poor alloying characteristics of indium have resulted in a non-homogeneous foil. It is estimated that these disks vary from .5 to 5% of the weight of the pressed disk foil. This increases the indium activity to coincide with the calculations while the iron and phosphorus remain at near constant level.

D. Sample Preparation

D.1 Metallic Foils

The samples of the elements were obtained in thin 1/2" circular disks from Reactor Experiments, Inc. Zinc samples were obtained by machining a 1/2" circular rod into disks. The foils were covered with cadmium covers after both had been thoroughly cleaned to remove all sodium traces. They were taped to the plastic stringer as shown in Figure 3.8. The sample alloys obtained from industrial firms were formed by stamping out at 1/2" diameter disk. The alloy 2509 is produced only in ingot form. There the bar was machined to 1/2" diameter and then small thin disks were cut off the rod. All samples were marked, cleaned and weighted to within .0001 gm on Ainsworth electric scales.

D.2 Powder Foils

The phosphorus and In-P-Fe disks were placed in a water-tight polyethylene containers as shown in Figure 3.5. The phosphorus powder was placed in a small polyethylene container inside a cadmium cover, and in the water tight container. The powder disk was taped at the same level as the metallic foils inside the cadmium cover and water-tight container. The powder was placed in previous weighed aluminum tins for counting purposes and determining the weight of the powder.

D.3 Foil Placement

All samples were placed in grid position D.2 for identical flux exposure. A nylon stringer was used to raise and lower the sample holders in grid position D.2.

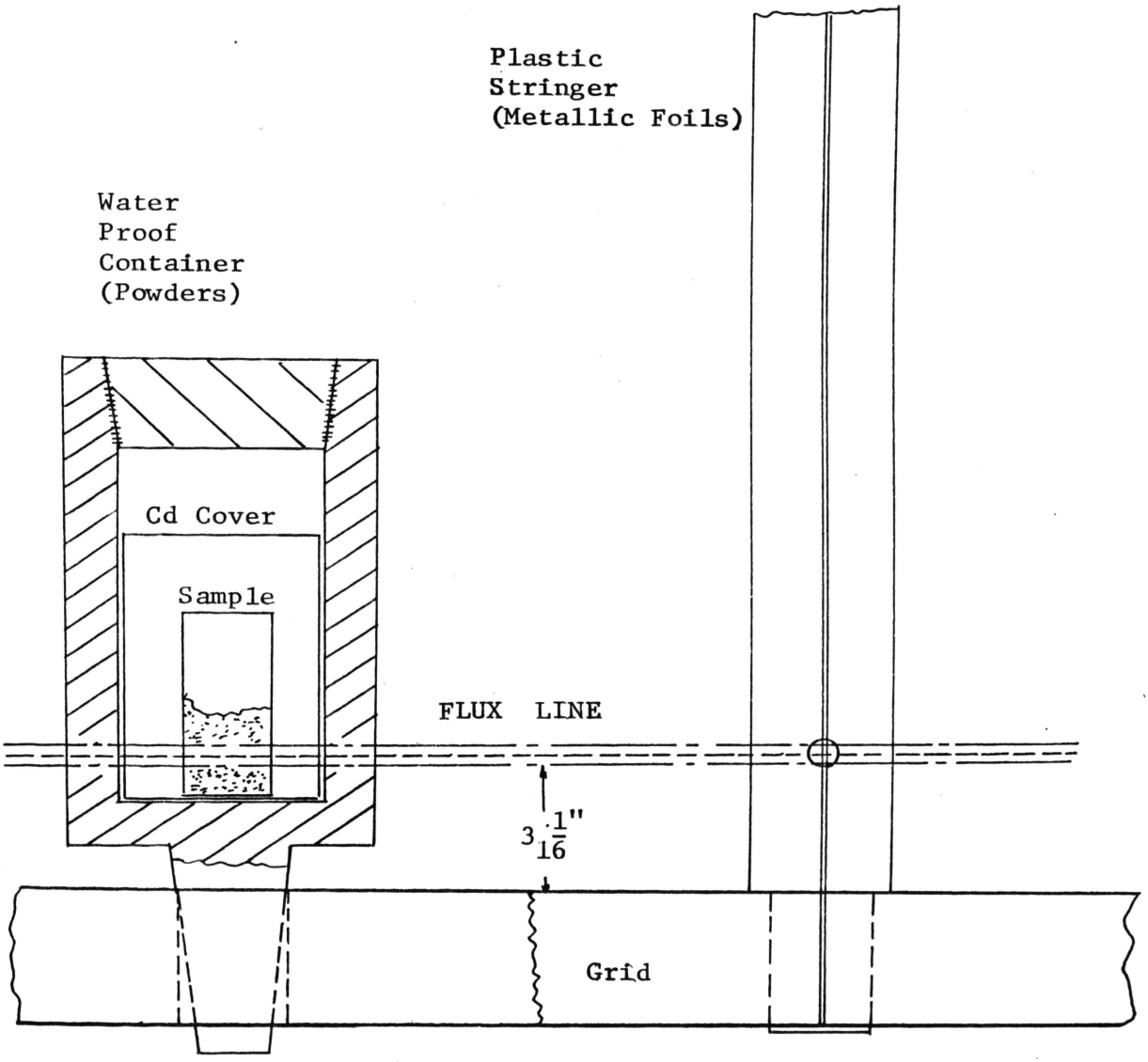

Core Position D-2
Power Level 10kw

Figure 3.8 Sample Holders

IV. COUNTING TECHNIQUES

A. Counting Methods

The characteristics and properties of the scintillation probe and multi-channel analyzer are described in Appendix II. The crystal was a RIDL 1 3/4" sodium-iodide thallium-activated crystal.

The light pulses from the scintillation detector are proportional to the energy of the gamma ray incident on the sodium-iodide crystal. After conversion to a current and subsequent amplification, this proportionality is still retained. By the discrimination circuitry in the computer, current pulse below a certain level are disregarded. Thus, only those radiations above a particular energy will be counted. In addition an upper discriminator may be used at a pre-determined energy level. The computer subtracts the pulses and thereby indicates the number of gamma disintegrations. Using this means, the energy spectrum of the radioactive source may be analyzed as a count rate versus energy spectrum. The output was then fed into the typewriter and recorder. The multi-channel analyzer is able to look at the entire gamma ray spectrum simultaneously. A schematic diagram of the counting method is shown in Figure 3.6.

The analyzer was calibrated by using gamma reference sources supplied by the New England Nuclear Corporation. A Cs^{137} and Co^{60} source were used to produce photopeaks at .661 Mev, 1.17 Mev and 1.33 Mev. The analyzer was set to be within 1 channel or .005 Mev of the true reading. This accuracy is within .0025 per cent of the true value.

Prior to the gamma spectra being recorded, a background count was taken for 10 minutes, utilizing 400 channels over a 2 Mev range. The identical parameters are used in taking the gamma spectra or the

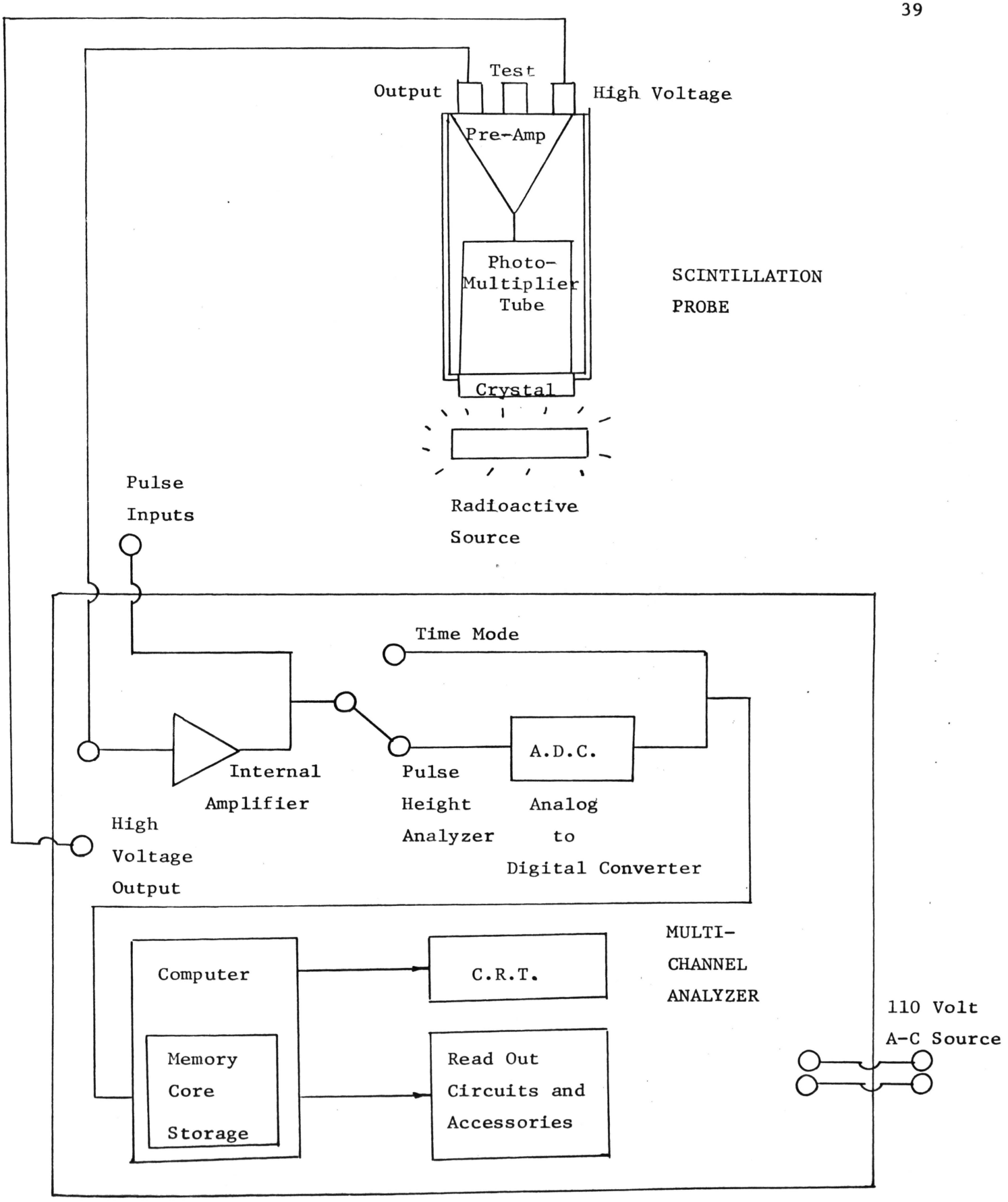

Figure 4.1 Schematic Diagram of Scintillation Probe

individual samples. Care was taken to note the condition of the reactor during counting times. In addition, the background of analyzer was taken at zero reactor power and at full power. The results of the background count are identical, there need be no further correction.

Interfering nuclides and other undesired effects were eliminated (as shown in Chapter III) by the following methods. One can wait until the short lived impurities or isotopes decay before counting the sample. If two nuclides are together, wait for the desired activity to decay, then recount and subtract the long lived impurity. Each of these methods were demonstrated in Appendix B.1.

B. Correction Factors

The gamma photopeaks of each reaction corrected to actual counts using calculated source intrinsic efficiencies of NaI crystals (17). The values were linearly interpreted from the data in Figure 4.2 by Crouthamel. This correction factors were used by Dr. D. R. Edwards in the gamma spectra analysis. The dead time was compensated for by using the live time mode on the multi-channel analyzer.

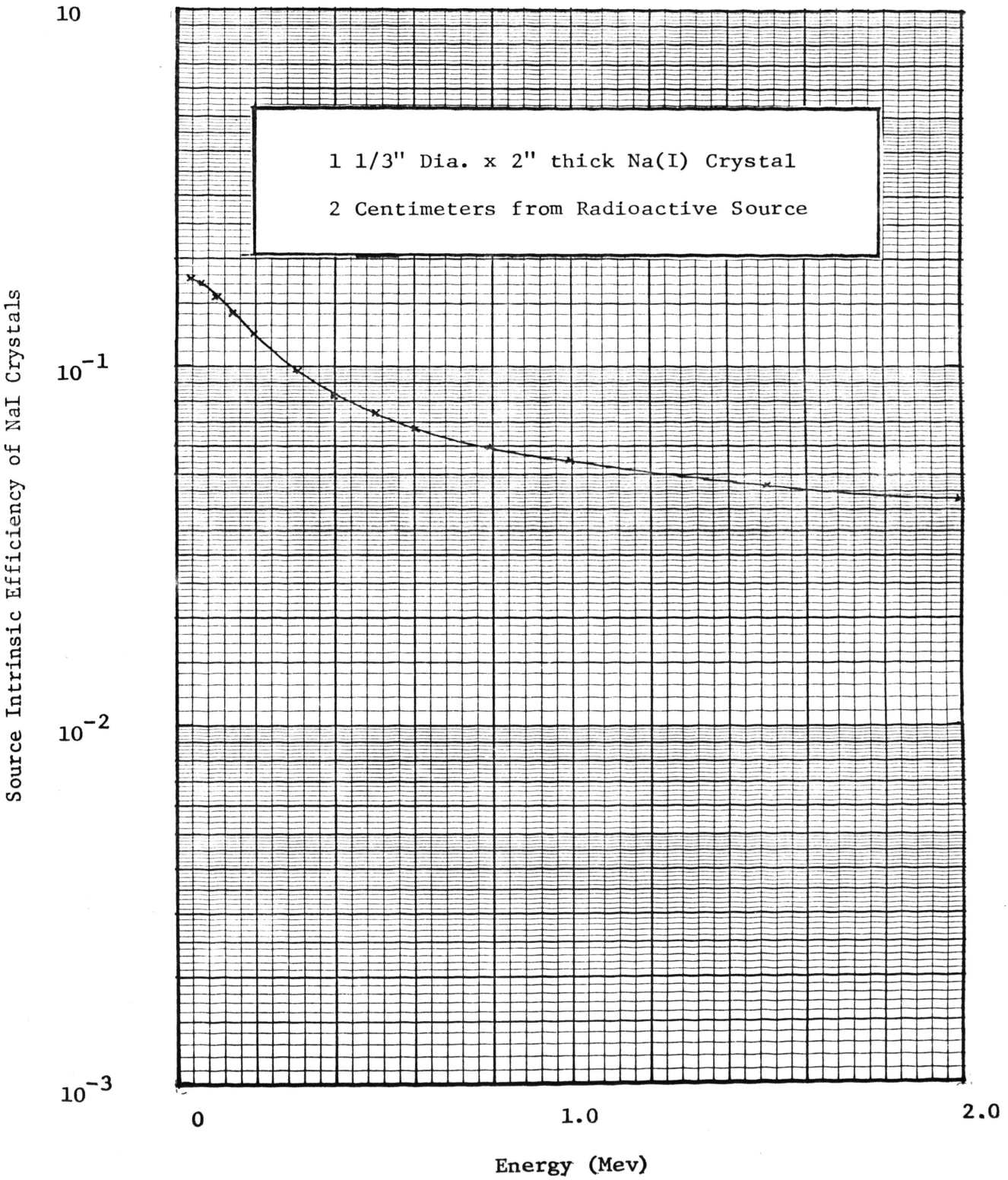

Figure 4.2 Source Intrinsic Efficiencies of NaI Crystals versus Energy

V. MATHEMATICAL INTERPRETATION

The mathematics of determining the fast flux spectra may be divided into two parts: 1) gamma spectra analysis for the activity of each element of Multi-foil, and 2) flux calculations based on the activity of each element.

A. Gamma Spectrum Analysis

The gamma spectrum of each multi-threshold foil was anslyzed using a modified version of the computer program PPA. This program was developed by M. Murphy, Jr. for the quantitative analysis of radioactive samples by the least-squares resolution of the gamma ray spectra. Essentially PPA fits the multi-foil data to a library of standards of each element with a Gaussian distribution and "strips" each reaction from the composite spectrum. The program was altered by Dr. Doyle Ray Edwards to fit the IBM-1620 computer and also modified for threshold foil analysis. A flow diagram is shown in Figure 5.1. The program takes into account several corrections as background subtraction, counting time, decay time, automatic compensation for gain and threshold shifts, sample fraction, crystal efficiency, and volume reduction prior to counting.

A listing of PPA is displayed in Appendix C.1. The gamma spectrum of each reaction for the elements listed in Table 3.4 was used for the library of standards. this data was obtained using a print out system of the multi-channel analyzer described in Section IV.

B. Flux Calculations

The weighted orthonormal method as presented by Rydin was selected for use in this thesis. The data obtained from a threshold foil activation can be conveniently expressed in the following form.

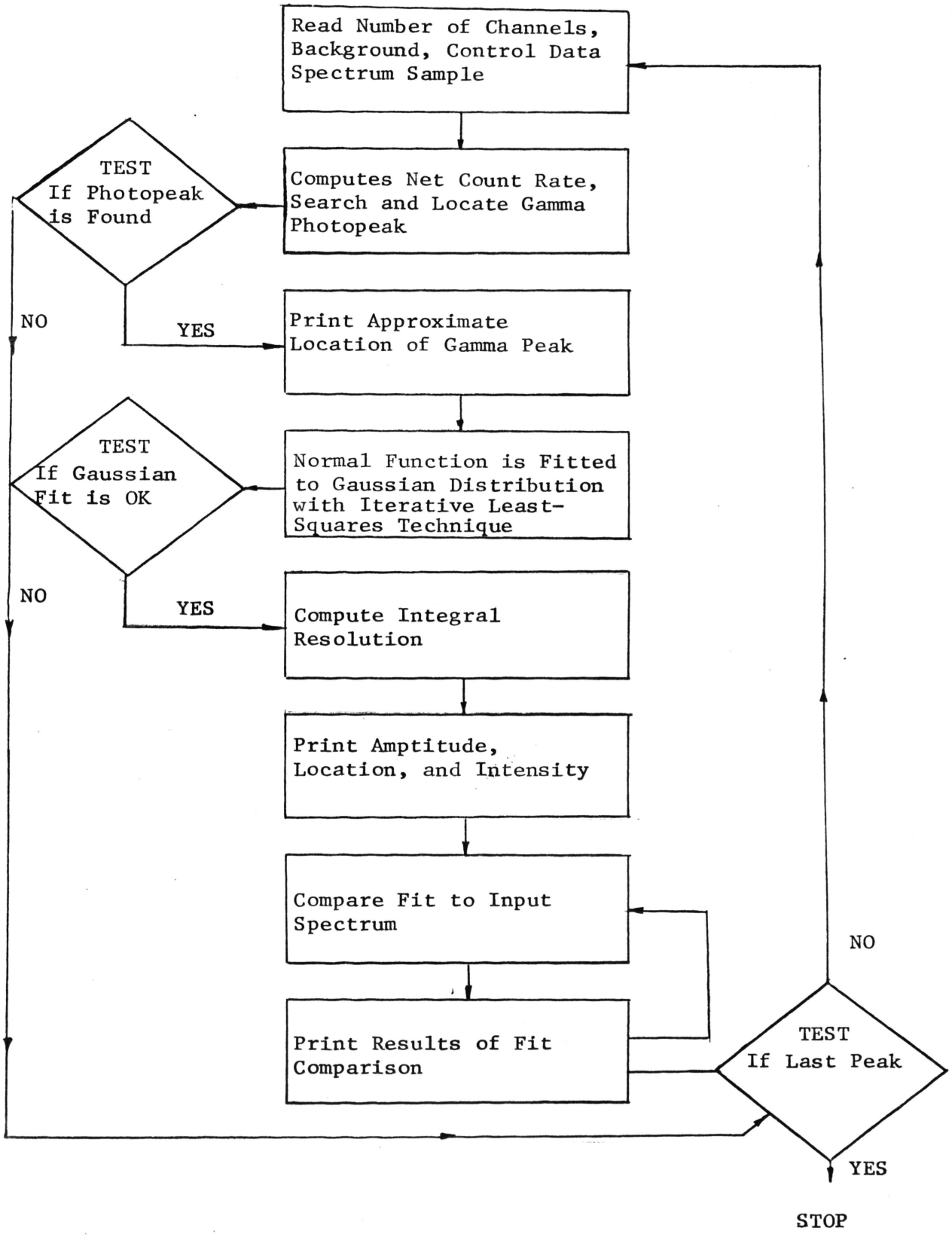

Figure 5.1 Schematic Flow Diagram of PPA Main Program

$$K_i(t) = \int_0^{\infty} \sigma_i (E)\ \phi(E)\ dE \qquad 5.1$$

where $K_i(t)$ is experimental foil activity result corrected for foil weight, irradiation time, counting time, abundance, counting efficiency, etc. and previously outlined in spectra analysis; σ_i (E) the fast neutron absorption cross section for the ith reaction as a function of energy; and $\phi(E)$ is the differential flux.

The primary program is to extract the differential spectrum, $\phi(E)$, from the experimental quantities.

As outlined in the literature review there are several methods to treat foil activation data. The solution of the problem is approached in the following general fashion: 1) the appropriate form of spectral shape is assumed, which has unspecified coefficients, 2) the foil activation cross-section curves are numerically integrated over an energy interval with respect to the assumed spectral shape according to equation 5.1, and 3) the experimentally measured activations are used to specify the appropriate coefficients of the assumed shape and hence specify the measured spectrum.

All methods expect to extract a large amount of differential information from a few integral measurements. In this work, the weighted orthonormal method is chosen since it can fit arbitrary spectra. The other methods are restricted to spectra with certain distinct features.

The flux is assumed to be given by a weighting function times an expansion of known functions of energy which are required to form an orthonormal set

$$\phi(E) = W(E) \sum_{i=1}^{n} B_i\ \psi_i(E) \quad \frac{\text{neutrons}}{\text{cm}^2\ \text{-sec -Mev}} \qquad 5.2$$

where $\phi(E)$ is the differential flux; $W(E)$ is the weighting function; B_i is the coefficient term determined by experimental values of $K_i(t)$; and $\psi_i(E)$ is a linear combination of the cross-section curves used in the measurements and are defined to be orthonormal with respect to a weighting function, $W(E)$.

As many coefficients are used in the expansion as there are foils and thus, the coefficients can be determined from the foil activation data. Hence we can write

$$\psi_1(E) = A_{11}\,\sigma_1(E)$$

$$\psi_2(E) = A_{21}\,\sigma_1(E) + A_{22}\,\sigma_2(E)$$

$$\psi_n(E) = \sum_{i=1}^{n} A_{ni}\,\sigma_i(E) \qquad 5.3$$

or in matrix form

$$[\psi] = [A]\,[\sigma] \qquad 5.4$$

where $[A]$ is a diagonal flux lower triangular matrix. The A_{ij} are determined by the orthonormal condition

$$\int_0^{E_{max}} \psi_1(E)\;\psi_j(E)\;W(E)\;dE = \delta_{ij} \qquad 5.5$$

this leads to a set of linear and non-linear equations which can be solved uniquely (see Appendix C.2). If we solve equation 4.4 for the cross section in terms of $[\psi]$, we get (in matrix form)

$$[\sigma] = [A]^{-1}\,[\psi] \qquad \text{let } [A]^{-1} = [D] \qquad 5.6$$

$$[\sigma] = [D]\,[\psi] \qquad 5.7$$

We can use this to write the activation of the K^{th} foil

$$K_k(t) = \int_0^{E_{max}} \sigma_k(E)\ \phi(E)\ dE$$

$$= \int_0^{E_{max}} W(E) \sum_{j=1}^{k} D_{kj}\ \psi_j(E) \sum_{i=1}^{h} B_i\ \psi_i(E)\ dE \qquad 5.8$$

Using orthonormal relations, the equation simplified to

$$K_k = \sum_{i=1}^{k} B_i\ D_{ki} \qquad 5.9$$

In matrix form

$$[K] = [D]\ [B] \qquad 5.10$$

We can then solve for B_i using the experimentally determined values of K_k

$$[B] = [D]^{-1}\ [K] \qquad \text{but } [D]^{-1} = [A] \qquad [B] = [A]\ [K]$$

Placing this result into the flux expansion equation 4.2, we obtain the result

$$\phi(E) = W(E) \sum_{k=1}^{h} \sum_{i=1}^{h} A_{ki}\ K_i \sum_{j=1}^{h} A_{ki}\ \sigma_i(E) \qquad 5.11$$

Since we know the weighting function is an arbitrary value, calculated A_{ij}, know the $\sigma_i(E)$, and measured the K_i by PPA, we can evaluate the spectrum.

The orthonormal requirement essentially adds m additional constraints to the problem with m additional pieces of information. An important advantage of this method is that the expansion coefficients are determined in a best-fit in the least-square sense.

This method has been coded for the IBM 1620 Model II computer and is used in this report. A complete mathematical analysis and listing of

FUSE-3 is shown in Appendix C.2. A flow diagram of this program is shown in Figure 4.2. Appendix B. 2 shows the various reaction cross-sections versus energy.

B.1 Weighting Function

The weighting function and the activation values from Ispra I were selected as test data. This function varied as the formula below:

$$W(E) = \text{Constant} \cdot \sqrt{E} \cdot e^{-.775E} \qquad 5.12$$

where E is the energy point of the flux. The use of a proper weighting function leads to the best fit of the flux plot. On the experimental data, the weighting function weighting function below was utilized:

$$W(E) = e^{-E} \qquad 5.13$$

This follows the recommendation of Di Cola on recent work with Ispra I in 1964.

C. Error Analysis

As emphasized in Chapter II, the entire method depends on accurately knowing the cross section data for each nuclear reaction. As seen in Table 2.1, this data can vary ten percent either side of the value used in flux calculations. The correction factors of foil self-shielding and flux depression were not of the magnitude to warrant their use to the calculated flux. All of the factors involved would not deviate the flux values as much as the inaccuracy of the cross section data. All cross section data was assumed to be accurate within five percent for mathematical purposes.

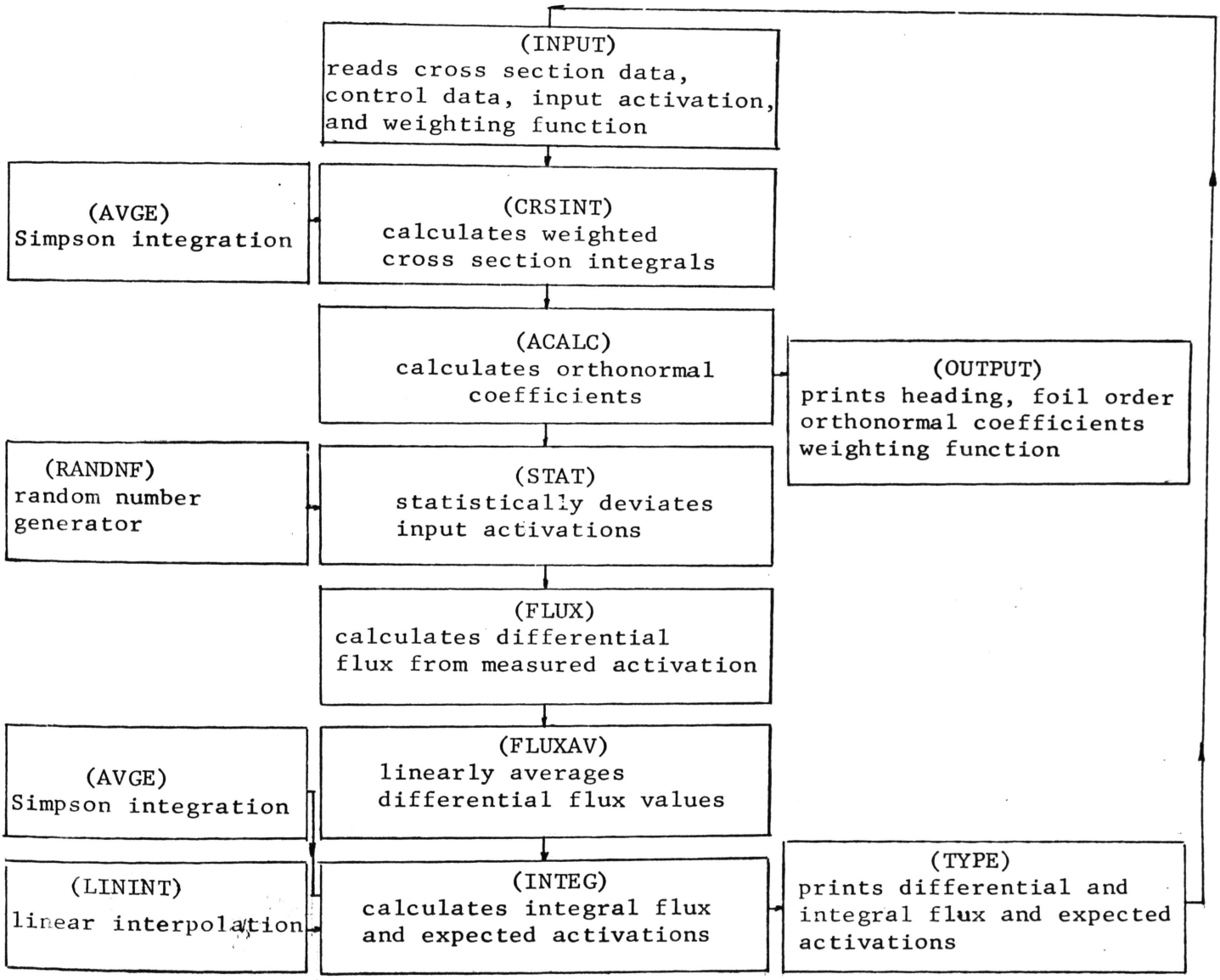

Figure 5.2 FUSE-3 Weighted Orthonormal Method Schematic Flow Diagram of Main Program (Written in Fortran for the IBM-1620 Model II Computer)

VI. RESULTS

A. Multi-Threshold Foils

The Alcoa 2509 alloy proved to be an inadequate threshold detector from the range of 2.9 to 8.1 Mev at a power level of 10 Kw. The three desired reactions were clearly indicated and the activations were of the same order of magnitude. The power level of the UMRR was not adequate to produce enough nickel activation for good statistical analysis. Higher activation could be obtained by longer irradiation times. However, the high activity of the aluminum thermal reaction would prohibit removal of the sample in time to count the desired $Al^{27}(n,p)$ reaction. The trace elements produced no interfering radiation. The optimum counting times for the Alcoa 2509 foils are 28 minutes and 60 hours after irradiation.

The In-P-Fe multi-threshold foil as constructed is inadequate as a multi-threshold foil. The gamma spectrum was completely dominated by the high activation cross-section of the indium reactions. The optimum counting time for determining the gamma photopeaks appears to be 16 to 17 hours after irradiation. At this time period the activity of the phosphorus and iron were quite small in comparison to the indium activity. Hence, the flux would be mostly dependent on the indium activation. However, the indium cross-section is not accurately known in the region of 5.5 to 15 Mev. In accordance with the "effective threshold concept", the indium cross-section was assumed to be constant from 5.5 to 15 Mev (Figure B.14). The accuracy of the flux spectrum would be of the same order as the accuracy of the assumption of the unknown cross-section.

B. Gamma Spectrum Analysis

The activity calculated by the least-squares Gaussian fit to the gamma photopeaks of the constituent reactions were in similar magnitude of the values of the individual reactions. Table 6.1 list the reactions for which their was enough statistical data for evaluation of the induced activity.

The activity of phosphorus and iron in the In-P-Fe foil could not be calculated due to the small magnitude of the gamma photopeaks at optimum counting time. The activity of the weak phosphorus reaction could not be determined in element form at 2 hours wait time. The Mg^{56} yields a clear concise photopeak at 3 hours wait time.

The Alcoa 2509 $Al^{27}(n,p)$ activity at .834 Mev was readily calculated by PPA at optimum wait time. The poor statistical data at 1.01 Mev photopeak prohibited the activity from being tabulated. The $Ni^{56}(n,p)$ product activity could be calculated in element form at 80 minutes wait time.

Since the $In^{115}(n,n')$, $Ni^{56}(n,p)$, $Al^{27}(n,p)$ and $Fe^{56}(n,p)$ activities could be calculated by the photopeak analysis program, this data was utilized for flux calculations. Each multi-threshold foil was inadequate as a flux detector, since the activity from one reaction could be determined for flux calculations.

C. Differential and Integral Flux

The flux plot of the In-P-Fe and Alcoa 2509 foils could not be evaluated due to the inadequate photopeak determination. The individual element activity was utilized to give information of the flux level of the reactor. The Watt fission spectrum was calculated by equation 2.1 to be used as a point of reference for the differential and integral flux. The results of the flux mappings using the

Table 6.1

Experimental and Calculated Activities, and Standard Deviation

Reaction	Experimental Activity	Calculated Activity	Standard Deviation
*$Ni^{58}(n,p)Co^{58}$	1.528255E+08	6.15230E+08	7.64127E+06
**$Ni^{58}(n,p)Co^{58}$	———	———	———
*$Al^{27}(n,p)Mg^{27}$	2.543588E+06	2.00492E+07	1.27179E+05
**$Al^{27}(n,p)Mg^{27}$	5.237471E+05	———	———
*$Al^{27}(n,\alpha)Na^{24}$	———	———	———
**$Al^{27}(n,\alpha)Na^{24}$	———	———	———
*$In^{115}(n,n')In^{115m}$	1.145658E+08	3.72556E+08	5.72829E+06
**$In^{115}(n,n')In^{115m}$	5.237471E+08	———	———
*$P^{31}(n,p)Si^{31}$	———	———	———
**$P^{31}(n,p)Si^{31}$	———	———	———
*$Fe^{56}(n,p)Mn^{56}$	5.577510E+06	7.17544E+06	3.72556E+08
**$Fe^{56}(n,p)Mn^{56}$	———	———	———

Note: The $Al^{27}(n,p)$ gamma photopeak at 1.01 Mev could not be calculated by PPA. The activity used is from the gamma photopeak at .834 Mev.

* Element Activation

** Activation from Multi-Threshold Foil

In, Ni, Al and Fe elements are shown in Figure 1 and 2. The nickel reaction was omitted to provide information on a theoretical multi-threshold foil with three reactions. The differential flux plot for 3 and 4 sets of foils oscillated during the lower magnitude of the energy ranges. This factor was due to the small number of foils used in this calculation and the inaccuracy of tabulated cross-section data. The use of 5 foils (or reactions) produced a more stable plot as shown in the sample flux calculation using ISPRA I data. The previous conditions were verified by Rydin (1). At 7.5 Mev, the oscillation's ended and the data followed the Watt Fission Spectrum.

The integral flux of the In, Ni, Al and Fe elements are displayed in Figure 6.2 with Watts Fission Spectrum. This data is in excellent accord to the work of Rydin and Ringle. The high energy neutron population drops off at a very rapid rate past the 12 Mev range as expected. The interpolation function of FUSE-3 is shown by the smooth flux curve. The value of the fast flux is similar in magnitude to the value of fast neutron flux calculated in the University of Missouri at Rolla Reactor Hazards Report. The general deviation of flux mappings from the fission spectrum for a thermal reaction are in agreement with several authors (1, 2, 32). The calculated activities and standard deviation from the experimental activity is also displayed in Table 6.1.

The high magnitude of the flux value at lower end of the fast neutron spectrum indicates the predominance of neutrons in the thermal region and epithermal region in a thermal reactor.

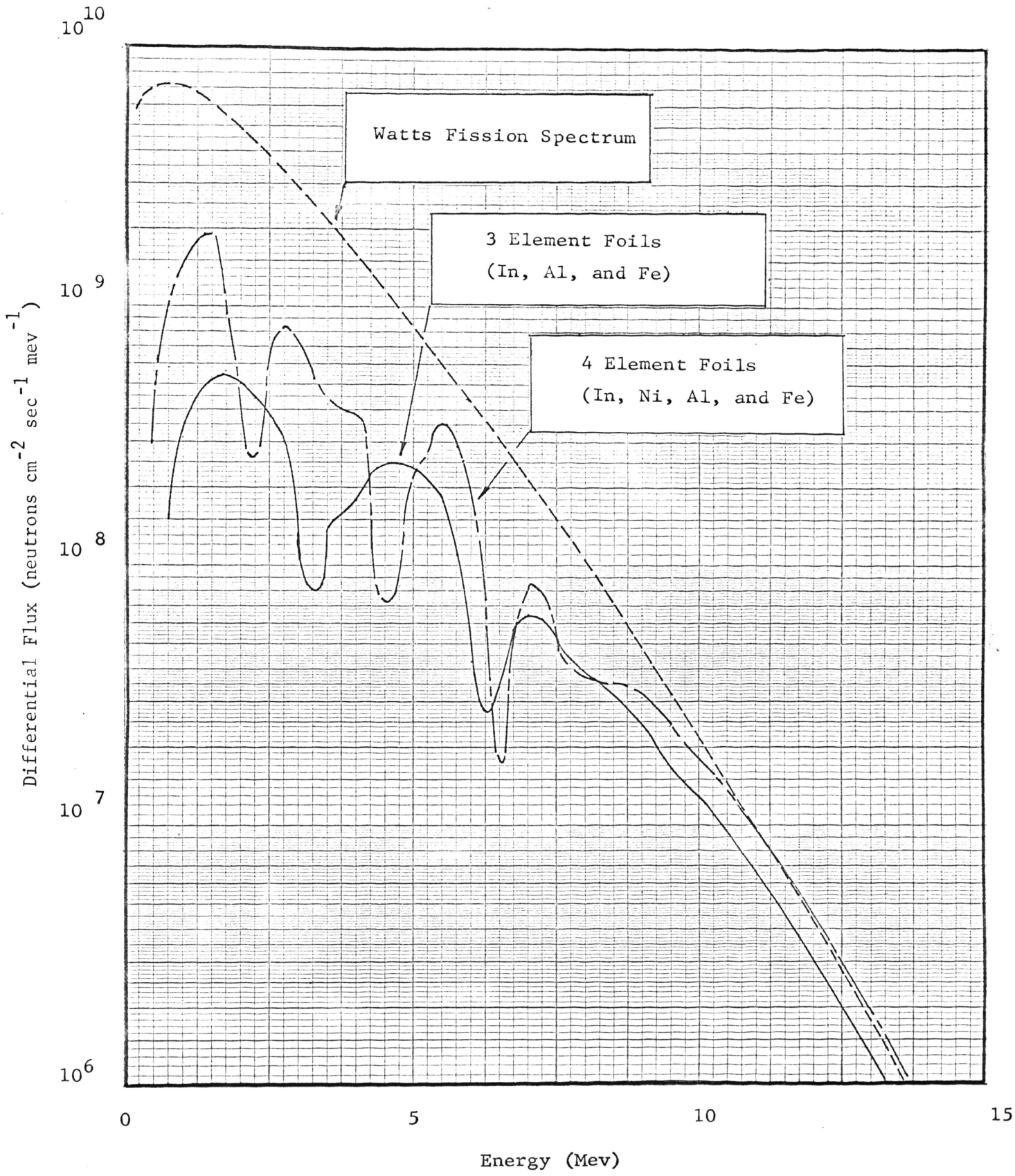

Figure 6.1 Fission Spectrum and Differential Flux of
In, Ni, Al, and Fe Elements
Flux versus Energy

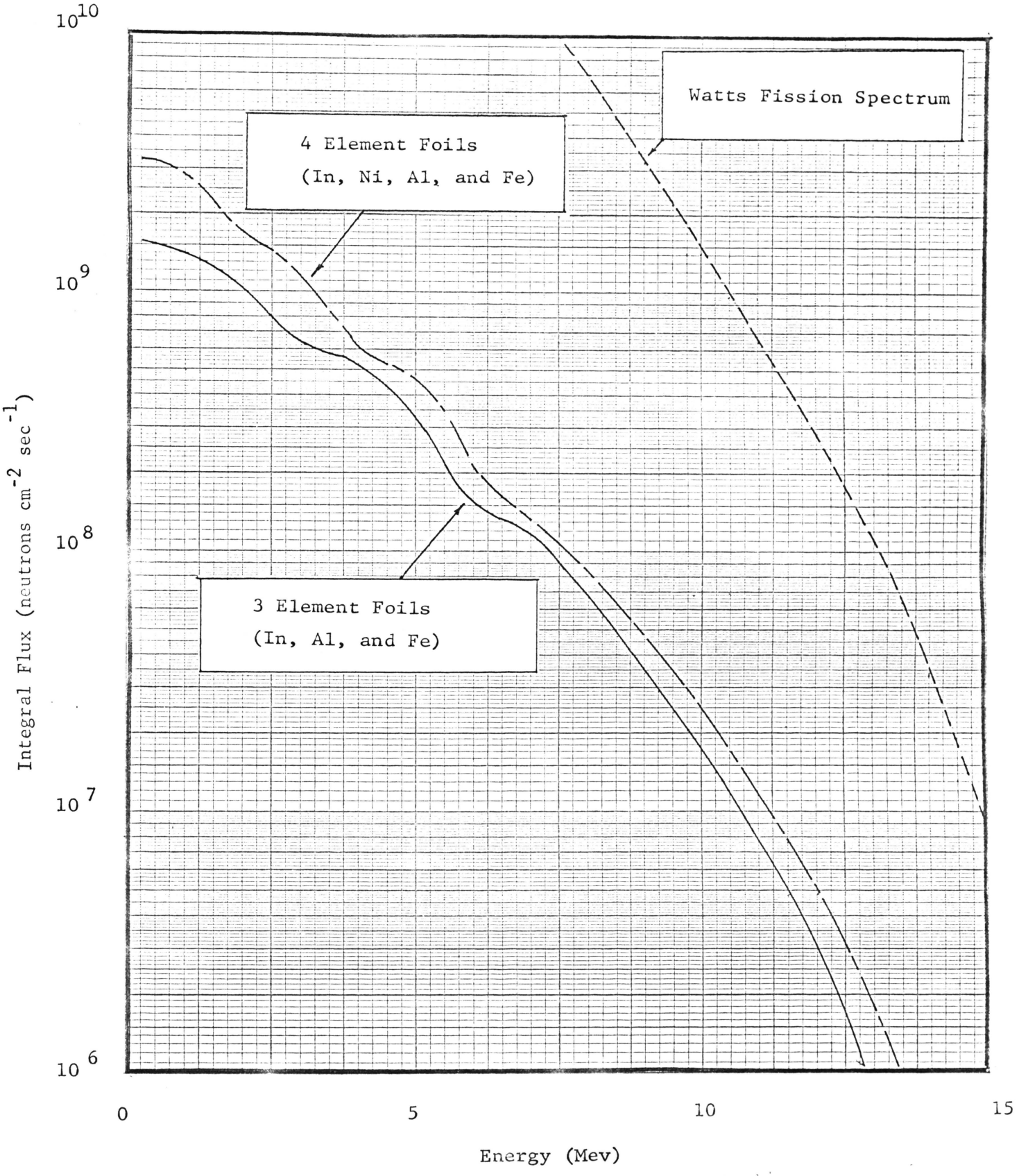

Figure 6.2 Fission Spectrum and Integral Flux of
In, Ni, Al, and Fe Elements
Flux versus Energy

VII. CONCLUSIONS

The Alcoa 2509 flux detector has excellent potential as a multi-threshold foil. The low power level of the reactor did not yield sufficient data on the $Ni^{58}(n,p)$ and $Al^{27}(n,\alpha)$ reactions. The In-P-Fe foil holds a good deal of promise as flux detector. The indium activity dominated the entire gamma spectra of the In-P-Fe foil for a 17 hour period. At this time length, the phosphorus and iron activity yields weak photopeaks. Indium is a low energy threshold detector, however, the cross-section of (n,n') reaction is large and not accurately tabulated. It is estimated the indium-phosphorus-iron foil contains as high as 5% indium. The author's results do not agree with the results tabulated by Holkenbrink.

The gamma spectrum analysis using the least-squares Gaussian fit have fair results. The multi-foil spectrum of all reactions could not be evaluated due to poor statistical data. A least-squares type gamma spectrum analysis is in accord with the recommendation of Ringle, Kholer and Murphy.

The fast flux spectrum can be determined using three reactions of threshold foils. However, the few reactions produce an oscillating curve for the differential flux plot. The integral flux plot displays a clearer flux profile of the neutron distribution. Four or five reactions would yield more accurate data for flux calculations. This method of measuring the fast-flux spectrum holds a great deal of promise in determining the fast neutron environment. The major drawbacks are 1) the inaccuracy to which the cross-section data is tabulated and 2) the small number and the range of threshold reactions in each multi-foil.

VIII. RECOMMENDATIONS

The author suggests the following recommendations for future work with multi-threshold foils. The $Fe^{56}(n,p)$ and $Al^{27}(n,p)$ reactions should be selected for further investigation. The $In^{115}(n,n')$ reaction holds much promise; however, the cross-section data has not been ac accurately tabulated. The $P^{31}(n,p)$ reaction should be eliminated from consideration as a threshold detector due to a weak gamma photo-peak. The In-Au alloy INCORO-60 merits study as a flux detector over the composite spectrum. An In, Fe, and another element could possibly be utilized as a multi-threshold detector if the amount of indium is controlled to .25 to 1 percent by weight. Alcoa 2509 is an adequate threshold detector and should be used at higher power levels for better statistical results.

Recommendations of a general nature are: 1) A multi-threshold foil with more than three desired reactions would yield flux data with a higher degree of accuracy, 2) A detector below the 1 Mev range is most desirable for detecting radiation damage, 3) The half lives and the cross-sections of the individual constituents should be approximately equal in value, 4) The least-squares analysis of the gamma spectrum gives accurate results. A program as ALPHA by Schonfeld which "strips" the individual constituents form the composite spectrum should yield better activity data (16), and 5) The method of flux calculation selected should be the most accurate in the particular range of study. For example, the Legendre method is good for continuous fluxes but poor for step function fluxes.

APPENDIX A

DESCRIPTION OF FACILITIES

This Appendix contains a brief description of the UMRR Reactor, the multi channel analyzer and the scintillation probe.

A.1 UMRR Nuclear Reactor

The University of Missouri at Rolla Reactor is a 10 Kw, heterogeneous, thermal, pool-type, research and training reactor. It is similar in design to the bulk shielding reactor, the original pool-type reactor at Oak Ridge, Tennessee.

Experimental facilities of the Reactor include a thermal column for irradiation requiring low energy neutrons, a beam tube for experiments which require a beam of neutrons at the external face of the reactor, and various irradiation facilities which can be placed in or near the core.

A.2 RIDL Model 34-12B Transistorized 400-Channel Analyzer

A 400-channel pulse height analyzer is similar to 400 single channel analyzers, except that it includes one input and data processing system. When it is operated in its time mode, it functions as a single-channel scaler for a basic time period, shifting to a new channel scaler for the basic time period. The basic analyzer includes a computer with a ferrite core memory, a data display system, and control circuitry for automatic operation.

The ferrite core memory includes a group of cores which are assigned to each of 400 channels. The built-in cathode-ray-tube display permits the operator to monitor data both during and after its accumulation in the memory. Data outputs are provided for recorders, typewriters, and tape punches. The multi-channel scaler stores gross count information through a preset time. At the end of the time interfal, the address is advanced to the next sequential channel. This operating cycle is repeated throughout the entire 400 channels.

A.3 Model 10-8 Scintillation Probe

The RIDL Model 10-8 Scintillation Probe is a convenient detector-preamplifier combination assembly, built into a cylindrical container. The housing includes a crystal holder at one end, a photomultiplier tube at the center, and a built-in two-transistor preamplifier at the opposite end.

A 1 3/4" sodium-iodide, thallium-activated crystal was used with the scintillation probe.

APPENDIX B

THRESHOLD FOIL DATA

The elements, isotopes, nuclear reactions, gamma peaks, reaction energies, half-life and the cross section at threshold energies for the elements are displayed in tabulated form. Sample forms, purity, vendors and the results of irradiation runs are also presented.

The cross sections of the individual nuclear reactions used in the flux calculations are shown in graphical form.

B.1.1 Aluminum - Al

Naturally Occurring Isotopes: Al^{27} - 100%

Nuclear Reactions:

Reaction	γ Peak Mev	Reaction Energy	Half Life	Cross Section
$Al^{27}(n,\gamma)Al^{28}$	1.78	Thermal	2.3 m	235 mb
$Al^{27}(n,p)Mg^{27}$	.834,1.01	E_t = 4.6 Mev	9.45 m	22 mb
$Al^{27}(n,\alpha)Na^{24}$	1.37	E_t = 8.1 Mev	15 h	60 mb
$Al^{27}(n,\gamma)Al^{28}$	1.78	E_r = 9.1 Kev	2.3 m	432 mb

Form: 1/2" circular metallic disks x 007" thick

Purity: 99.99%

Vendor: Reactor Experiments Inc.

Irradiation Results:

The aluminum has two reactions of interest in this work a $Al^{27}(n,p)$, and $Al^{27}(n,\alpha)$. The threshold reactions of these reactions are 4.6 and 8.1 Mev respectively. The (n,p) product has a short half life of 9.5 minutes, therefore, a count should be taken at approximately 30 minutes after irradiation. This time interval will allow the short 2.3 minute half-life $Al^{27}(n,\gamma)$ product to die out, as shown in Figure B.1. The 15 h half-life (n,α) product is displayed in Figure B.2.

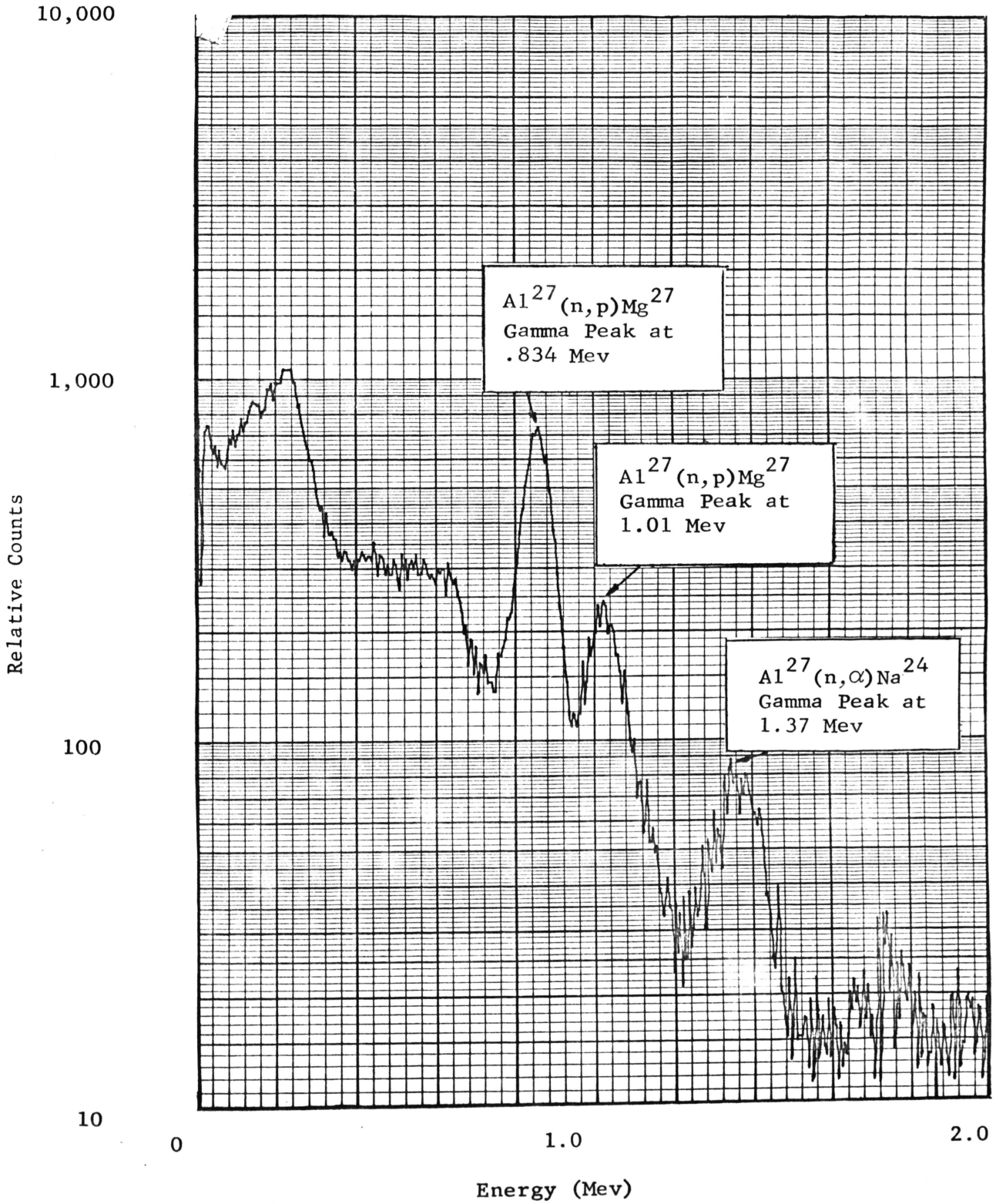

Figure B.1 Aluminum Gamma Spectrum 36 minutes after Irradiation
Relative Counts versus Energy

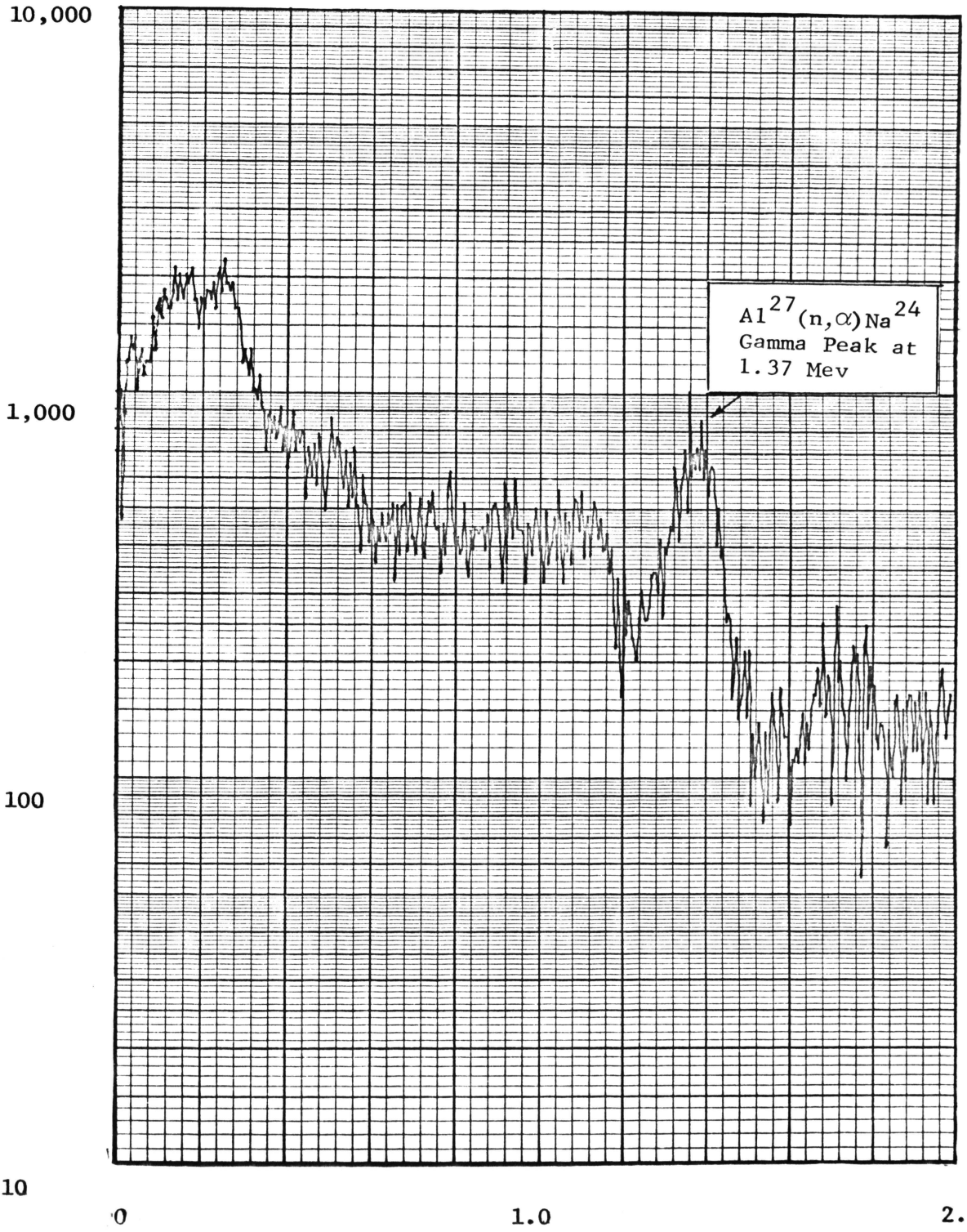

Figure B.2 Aluminum Gamma Spectrum 150 minutes after Irradiation Relative Counts versus Energy

B.1.2 Copper - Cu

Naturally Occurring Isotopes: Cu^{63} - 69.09%
Cu^{65} - 30.91%

Nuclear Reactions:

Reaction	γ Peak Mev	Reaction Energy	Half Life	Cross Section
$Cu^{63}(n,\gamma)Cu^{64}$	.51,1.34	E_r = 562 ev	12.9 h	1000 mb
$Cu^{63}(n,\gamma)Cu^{64}$	.51,1.34	Thermal	12.9 h	2400 mb
$Cu^{63}(n,2n)Cu^{62}$	.51,.69,.88,1.13,1.17	E_t = 11.4 Mev	9.73 m	500 mb
$Cu^{65}(n,2n)Cu^{64}$	.511	E_t = 2.9,11.4Mev	12.8 h	800 mb
$Cu^{65}(n,p)Ni^{65}$	.37,1.12,1.49	E_t = 1.32 Mev	2.6 h	36 mb
$Cu^{65}(n,\gamma)Cu^{66}$	.84,1.04	E_t = 2.9 Mev	5.1 m	9 mb

Form: 1/2" circular metallic disks x .005" thick

Purity: 99.99%

Vendor: Reactor Experiments Inc.

Irradiation Results:

The high annihilation radiation of the copper is clearly demonstrated in Figure B.3. It should be noted the gamma photopeak of Ni^{65} at .37 Mev is covered by annihilation radiation. Only the thermal reaction at 1.34 Mev can be detected in the Cu spectra. The $nickel^{65}$ threshold reaction at 1.32 Mev could not be determined. The annihilation radiation from the Cu^{62} was allowed to decay 2.5 h before measurement of the same radiation from the Cu^{64} reactions. The Cu^{64} is shown in Figure 3.3. The Cu^{64} can also be formed from a thermal reaction, hence threshold reactions at 11.4 Mev could not be determined accurately.

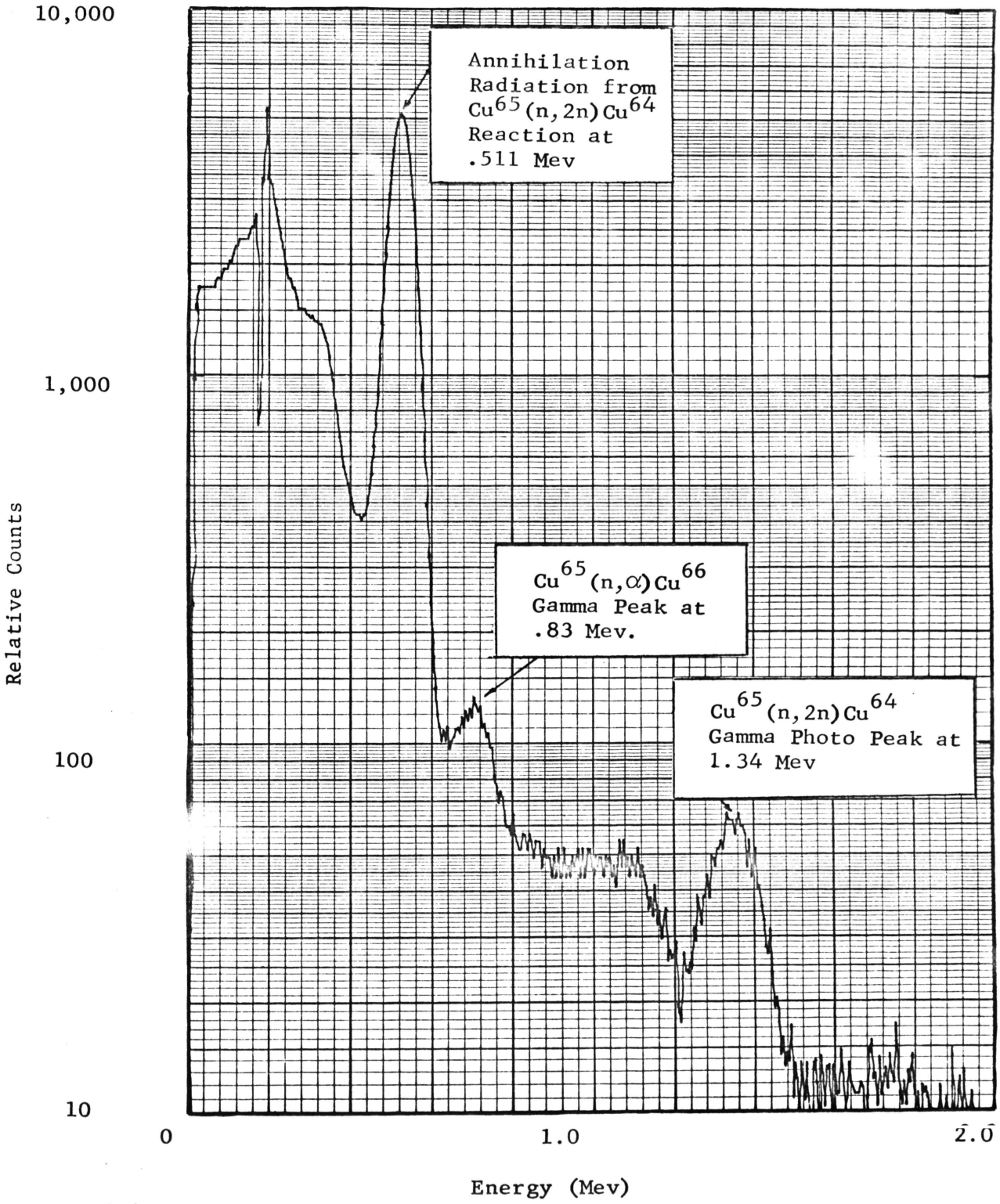

Figure B.3 Copper Gamma Spectrum 3.3 hours after Irradiation. Relative Counts versus Energy

B.1.3 Gold - Au

Naturally Occurring Isotopes: Au^{197} - 100%

Nuclear Reactions:

Reaction	γ Peak Mev	Reaction Energy	Half Life	Cross Section
$Au^{197}(n,\gamma)Au^{198}$	.411	Thermal	2.696 d	———
$Au^{197}(n,\gamma)Au^{198}$	.411	E_r = 4.9 ev	2.696 d	15,000 b

Form: 1/2" circular metallis disks x .002" thick

Purity: 99.99%

Vendor: Reactor Experiments Inc.

Irradiation Results:

The gold foils are useful thermal and resonance detectors for thermal and epithermal flux. The high cross section of the resonance reaction produces a dominant peak at .411 Mev.

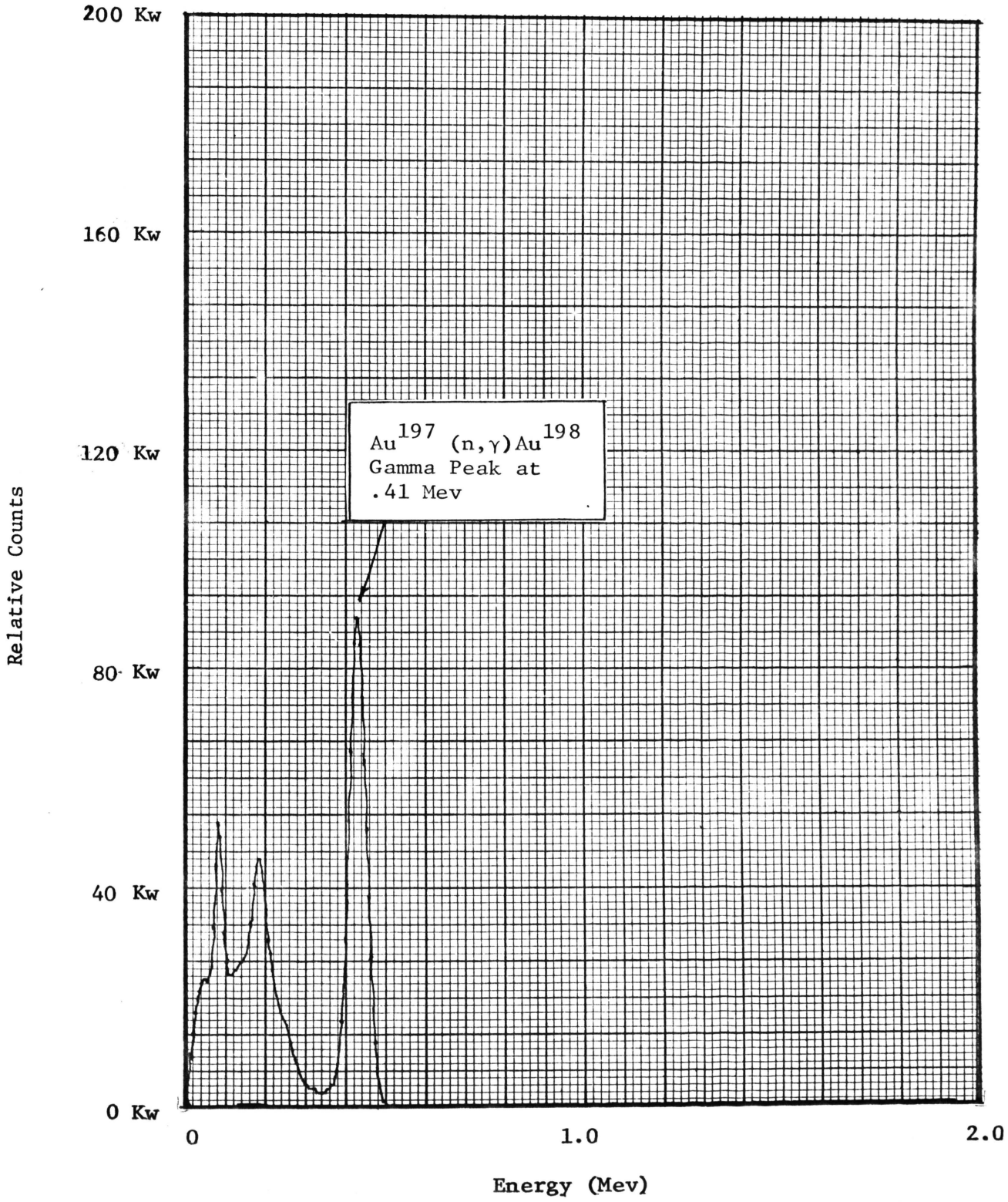

Figure B.4 Gold Gamma Spectrum 330 hours after Irradiation Relative Counts versus Energy

B.1.4 Indium - In

Naturally Occurring Isotopes: In^{113} - 4.28%
*In^{115} - 95.72%

* Naturally occurring or otherwise available but radioactive

Nuclear Reactions:

Reaction	γ Peak Mev	Reaction Energy	Half Life	Cross Section
$In^{113}(n,n')In^{113m}$	.392	———	104 m	———
$In^{115}(n,2n)In^{114m}$	.101	E_t = 10.6 Mev	50 d	1400 mb
$In^{115}(n,\gamma)In^{116m}$	.406,1.085,1.274	Thermal	54 m	8500 mb
$In^{115}(n,\gamma)In^{116m}$	.406,1.085,1.274	E_r = 1.44 ev	54 m	>1.95 mb
$In^{115}(n,n')In^{115m}$	.335,523	E_t = .45 Mev	4.5 h	400 mb

Form: 1/2" circular metallic disks x .005" thick

Purity: 99.99%

Vendor: Reactor Experiments Inc.

Irradiation Results:

The very high cross section of the In^{116m} daughter is shown by the gamma photopeak of .406, .820, 1.065 and 1.274 Mev of Figure B.4 at 9 hours after irradiation, the $In^{115}(n,n')$ product is nearly equal to $In^{115}(n,\gamma)$ product. The desired In^{115m} isotope is predominate only after 15 or 17 hours irradiation (Figure B.5). At this time, the 54 minute half-life In^{116m} isotope has decayed sufficiently for determining the desired reaction. The magnitude and half-life (50 days) of In^{114m} are displayed in Figure B.6. In order to clarify the $In^{115}(n,n')$ product, a count was taken several days later in order to subtract the background and In^{114m} reaction. This desired $In^{115}(n,n')$ reaction has a low threshold reaction at 0.45 Mev.

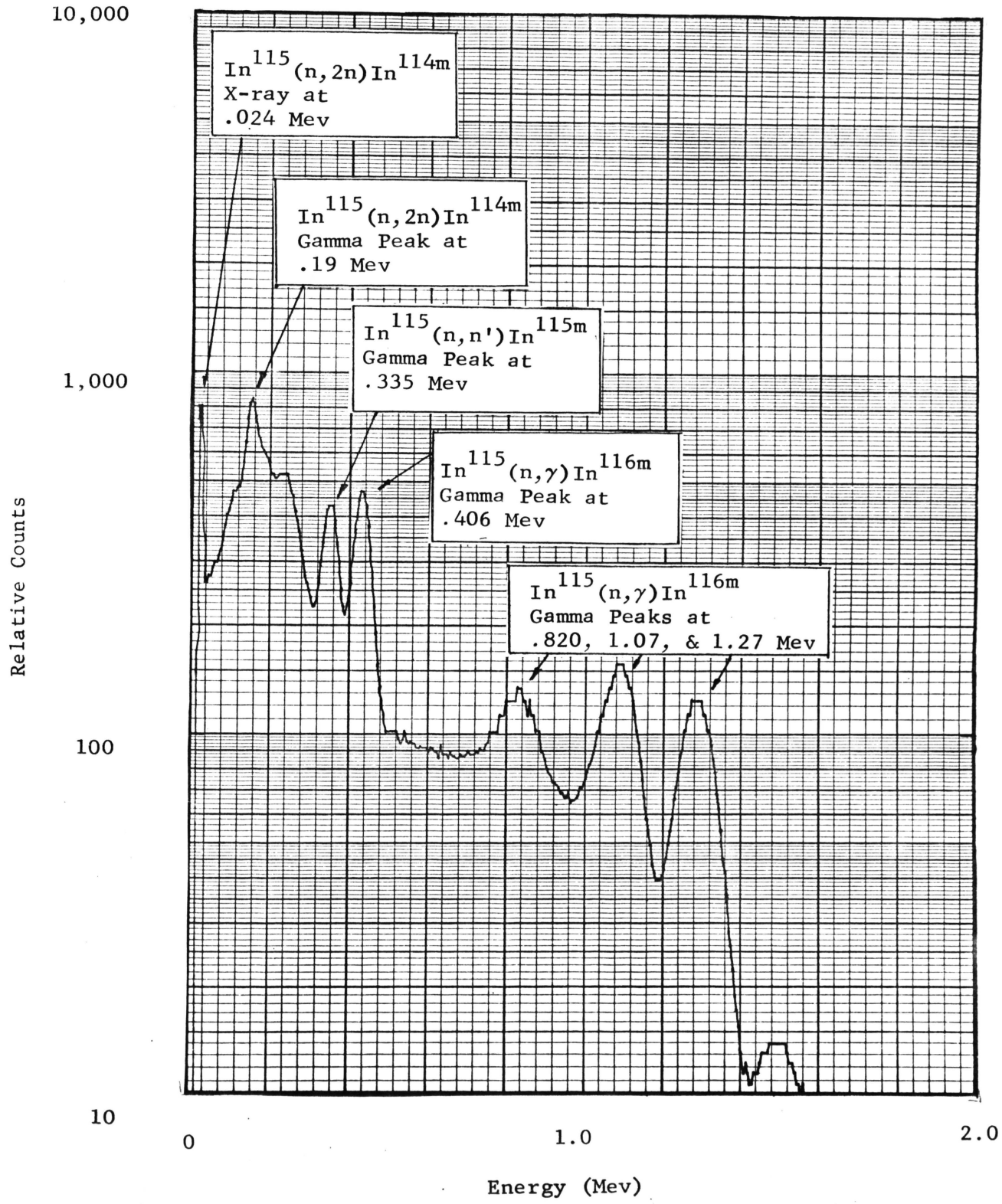

Figure B.5 Indium Gamma Spectrum 9.07 hours after Irradiation
Relative Counts versus Energy

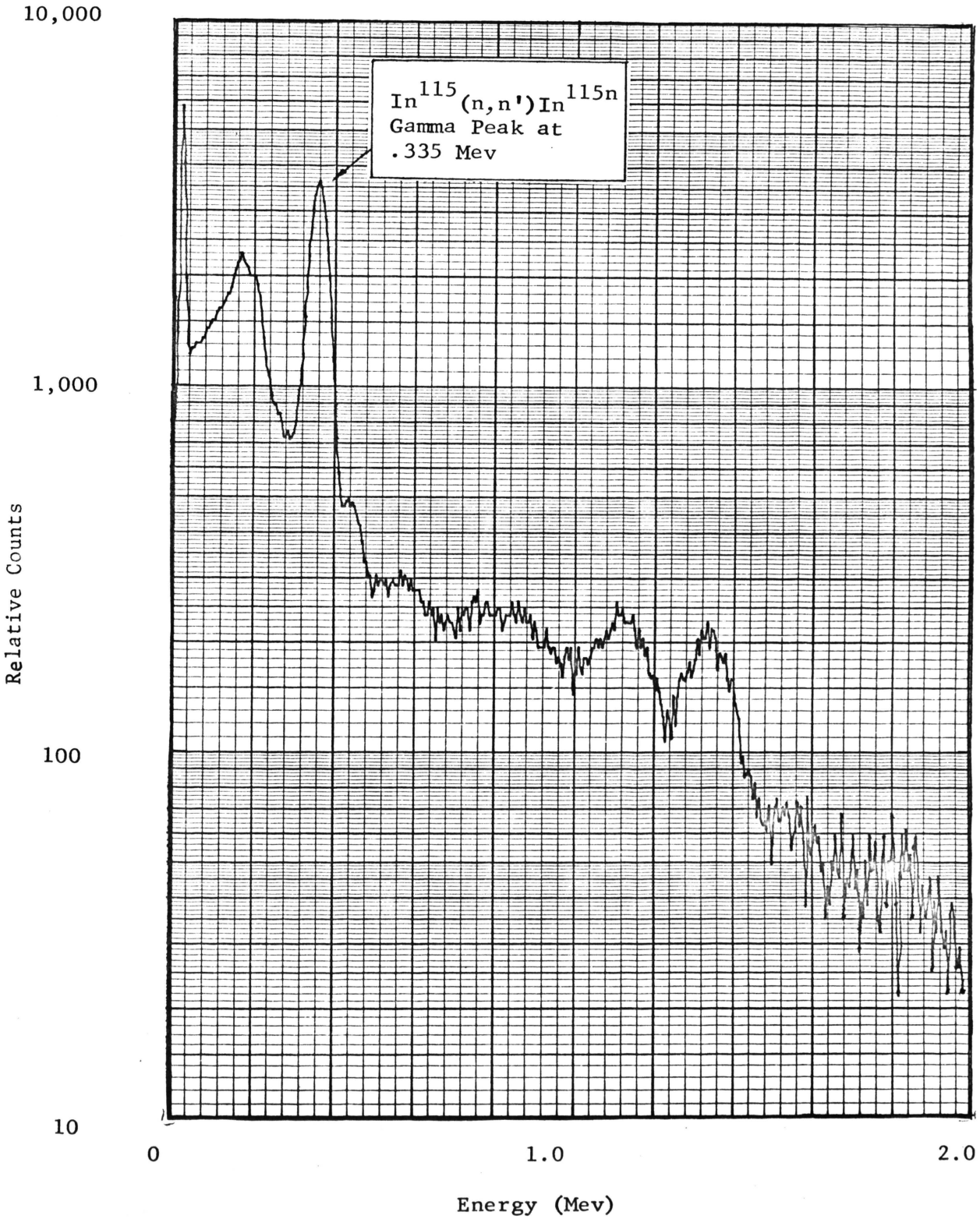

Figure B.6 Indium Gamma Spectrum 15.48 hours after Irradiation Relative Counts versus Energy

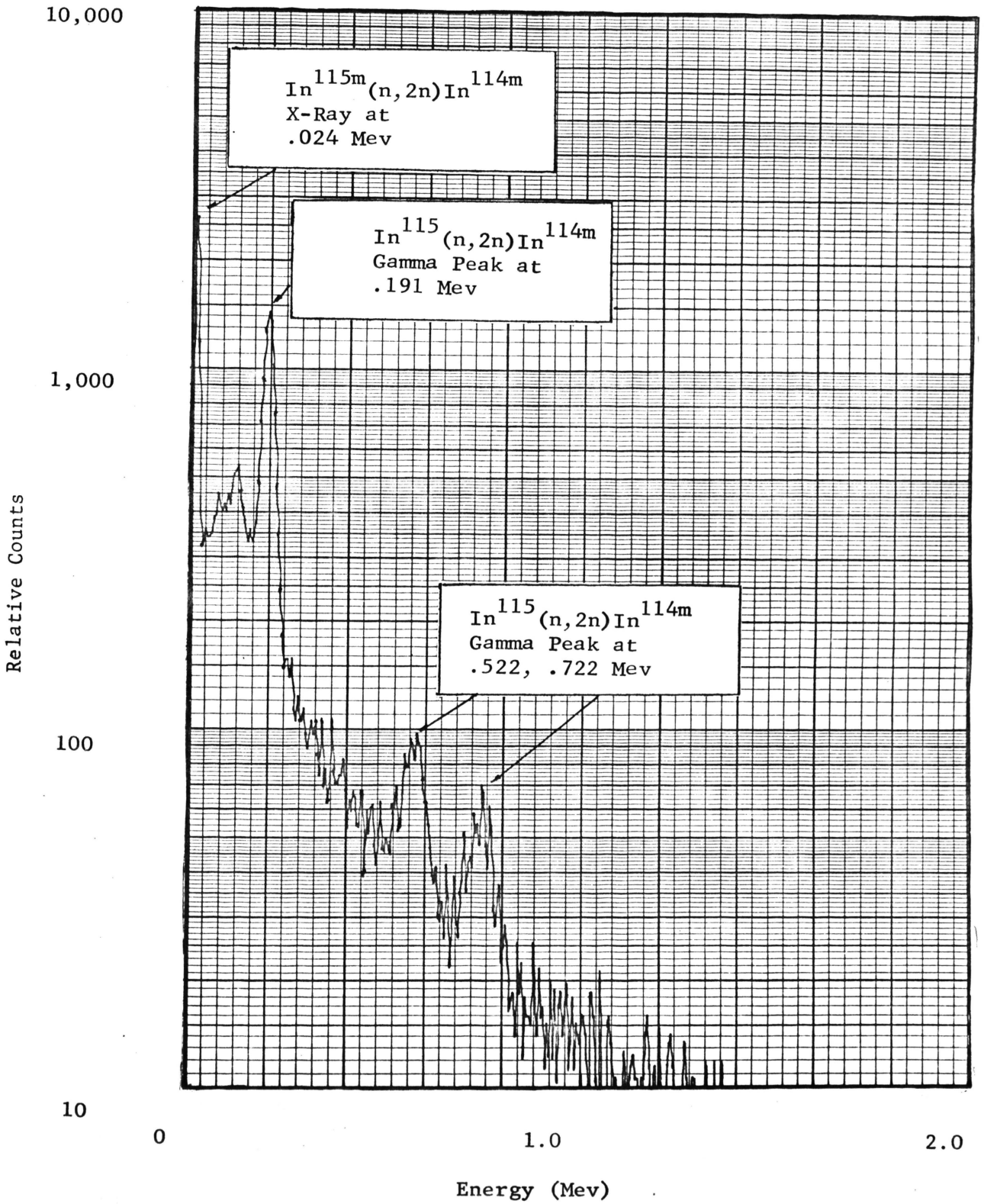

Figure B.7 Indium Gamma Spectrum 70.94 hours after Irradiation. Relative Counts versus Energy

B.1.5 Iron - Fe

Naturally Occurring Isotopes: Fe^{54} - 5.82%
Fe^{56} - 91.66%
Fe^{57} - 2.19%
Fe^{58} - 0.33%

Nuclear Reactions:

Reaction	γ Peak Mev	Reaction Energy	Half Life	Cross Section
$Fe^{54}(n,\gamma)Fe^{55}$	.22	Thermal	2.60 y	≈500 mb
$Fe^{54}(n,2n)Fe^{53}$	.37,.51	E_t = 13.9 Mev	8.9 m	10 mb
$Fe^{54}(n,p)Mg^{54}$	.84	———	——	———
$Fe^{56}(n,p)Mn^{56}$	.84,1.80	E_t = 5.3 Mev	2.576 h	120 mb
$Fe^{58}(n,\gamma)Fe^{59}$	1.10,1.20	Thermal	2.60 y	———

Form: 1/2" circular metallic disks x .005" thick

Purity: 99.9%

Vendor: Reactor Experiments Inc.

Irradiation Results:

The iron demonstrates a clear gamma photopeak at .84 Mev as shown in Figure 3.4. The two reactions are the $Fe^{56}(n,p)$ and $Fe^{54}(n,p)$. The Fe^{56} reaction has a threshold 5.3 Mev and a product with a half-life of 2.576 hours, and yields a countable production. The fast reaction has a half-life of 8.0 minutes and yields no countable activity. The Mn^{56} iron photopeak may be detected up to 8 half-lives.

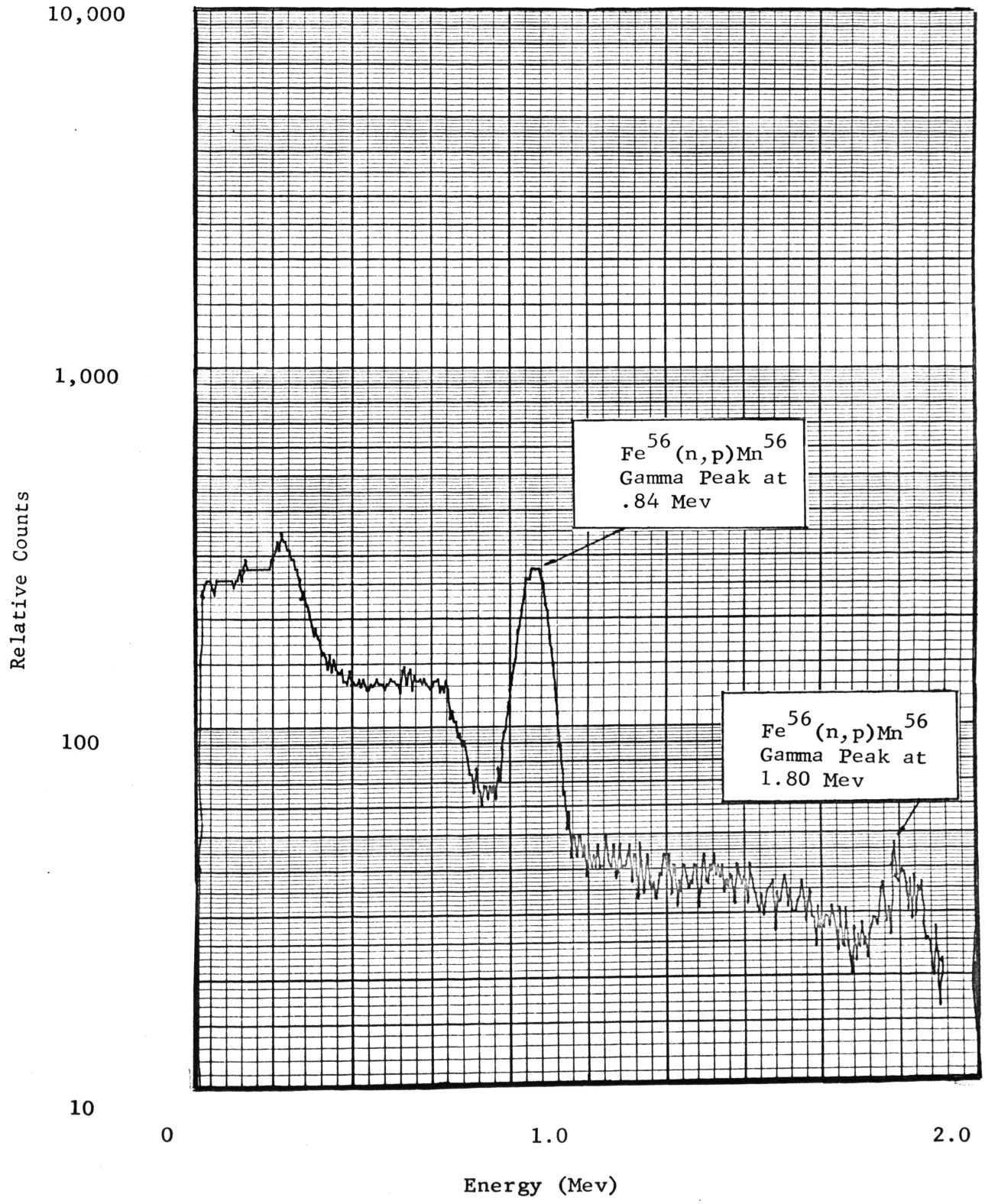

Figure B.8 Iron Gamma Spectrum 3.05 hours after Irradiation. Relative Counts versus Energy

B.1.6 Nickel - Ni

Naturally Occurring Isotopes: Ni^{58} - 67.88%
Ni^{60} - 26.23%
Ni^{61} - 1.19%
Ni^{62} - 3.66%
Ni^{64} - 1.08%

Nuclear Reactions:

Reaction	γ Peak Mev	Reaction Energy	Half Life	Cross Section
$Ni^{58}(n,p)Co^{58}$	.81	E_t = 2.9 Mev	72 d	92 mb
$Ni^{58}(n,p)Co^{58m}$	.81	E_t = 4.1 Mev	9.2 h	10 mb
$Ni^{58}(n,2n)Ni^{57}$	1.37,1.89,.127	E_t = 11.7 Mev	36 h	.0012 mb
$Ni^{60}(n,p)Co^{60}$	1.17,1.33	E_t = 2.07 Mev	5.24 y	3.5 mb
$Ni^{61}(n,p)Co^{61}$	.068	E_t = 5.41 Mev	1.65 h	———
$Ni^{62}(n,\alpha)Fe^{59}$	1.10,1.28	E_t = .884 Mev	45.1 d	.014 mb
$Ni^{62}(n,p)Co^{62}$	1.17,1.47,1.74	E_t = 8.92 Mev	13.9 m	———

Form: 1/2 circular disks x .010" thick

Purity: 99.87%

Vendor: Reactor Experiments Inc.

Irradiation Results:

The Co^{58} obtained from the $Ni^{58}(n,p)$ reaction may be detected free from interference by all other reactions produced by neutrons on nickel. This product has gamma photopeak at .810 Mev, and a threshold reaction at 2.9 Mev. The long half-life of Co^{58} (72 days) allows for the Ni^{57} and Ni^{65} to be eliminated allowing a few days for decay. The long half-life (5.24 years) plus the low cross section of the $Ni^{60}(n,p)$ reaction eliminates interference from Co^{60}. Due to the low power levels of the UMRR, no correction was necessary for the thermal neutron

burnout of Co^{58}. The Fe^{59} activity is shown with the Co^{58} in Figure B.8. The desired reaction is clearly indicated in Figure B.9.

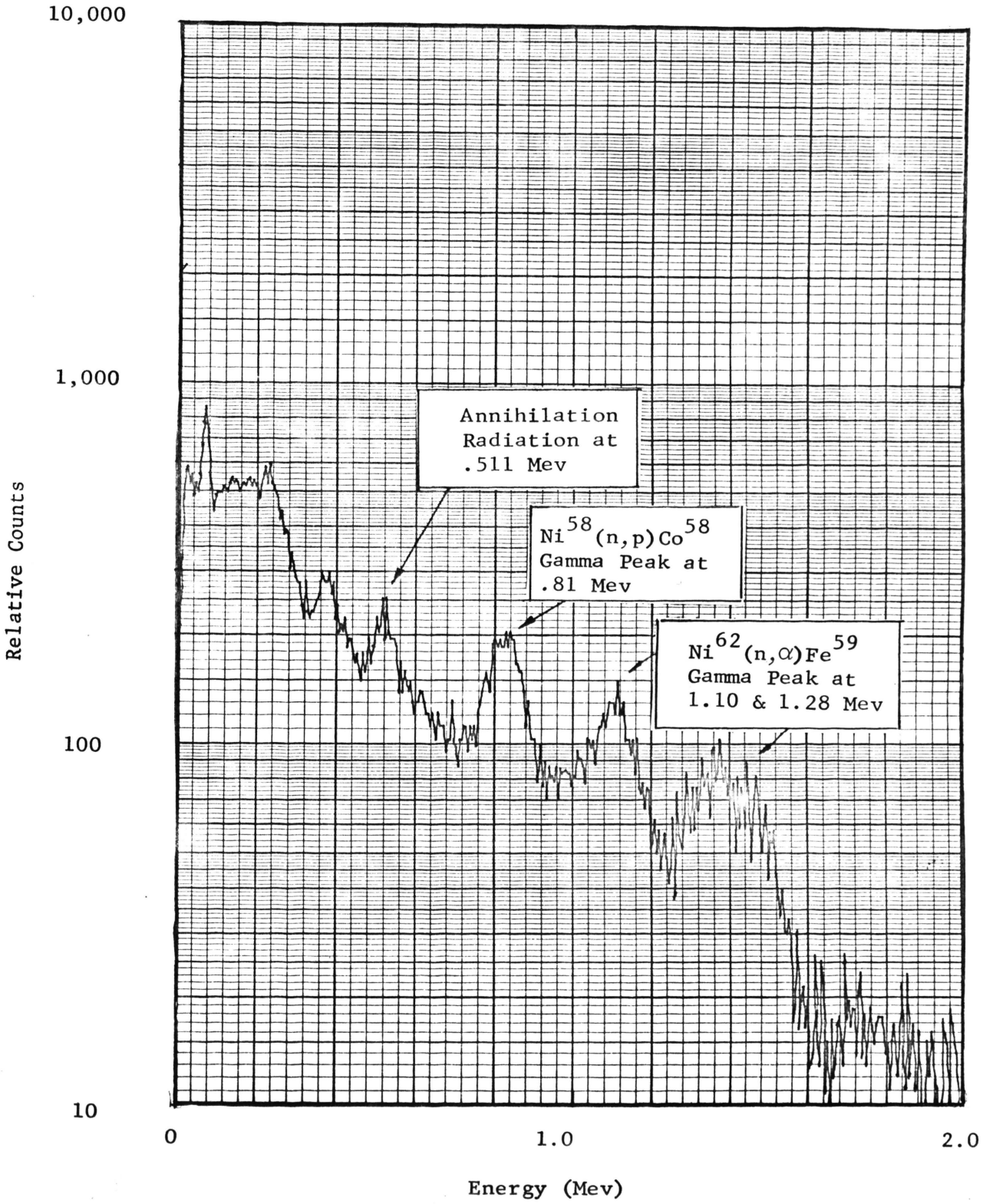

Figure B.9 Nickel Gamma Spectrum 81 minutes after Irradiation Relative Counts versus Energy

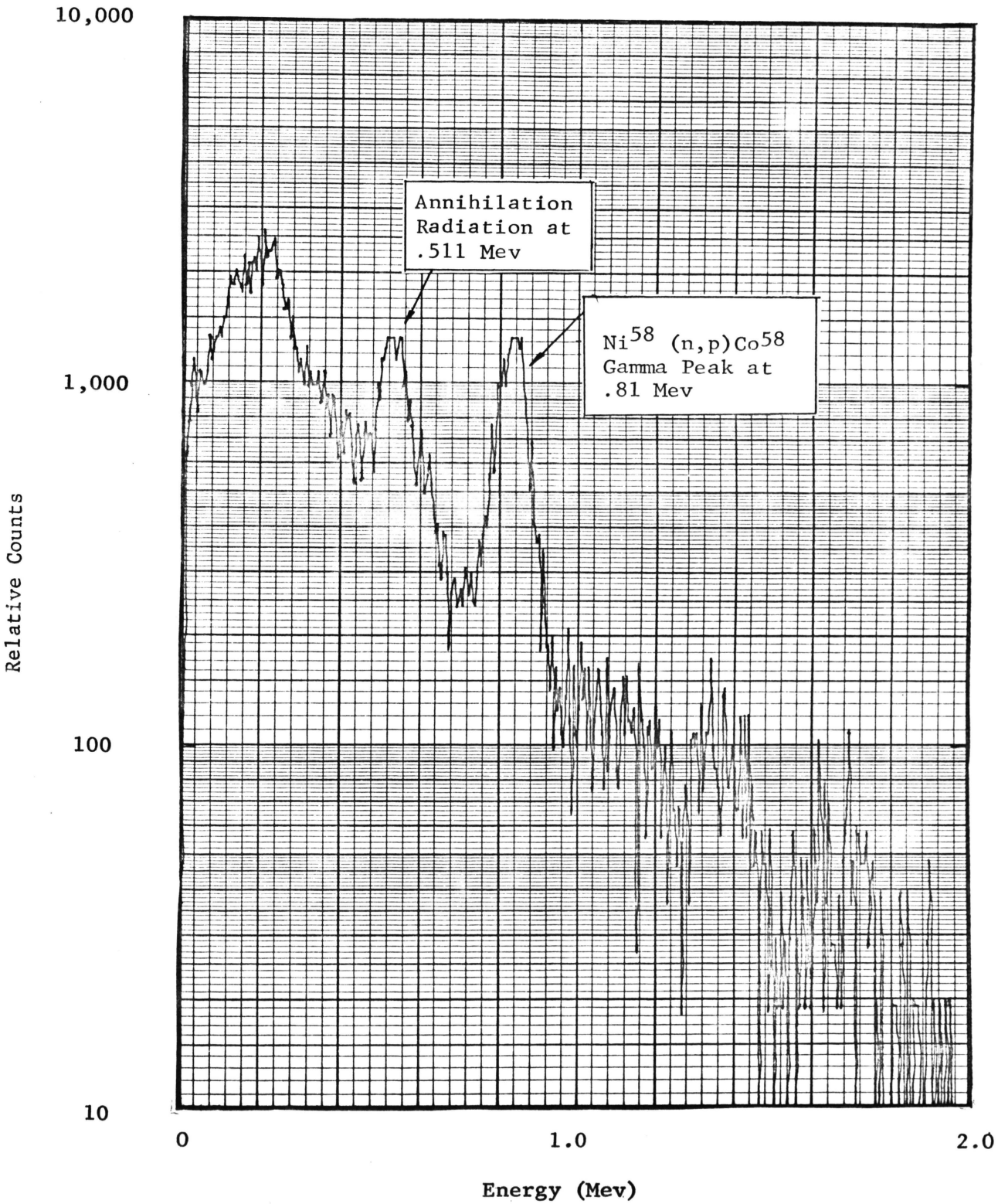

Figure B.10 Nickel Gamma Spectrum 60.4 hours after Irradiation
Relative Counts versus Energy

B.1.7 Phosphorus - P

Naturally Occurring Isotopes: P^{31} - 100%

Nuclear Reactions:

Reaction	γ Peak Mev	Reaction Energy	Half Life	Cross Section
$P^{31}(n,p)Si^{317}$	1.26	E_t = 2.4	2.6 h	130 mb
$P^{31}(n,\alpha)P^{32}$	1.49	———	14.3 d	———

Form: Homogenous Powder

Purity: Reagent Phosphorus

Vendor: Cerac Corporation

Irradiation Results:

The phosphorus gamma spectra is dominated by the Bremstrahlung as shown in Figure B.10. A weak gamma photopeak (small in magnitude to Bremstrahlung) may be detected 1.26 Mev. The phosphorus threshold reaction is at 2.42 Mev.

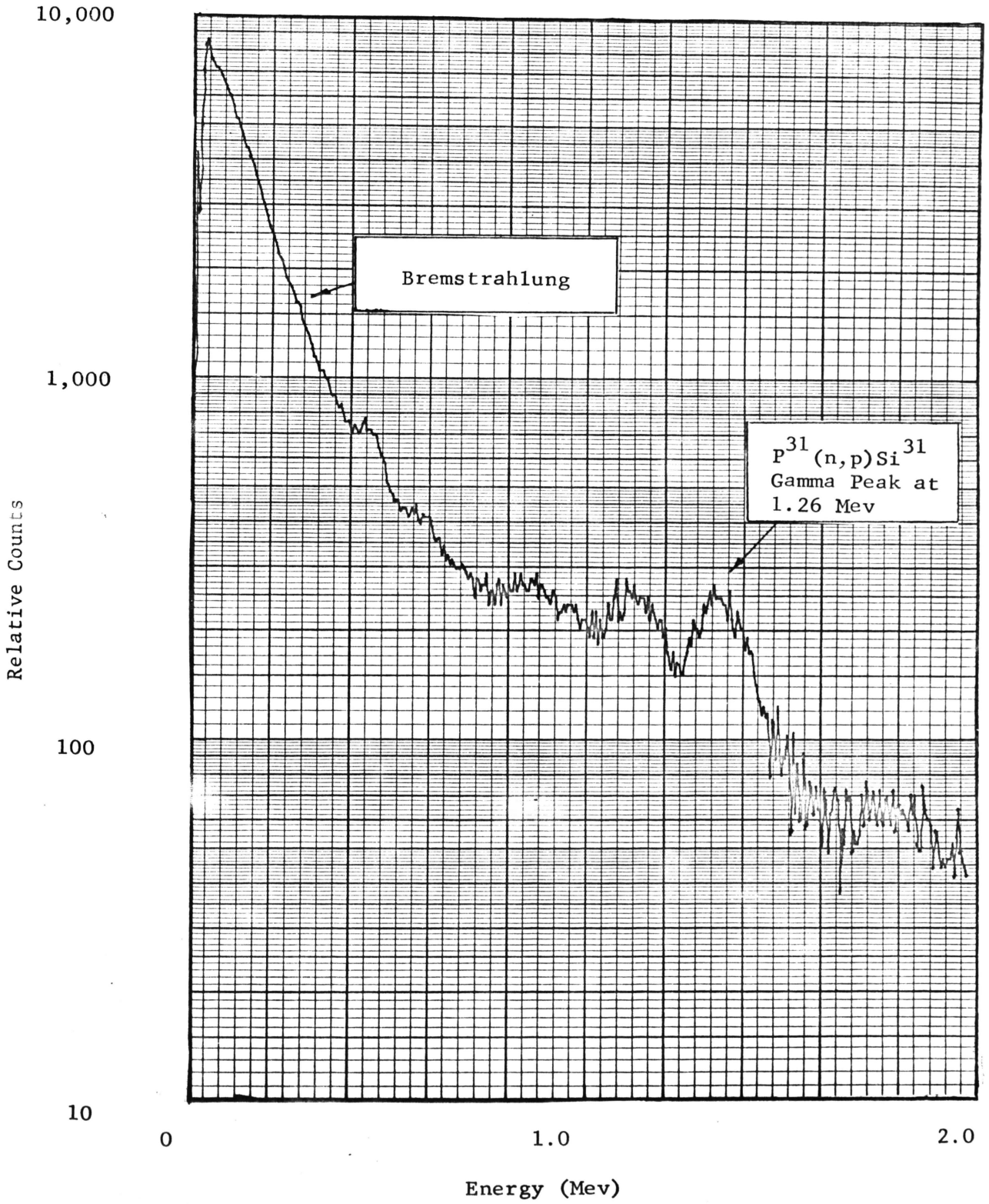

Figure B.11 Phosphorus Gamma Spectrum 119 minutes after Irradiation
Relative Counts versus Energy

B.1.8 Silver - Ag

Naturally Occurring Isotopes: Ag^{107} - 51.82%
Ag^{109} - 48.18%

Nuclear Reactions:

Reaction	γ Peak Mev	Reaction Energy	Half Life	Cross Section
$Ag^{107}(n,\gamma)Ag^{108}$	.63	Thermal	2.3 m	———
$Ag^{107}(n,2n)Ag^{106}$	.51	E_t = 9.6 Mev	24.3 m	42 mb
$Ag^{109}(n,\gamma)Ag^{110}$	.66,.88	Thermal	253 d	
$Ag^{109}(n,\gamma)Ag^{110}$	.66	E_r = 5.12 ev	24 s	7.600 b
$Ag^{109}(n,p)Pd^{109}$	.022	E_t = 0.4 Mev	13.6 h	2 mb

Form: 1/2 circular metallic disks x .005" thick

Purity: 99.97%

Vendor: Reactor Experiments Inc.

Irradiation Results:

The silver gamma spectra is displayed in Figure B.10. The Ag^{110} activity dominates the other silver reactions. The $Ag^{107}(n,2n)$ reaction may be determined due to its short half life. The long half life (253 days) of the Ag^{109} thermal reaction may be subtracted by allowing 6 hours for the Ag^{106} decay. The weak $Ag^{109}(n,p)Pd^{109}$ X-ray could not be determined 3 hours after irradiation.

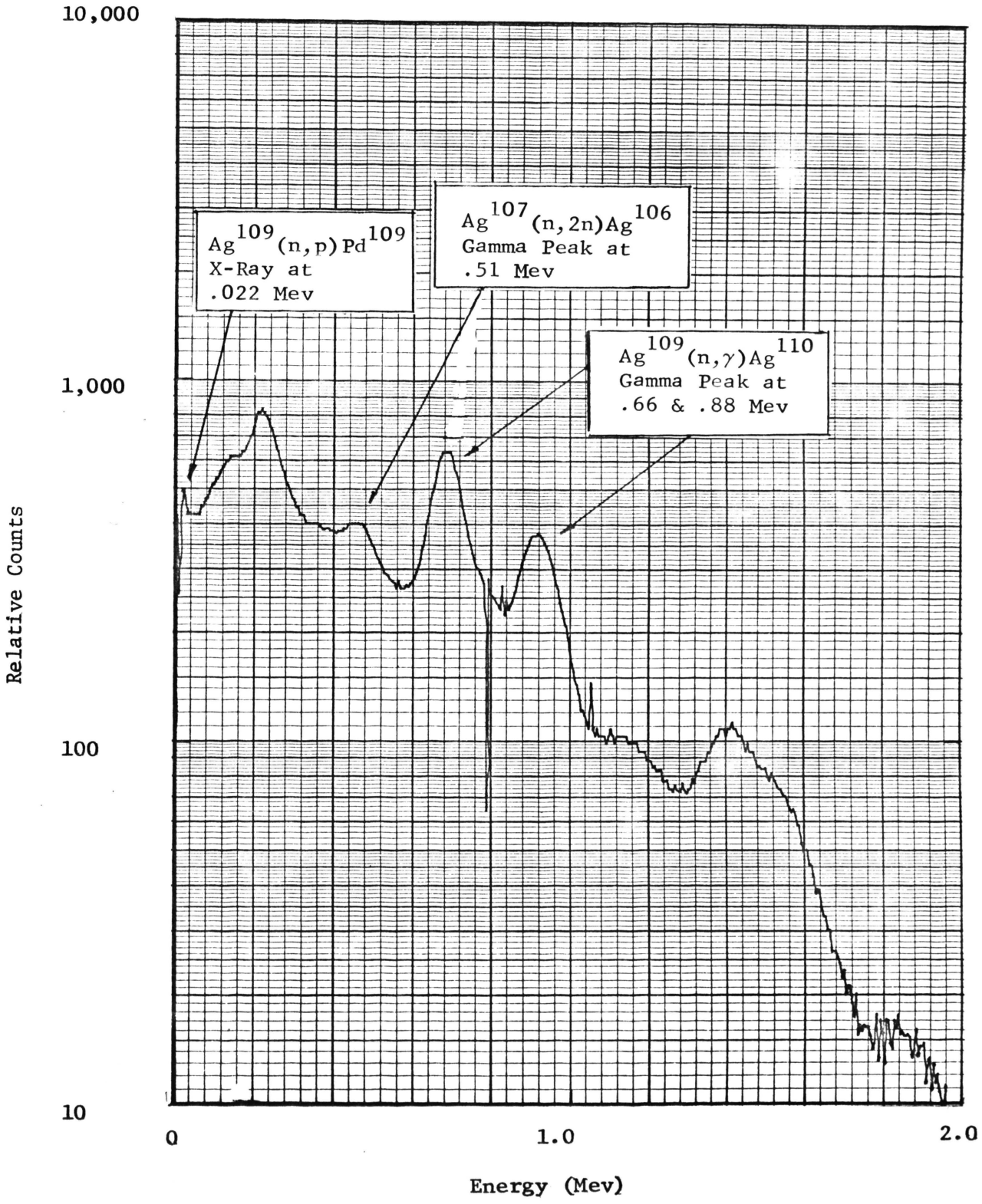

Figure B.12 Silver Gamma Spectrum 3.05 hours after Irradiation Relative Counts versus Energy

B.1.9 Zinc - Zn

Naturally Occurring Isotopes: Zn^{64} - 48.89%
Zn^{66} - 27.81%
Zn^{67} - 4.11%
Zn^{68} - 18.57%
Zn^{70} - 0.62%

Nuclear Reactions:

Reaction	γ Peak Mev	Reaction Energy	Half Life	Cross Section
$Zn^{64}(n\ p)Cu^{64}$	1.34	4.7	12.9 h	90 mb
$Zn^{64}(n,2n)Zn^{63}$	.67,.81,.97	10.4	38 min	500 mb
$Zn^{67}(n,p)Cu^{67}$	.090,.182	4.7	61 h	———
$Zn^{66}(n,p)Cu^{66}$	.83,1.04	——	5.1 min	———
$Zn^{68}(n,\alpha)Ni^{65}$	.37,1.11,1.48	10.0	2.56 h	7 mb
$Zn^{68}(n,\gamma)Zn^{69m}$	.44 (IT)	——	14.0 h	———

Form: 1/2" circular metallic disks x 1/16" thick

Purity: 99.97%

Vendor: University of Missouri at Rolla, Metallurgy Department

Irradiation Results:

The 38 minute Zn^{63} and 5 minute Cu^{66} must be allowed to decay before detecting the Cu^{64} reaction. The overlapping photopeak of the Zn^{65} annihilation radiation at .51 Mev and Zn^{65m} radiation at .438 Mev are clearly shown in Figure 3.12.

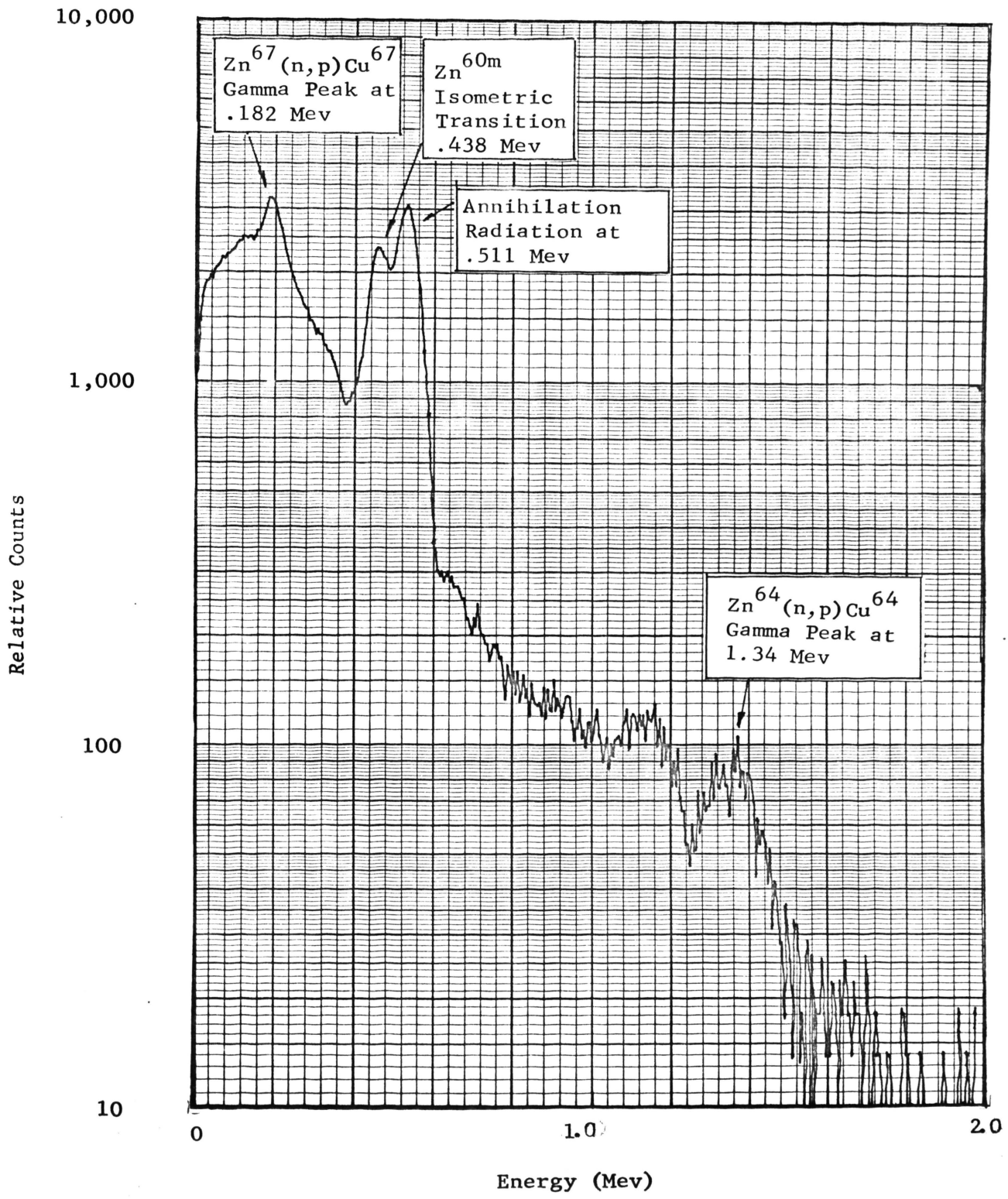

Figure B.13 Zinc Gamma Spectrum 3.56 hours after Irradiation Relative Counts versus Energy

APPENDIX B.2

CROSS-SECTION ELEMENT DATA

A thorough literature search was performed to obtain cross-sections of the desired reactions in the range of 0 to 15 Mev. The resulting data is shown in Figure B.14 and B.15. Note the value of the In^{115m} reaction was extrapolated to form 5.5 Mev to zero at 10 Mev. In some cases the data used was a composite of different sources (10, 13, 25).

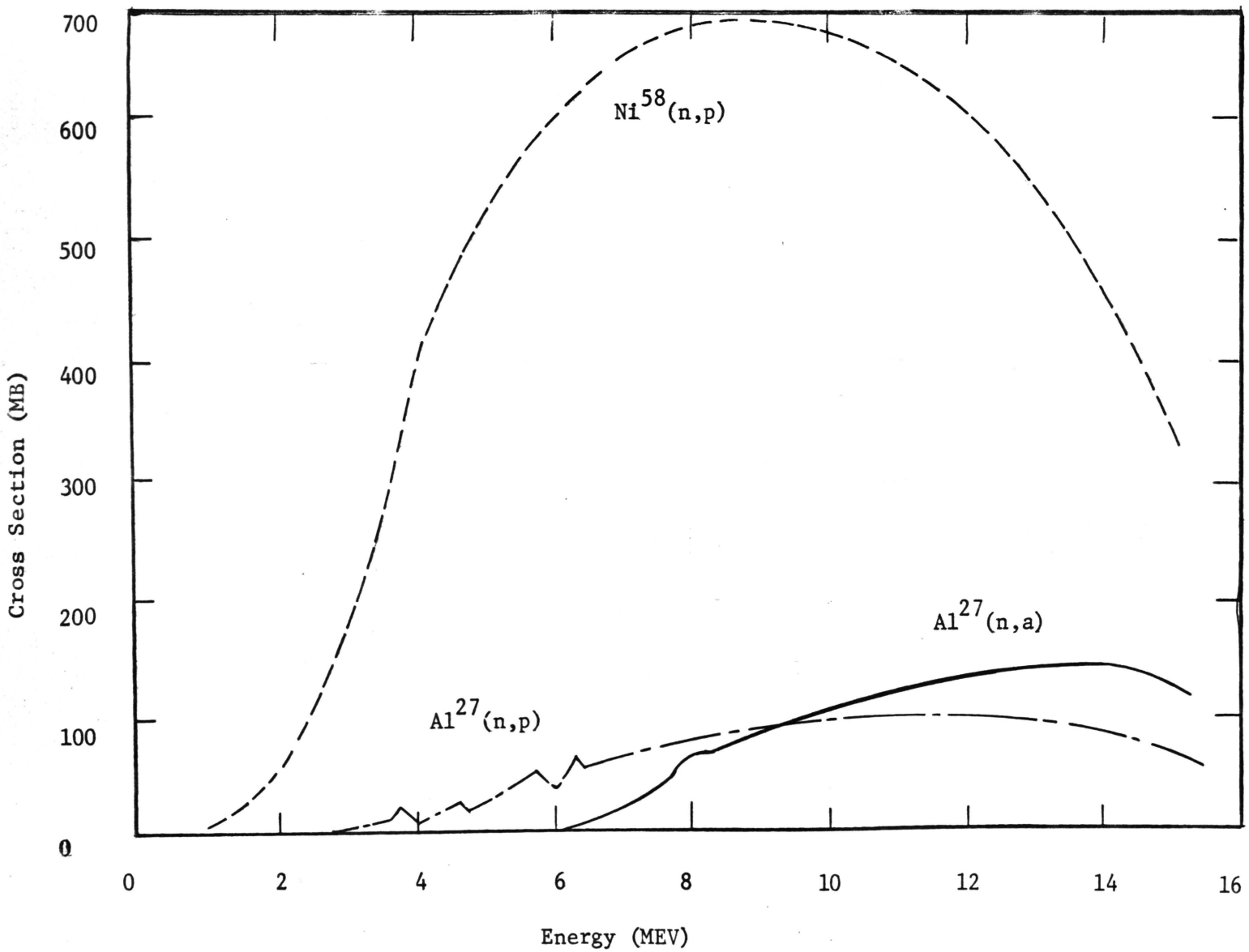

Figure B. 14 Threshold Cross Section vs Energy
$Ni^{58}(n,p)$; $Al^{27}(n,p)$; $Al^{27}(n,a)$

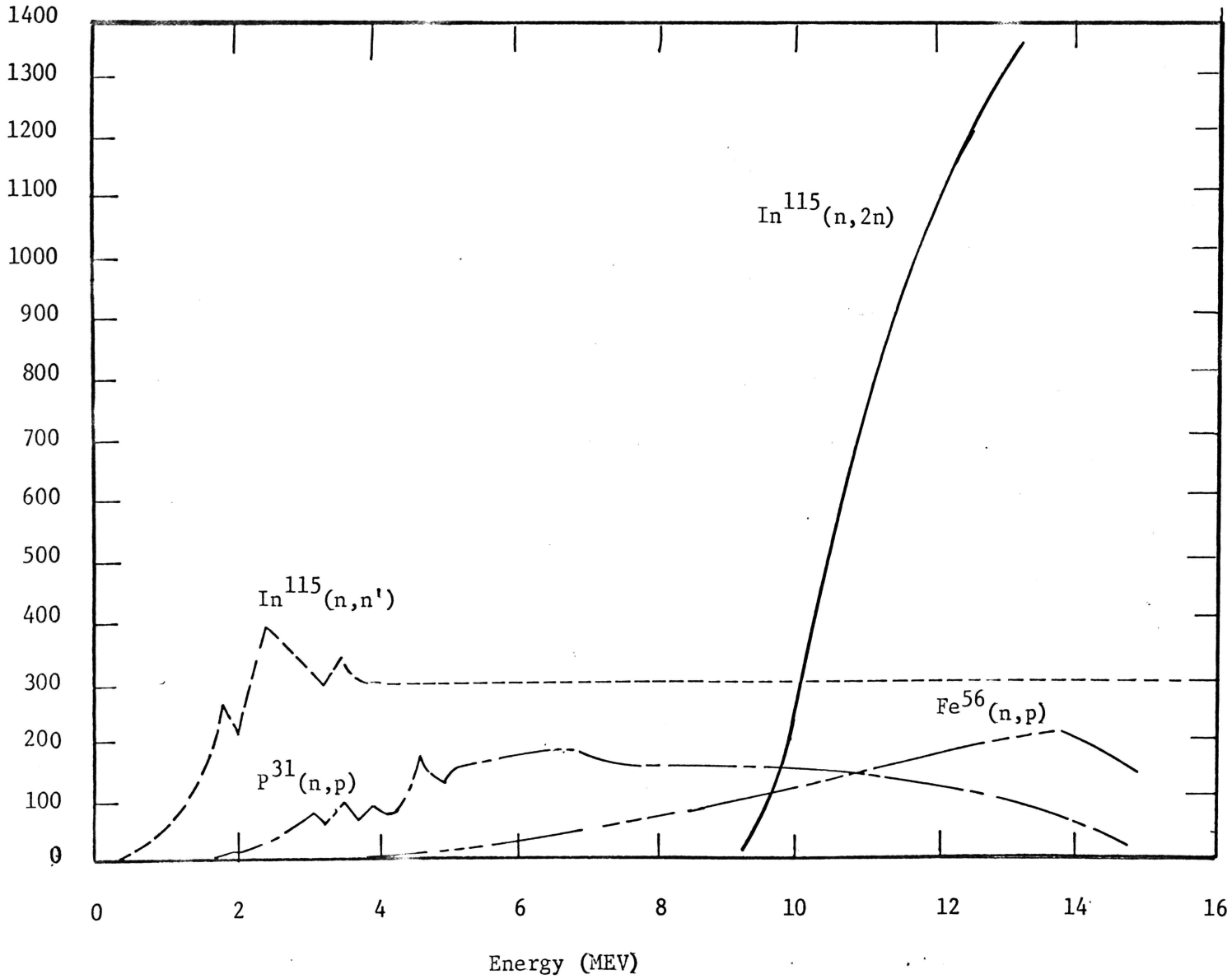

Figure B. 15 Threshold Cross Section vs Energy
$In^{115}(n,2n)$; $In^{115}(n,n')$; $P^{31}(n,p)$; $Fe^{56}(n,p)$

Table B.1

Multi-Threshold Foil Data

Material	Form	Fabrication	Vendor
Alcoa 2509	1/2" circular metallic disk x 1/16" thick	machined to rod and cut-off	Aluminum Company of America
CDA Alloy 735	1/2" circular metallic disk x .010" thick	stamped from sheet	Waterbury Rolling Mills, Inc.
IncoSIL-10	1/2" circular metallic disk x .010" thick	stamped from sheet	Western Gold and Platinum Works
Incoro-60	1/2" circular metallic disk x .010" thick	stamped from sheet	Western Gold and Platinum Works
In-P-Fe	1" circular powder disk x 1/8" thick	pressed into disks	Cerac, Incorporated

APPENDIX C

COMPUTER CODES AND ORTHONORMALIZATION OF FUNCTIONS

A listing of the least-squares method of gamma spectra analysts (PPA) appears in Section C.1. This program was modified by Dr. D. R. Edwards for use on the IBM 1620 Model II computer from a photopeak analysis program by H. M. Murphy, Jr.

The orthonormalization of the flux function is presented in Appendix C.2 with the computer program listed for the weighted orthonormal method of flux calculation. The program, FUSE-3, originally written by R. A. Rydin, was altered for use on an IBM 1620 Model II computer by K. L. Cage.

C.1 PPA Computer Code

The gamma spectrum of each multi-threshold foil was analyzed using a modified version of the computer program PPA (Photo Peak Analysis). This program was developed by H. M. Murphy, Jr. for photopeak analysis of pulse-height gamma-ray scintillation spectra. As many as five photopeaks can be fitted by PPA in any given experimental spectrum with the following results: 1) the exact channel location of the photopeak; 2) the width of the photopeak; 3) the peak count rate; 4) the integrated photopeak count rate; and 5) the integrated photopeak count rate corrected for radioactive decay to "zero-time". A listing of this program follows.

```
*LIST PRINTER
*ALL STATEMENT MAP
C      PPA,(PHOTOPEAK ANALYSIS), AN EXPERIMENTAL ROUTINE WRITTEN TO FIT
C      A GAUSSIAN FUNCTION TO SELECTED PHOTOPEAKS IN A SCINTILLATION
C      PULSE HEIGHT SPECTRUM AND TO REPORT THE RESULTS OF THE FIT IN
C      TERMS THAT ARE FAMILIAR TO THE GAMMA RAY SPECTROSCOPIST.
C
C      AFWL-TR-65-111
C
       DIMENSION BK(400),Y(400),PK(5),HOBB(15),HOBT(15),HOBX(15),HZB(4),
      2HNB(4)
C
       HZB(1)=0.69455956
       HZB(2)=0.00424143
       HZB(3)=0.52475956
       HZB(4)=0.64554400
       HNB(1)=0.55660042
       HNB(2)=0.41435247
       HNB(3)=0.59566455
       HNB(4)=0.44000000
       INDEX=1
       JNDEX=1
C
C      *RELOAD AND START.
C
     1 READ 54,NC
       IF(NC)45,45,2
     2 IF(NC-401)3,45,45
C
C      *ZEROB
C
     3 DO 4 I=1,NC
     4 BK(I)=0
       DO 904 I=1,4
   904 HOBB(I)=HZB(I)
       DO 5 I=5,15
     5 HOBB(I)=0
       KBF=0
C
C      READ INPUT DATA.
C
     6 READ 55,HOBX
       J=JTEST(HOBX(1),JNDEX)
       GO TO (7,37,41,43,3,1,46),J
C
C      READ UNKNOWN SPECTRUM.
C
     7 READ 56,TX,TZ,T12,PK
       READ 57, (Y(I),I=1,NC)
       J=1
       CT=Y(1)/100.
       IF(CT)8,9,9
     8 CT=1.
     9 IF(KBF)10,13,10
    10 DO 12 I=1,NC
```

```
      Y(I)=(Y(I)/CT)-BK(I)
      IF(Y(I))11,12,12
   11 Y(I)=0
   12 CONTINUE
      GO TO 15
   13 DO 14 I=1,NC
   14 Y(I)=Y(I)/CT
   15 DT=TX-TZ
      IF(T12)16,16,17
   16 CF=1.
      GO TO 21
   17 IF(DT)18,16,19
   18 DT=-DT
   19 CFXP=0.6931471 8*DT/T12
      IF(CFPX-88.)20,16,16
   20 CF=EXPF(-CFXP)
C
C     FIT UNKNOWN SPECTRUM AT P(K).
C
   21 PRINT 58,HOBX
      PRINT 59,HOBB
      PRINT 60,TX,TZ,DT,CF,T12
      PRINT 61,CT
      PRINT 62,PK(J)
      IB=0.90*PK(J)
      IT=(1.10*PK(J))+0.5
      IF(5-IB)23,23,22
   22 IB=5
   23 IF(IT-NC)25,25,24
   24 IT=NC
   25 D=PEACH(Y,IB,IT,NC,INDEX)
      IF(D)47,47,26
   26 PRINT 63,D
      DDD=D
C
      CALL DREPK(Y,NC,A,B,C,D,E)
C
      IF(C)48,48,27
27    SIGMA=SQRTF(-1./(E+E))
      TOTX=2.506628*SIGMA*C
      TOTZ=TOTX/CF
      RES=235.02*SIGMA/D
      PRINT 65,C,D
      PRINT 66,SIGMA,RES
      PRINT 67,TOTX,TOTZ
      PRINT 68
      IB=D-3.*SIGMA
      IF(IB)28,28,29
   28 IB=1
   29 IT=(D+3.*SIGMA)+0.5
      IF(IT-NC)31,31,30
   30 IT=NC
   31 SY=0
```

```
      SG=0
C
C     COMPARE RESULTS OF FIT WITH ORIGINAL DATA.
C
      DO 34 I=IB,IT
      X=I
      DIX=D-X
      YG=C*EXPF(E*DIX*DIX)
      YF=A+B*X+YG
      SY=SY+Y(I)
      SG=SG+YG
      IF(KBF)32,32,33
   32 TBK=0
      GO TO 34
   33 TBK=BK(I)
   34 PRINT 69,I,TBK,Y(I),YF,YG,SY,SG
   35 J=J+1
      IF(J-6)36,6,6
   36 IF(PK(J))6,6,21
C
C     *BACKG
C
   37 READ 55,HOBB
      READ 57, (BK(I),I=1,NC)
      CT=BK(1)/100.
      IF(CT)38,38,39
   38 CT=1.
   39 DO 40 I=1,NC
   40 BK(I)=BK(I)/CT
      KBF=1
      GO TO 6
C
C     *NOBAC
C
   41 KBF=0
      DO 42 I=1,15
      HOBT(I)=HOBB(I)
   42 HOBB(I)=0.
      DO 942 I=1,4
  942 HOBB(I)=HNB(I)
      GO TO 6
C
C     *RECAL
C
   43 KBF=1
      DO 44 I=1,15
   44 HOBB(I)=HOBT(I)
      GO TO 6
C
C     ERROR DIAGNOSTICS.
C
   45 PRINT 70,NC
   46 PRINT 72
```

```
      CALL EXIT
C
C     PROGRAM EXIT.
C
C
C     NO PEAK COMMENT.
C
   47 PRINT 64,PK(J)
      GO TO 35
C
C     LIST INPUT DATA ON WHICH GAUSS FAILED TO CONVERGE.
C
   48 PRINT 73
      IB=0.85*DDD
      IT=1.15*DDD+0.5
      IF(IB)49,49,50
   49 IB=1
   50 IF(IT-NC)52,52,51
   51 IT=NC
   52 DO 53 I=IB,IT
   53 PRINT 69,I,BK(I),Y(I)
      GO TO 35
C
C                    =====    FORMATS    =====
C
   54 FORMAT (I3)
   55 FORMAT (15A4)
   56 FORMAT (8E10.4)
   57 FORMAT (10F8.0)
   58 FORMAT (9H1      PPA 2X 15A4/1X)
   59 FORMAT (11X 15A4/1X)
   60 FORMAT (6X 4HTX = F10.4 3X 4HTZ = F10.4 3X 4HDT = F9.4/6X 18HTHE D
     2ECAY FACTOR = F13.8 3X 6HT1/2 = F9.3 6H DAYS.)
   61 FORMAT (6X 17HTHE COUNT TIME IS F7.2 9H MINUTES.)
   62 FORMAT (6X 31HTHE PEAK IS EXPECTED IN CHANNEL F7.2 1H./31H0      ST
     2ART PHOTOPEAK ANALYSIS./1X)
   63 FORMAT (6X 35HTHE PEAK APPEARS TO BE NEAR CHANNEL F7.2 1H.)
   64 FORMAT (33H0      NO PEAK EXISTS NEAR CHANNEL F7.2 1H.)
   65 FORMAT (27H0      THE PEAK AMPLITUDE IS F8.2 18H CPM/CH AT CHANNEL
     2F7.2 1H.)
   66 FORMAT (6X 25HTHE STANDARD DEVIATION IS F6.2 12H CHANNELS, ( F6.2
     215H PERCENT FWHM).)
   67 FORMAT (6X 27HTHE PHOTOPEAK COUNT-RATE IS F9.2 29H CPM AT TX, WHIC
     2H CORRESPONDS/6X 18HTO A COUNT-RATE OF   E11.4 11H CPM AT TZ.)
   68 FORMAT (9H0        I 6X 4HB(I) 6X 4HY(I) 7X 3HFIT 5X 5HGAUSS 6X 4HS
     2UMY 8X 2HSG/1X)
   69 FORMAT (5X I4 4F10.2 2F10.1)
   70 FORMAT (42H1      THE NUMBER OF CHANNELS IS INCORRECT./6X 4HNC = I4
     2/1H0)
   71 FORMAT (20H0      END FILE READ./1X)
   72 FORMAT (25H0      END OF COMPUTATION./1H1)
   73 FORMAT (9H0        I 6X 4HB(I) 6X 4HY(I)/1X)
      END
```

PPA PHOTOPEAKS ARE ANALYZED AT 169, 202, AND 274.

TEST OF PPA WITH ALCOA 2509

TX = 0.0000 TZ = 0.0000 DT = 0.0000
THE DECAY FACTOR = 1.00000000 T1/2 = 0.000 DAYS.
THE COUNT TIME IS 100.00 MINUTES.
THE PEAK IS EXPECTED IN CHANNEL 169.00.

START PHOTOPEAK ANALYSIS.

THE PEAK APPEARS TO BE NEAR CHANNEL 170.53.
5 ITERATIONS.

THE PEAK AMPLITUDE IS 72.63 CPM/CH AT CHANNEL 170.32.
THE STANDARD DEVIATION IS 6.86 CHANNELS, (9.47 PERCENT FWHM).
THE PHOTOPEAK COUNT-RATE IS 1250.68 CPM AT TX, WHICH CORRESPONDS TO A COUNT-RATE OF 1.2506E+03 CPM AT TZ.

I	B(I)	Y(I)	FIT	GAUSS	SUMY	SG
149	8.90	7.71	14.29	.58	7.7	.5
150	8.30	8.97	14.29	.91	16.6	1.5
151	8.20	9.69	14.43	1.39	26.3	2.8
152	9.00	9.93	14.78	2.07	36.3	4.9
153	8.60	11.78	15.40	3.02	48.0	7.9
154	9.30	12.52	16.36	4.31	60.6	12.3
155	8.00	15.30	17.75	6.03	75.9	18.3
156	7.90	18.65	19.64	8.26	94.5	26.6
157	7.70	21.07	22.12	11.08	115.6	37.6
158	6.60	26.79	25.25	14.54	142.4	52.2
159	7.40	28.92	29.06	18.68	171.3	70.9
160	7.80	32.58	33.54	23.49	203.9	94.4
161	6.90	40.29	38.65	28.93	244.2	123.3
162	8.20	43.35	44.26	34.87	287.5	158.2
163	8.30	50.06	50.22	41.16	337.6	199.3
164	7.60	56.29	56.29	47.56	393.9	246.9
165	8.40	62.08	62.20	53.81	455.9	300.7
166	9.10	66.63	67.65	59.60	522.6	360.3
167	6.70	74.09	72.35	64.63	596.7	425.0
168	8.60	77.74	76.00	68.61	674.4	493.6
169	10.10	76.80	78.36	71.31	751.2	564.9
170	10.80	77.69	79.28	72.56	828.9	637.4
171	9.10	77.97	78.67	72.28	906.9	709.7
172	9.50	77.52	76.56	70.49	984.4	780.2
173	9.80	73.16	73.04	67.31	1057.5	847.5
174	8.60	69.63	68.32	62.92	1127.2	910.5
175	9.30	62.69	62.65	57.59	1189.9	968.1
176	8.80	56.40	56.33	51.60	1246.3	1019.7
177	8.70	48.72	49.66	45.27	1295.0	1064.9
178	7.70	43.42	42.94	38.87	1338.4	1103.8
179	7.80	36.13	36.42	32.69	1374.5	1136.5
180	6.70	30.65	30.31	26.91	1405.2	1163.4
181	7.20	23.09	24.75	21.68	1428.3	1185.1
182	5.50	20.70	19.84	17.11	1449.0	1202.2

183	5.70	15.54	15.62	13.21	1464.5	1215.4
184	5.20	13.27	12.06	9.99	1477.8	1225.4
185	6.70	8.42	9.14	7.40	1486.2	1232.8
186	4.10	8.66	6.77	5.36	1494.9	1238.2
187	5.00	6.94	4.88	3.80	1501.8	1242.0
188	3.70	8.11	3.38	2.64	1509.9	1244.7
189	5.30	5.82	2.20	1.79	1515.7	1246.5
190	4.20	6.79	1.27	1.19	1522.5	1247.7
191	5.10	6.81	.52	.78	1529.3	1248.4

```
*LIST PRINTER
*ALL STATEMENT MAP
C       PPA CORRECTION FACTORS,WEIGHT,IRRADIATION  AND WAIT TIME,
C       ISOTOPE PERCENTAGE, DECAY SCHEME
C       ACTIVATION STANDARDIZATION - K.L.C.
        DIMENSION A(25),AB(25),ACD(25),WT(20),C1(25),C2(25),C3(25),C4(25)
        DIMENSION T1(25),T2(25),T3(25),T12(25),C5(25),C6(25),C7(25)
        DIMENSION FOIL(25)
        MAX=6
      1 READ 9,(FOIL(I),I=1,MAX)
        READ 10,(A(I),I=1,MAX),(WT(I),I=1,MAX),(T2(I),I=1,MAX),
       1(T1(I),I=1,MAX),(T12(I),I=1,MAX),(C4(I),I=1,MAX),(C5(I),I=1,MAX),
       2(C6(I),I=1,MAX)
        PRINT 200
        DO 100 I=1,MAX
        Y=.6931/T12(I)
        C1(I)=(1.0-EXPF(-Y*T1(I)))
        C2(I)=EXPF(-Y*T2(I))
        C3(I)=1.
        AB(I)=A(I)/(WT(I)*C1(I)*C2(I)*C3(I)*C4(I)*C5(I)*C6(I))
  100   PRINT 500,FOIL(I),AB(I)
    9   FORMAT (36A2)
   10   FORMAT(4E18.2)
  200   FORMAT (//6X,12H FOIL NUMBER,15X,19H SATURATED ACTIVITY//)
  500   FORMAT(6XA2,19X,E16.8)
        GO TO 1
  600   CONTINUE
        CALL EXIT
        END
```

FOIL NUMBER	SATURATED ACTIVITY
I	.11456584E+09
P	
F	.55775102E+07
N	.15282557E+09
A	.25435883E+07
A	

FOIL NUMBER	SATURATED ACTIVITY
I	.23506583E+09
P	
F	
N	
A	.52374719E+06
A	

APPENDIX C.2

ORTHONORMALIZATION OF THE FLUX FUNCTION

The flux is assumed to be given as a weighting function times an expansion of known functions of energy which are required to form an orthonormal set. As many coefficients are used in the expansions as there are threshold elements in the multi-threshold foil.

The flux spectrum

$$\phi(E) = W(E) \sum_{i=1}^{n} B_i \psi_i (E) \frac{\text{neutrons}}{\text{cm}^2\text{- sec}} \text{ - Mev} \qquad \text{C.2.1}$$

where ψ_i is a linear combination of coefficients and cross section data, $0 < E < \infty$, and have the property

$$\int_0^{E_{max}} \psi_i(E)\ \psi_j(E)\ W(E)\ dE = \delta_{ij} = \begin{cases} 1 \text{ when } i = j \\ 0 \text{ when } i \neq j \end{cases} \qquad \text{C.2.2}$$

where E_{max} corresponds to 15 Mev

$$\psi_n(E) = \sum_{i=1}^{n} An_i\ \sigma_i (E) \qquad \text{C.2.3}$$

Expanding the function

$$\psi_1 (E) = A_{11}\ \sigma_1 (E) \qquad n = 1$$

$$\psi_2 (E) = A_{21}\ \sigma_1 (E) + A_{22}\ \sigma_2 (E) \qquad n = 2$$

$$\psi_3 (E) = A_{31}\ \sigma_1 (E) + A_{32}\ \sigma_2 (E) + A_{33}\ \sigma_3 (E) \qquad n = 3$$

$$\psi_4 (E) = A_{41}\ \sigma_1 (E) + A_{42}\ \sigma_2 (E) + A_{43}\ \sigma_3 (E) + A_{44}\ \sigma_4 (E) \qquad n = 4$$

Rewriting in matrix form

$$[\psi] = [A]\,[\sigma] \qquad \text{C.2.4}$$

$$\begin{bmatrix} \psi_1(E) \\ \psi_2(E) \\ \psi_3(E) \\ \psi_4(E) \\ \\ \psi_n(E) \end{bmatrix} = \begin{bmatrix} A_{11} & 0 & 0 & 0 & \\ A_{21} & A_{22} & 0 & 0 & \\ A_{31} & A_{32} & A_{33} & 0 & \\ A_{41} & A_{42} & A_{43} & A_{44} & \\ & & & & \\ A_{n1} & & & & A_{nn} \end{bmatrix} \begin{bmatrix} \sigma_1(E) \\ \sigma_2(E) \\ \sigma_3(E) \\ \sigma_4(E) \\ \\ \sigma_n(E) \end{bmatrix}$$

Substituting Equations C.2.3 into Equation C.2.4 at

$i = j$ $(\psi_1(E) \cdot \psi_j(E) = 1)$

$n = 1,1$

$$A_{11}^2 \int_0^{E_{max}} \sigma_1^2(E)\, W(E)\, dE = 1 \qquad \text{C.2.4.1}$$

$n = 2,2$

$$A_{21}^2 \int_0^{E_{max}} \sigma_1^2(E)\, W(E)\, dE + 2A_{21} A_{22} \int_0^{E_{max}} \sigma_1(E)\ \sigma_2(E)\, W(E)\, dE + A_{22}^2 \int_0^{E_{max}} \sigma_2^2(E)\, W(E)\, dE = 1 \qquad \text{C.2.4.2}$$

$n = 3,3$

$$A_{31}^2 \int_0^{E_{max}} \sigma_1(E)\, W(E)\, dE + 2A_{31} A_{22} \int_0^{} \sigma_1(E)\ \sigma_2(E)\, W(E)\, dE + 2A_{31} A_{33} \int_0^{E_{max}} \sigma_1(E)\ \sigma_3(E)\, W(E)\, dE + 2A_{22} A_{33} \int_0^{E_{max}} \sigma_2(E)\ \sigma_3(E)\, W(E)\, dE + A_{22}^2 \int_0^{} \sigma_2^2(E)\, W(E)\, dE + A_{33}^2 \int_0^{E_{max}} \sigma_3^2\, W(E)\, dE = 1 \qquad \text{C.2.4.3}$$

At $i \neq j$ $(\psi_1(E) \cdot \phi_2(E) = 0)$

$n = 1,2$

$$A_{11} A_{21} \int_0^{E_{max}} \sigma_1^2(E)\, W(E)\, dE + A_{11} A_{22} \int_0^{E_{max}} \sigma_1(E)\, W(E)\, dE = 0 \qquad \text{C.2.4.4}$$

$$n = 2,3$$

$$A_{21}\,A_{31}\int_0^{E_{max}} \sigma_1^{\,2}(E)\,W(E)\,dE + A_{21}\,A_{32}\int_0^{E_{max}} \sigma_1(E)\,\sigma_2(E)\,W(E)$$
$$+ A_{21}\,A_{33}\int_0^{E_{max}} \sigma_1(E)\,\sigma_3(E)\,W(E)\,dE + A_{22}\,A_{31}\int_0^{E_{max}} \sigma_1(E)\,\sigma_2(E)\,W(E)\,dE$$
$$+ A_{22}\,A_{31}\int_0^{E_{max}} \sigma_2^{\,2}(E)\,W(E)\,dE + A_{22}\,A_{33}\int_0^{E_{max}} \sigma_2(E)\,\sigma_3(E)\,W(E)\,dE = \qquad \text{C.2.4.5}$$

$$n = 1,3$$

$$A_{11}\,A_{31}\int_0^{E_{max}} \sigma_1^{\,2}(E)\,W(E)\,dE + A_{11}\,A_{32}\int_0^{E_{max}} \sigma_1(E)\,\sigma_2(E)\,W(E)\,dE$$
$$+ A_{11}\,A_{13}\int_0^{E_{max}} \sigma_1(E)\,\sigma_2(E)\,W(E)\,dE = 0 \qquad \text{C.2.4.6}$$

Defining a new term

$$S_{ij} = S_{ji} = \int_0^{E_{max}} \sigma_i(E)\,\sigma_j(E)\,W(E)\,dE \qquad \text{C.2.5}$$

Substituting C.2.5 into the C.2.4 series where k is the highest order of i or j,

$k = 1$ $\quad A_{11}^{\,2}\,S_{11} = 1$ C.2.5

$k = 2$ $\quad A_{21}^{\,2}\,S_{11} + 2A_{21}\,A_{22}\,S_{12} + A_{22}^{\,2}\,S_{22} = 1$ C.2.6.2

$$A_{11}\,A_{21}\,S_{11} + A_{11}\,A_{22}\,S_{12} = 0 \qquad \text{C.2.6.3}$$

$k = 3$ $\quad A_{21}\,A_{31}\,S_{11} + A_{21}\,A_{32} + A_{21}\,A_{31}\,S_{13} = 0$ C.2.6.4

$$A_{21}\,A_{31}\,S_{11} + A_{21}\,A_{32} + A_{21}\,A_{33}\,S_{13}$$
$$+ A_{22}\,A_{31}\,S_{12} + A_{22}\,A_{32}\,S_{22} + A_{22}\,A_{33}\,S_{23} = 0 \qquad \text{C.2.6.5}$$

$$A_{31}^{\,2}\,S_{11} + A_{31}\,A_{32}\,S_{12} + A_{31}\,A_{33}\,S_{13}$$
$$+ A_{32}\,A_{31}\,S_{12} + A_{32}^{\,2}\,S_{22} + A_{32}\,A_{33}\,S_{23}$$
$$+ A_{33}\,A_{31}\,S_{13} + A_{33}\,A_{32}\,S_{23} + A_{33}^{\,2}\,S_{33} = 1 \qquad \text{C.2.6.6}$$

Rearranging, substituting, solving yields

$k = 1$ $\quad A_{11} = \left(\frac{1}{S_{11}}\right)^{1/2}$ C.2.7.1

$$k = 2 \qquad A_{21} = -A_{22} \frac{S_{12}}{S_{11}} \qquad \text{C.2.7.2}$$

$$A_{22} = \frac{1}{\left(\frac{S_{12}^2}{S_{11}} + S_{22}\right)^{1/2}} \qquad \text{C.2.7.3}$$

and so on.

It should be noted that each k set of Equations yields (k - 1) linear equations and 1 non-linear equation, and the number of terms greatly increases as k increases.

Factoring and simplifing the k = 3 equations

$$A_{31} S_{11} + A_{32} S_{12} + A_{33} S_{13} = 0 \qquad \text{C.2.8.1}$$

k - 1 Linear $A_{33}(A_{31} S_{12} + A_{32} S_{22} + A_{33} S_{23}) = 0$ C.2.8.2

Non-Linear $A_{31} S_{13} + A_{32} S_{23} + A_{33} S_{33} = 1$ C.2.8.3

Defining new coefficients

$$Cij = \sum_{k=1}^{i} Aik\ Skj \qquad \text{C.2.9}$$

Expanding the values for C's

At i = 1, j = 1 $C_{11} = A_{11} S_{11}$ C.2.10.1

At i = 1, j = 2 $C_{12} = A_{11} S_{12}$ C.2.10.2

At i = 1, j = 3 $C_{13} = A_{11} S_{13}$ C.2.10.3

At i = 1, j = 2 $C_{22} = A_{21} S_{12} + A_{22} S_{22}$ C.2.10.4

At i = 2, j = 3 $C_{23} = A_{21} S_{13} + A_{22} S_{23}$ C.2.10.5

At i = 2, j = 1 $C_{21} = A_{21} S_{11} + A_{22} S_{12} = 0$ C.2.10.6

At i = 3, j = 1 $C_{31} = A_{31} S_{11} + A_{32} S_{12} + A_{33} S_{13} = 0$ C.2.10.7

If we define

$$A'_{km} = \frac{A_{km}}{A_{kk}} \qquad \text{C.2.11}$$

The $k - 1$ linear equations of the k^{th} set may be put into the following form:

$$\begin{bmatrix} C_{11} & C_{12} & C_{1,\,k-1} \\ 0 & C_{22} & C_{2,\,k-1} \\ 0 & 0 & \\ & & \\ 0 & 0 & C_{K-1,\,k-1} \end{bmatrix} \begin{bmatrix} A'_{k,1} \\ A'_{k,2} \\ \\ \\ A'_{k,\,k-1} \end{bmatrix} = \begin{bmatrix} C_{1,k} \\ C_{2,k} \\ \\ \\ C_{k-1,\,k} \end{bmatrix} \qquad \text{C.2.12}$$

The [C] matrix is diagonal plus upper triangular and there can be algebraical solved for each A'_{km} term from the bottom up. The A'_{km} term can then be put into the equation for A_{kk} which is a generalization of the non-linear equation C.2.8.3.

$$A_{kk} = \left[\sum_{m=1}^{k-1} A'_{km}\, S_{mk} + S_{kk} \right]^{-1/2} \qquad \text{C.2.13}$$

and we obtain A_{km} from

$$A_{km} = \frac{A'_{km}}{A_{kk}} \qquad \text{C.2.14}$$

Using equation C.2.4 and solving for the cross section in terms of $[\psi]$ we have

$$[\sigma] = [A]^{-1}\,[\psi] \qquad \text{letting } [D] = [A]^{-1}$$

$$[\sigma] = [D]\,[\psi] \qquad \text{C.2.14}$$

The activation of the K^{th} foil may be written as

$$K_k = \int_0^{E_{max}} \sigma_k\,(E)\;\phi(E)\;dE \qquad \text{C.2.15}$$

Substituting in equations C.2.1 and C.2.14 into C.2.15 yields

$$K_k = \int_0^{E_{max}} \sum_{j=1}^{k} D_{kj}\ \psi_j\ (E) \quad W(E) \sum_{i=1}^{n} B_i\ \psi(E)\ dE \qquad C.2.16$$

Using the orthonormal relations, i - j and $\int_0^{E_{max}} W(E)\ \psi_1\ (E)\ \psi_j\ (E) = 1$ the equation simplifies to

$$K_k = \sum_{i=1}^{k} B\ D_{ki} \qquad C.2.16.1$$

In matrix form

$$[K] = [D]\ [B] \qquad C.2.16.2$$

We can solve for B_i using the experimentally determined values of K_k calculated by the computer program alpha

$$[B] = [D]^{-1}\ [K] \qquad C.2.16.3$$

Substituting

$$[B] = [A]\ [K]$$

Placing this result into equation C.2.1 and equation C.2.4, we obtain the result in general form

$$\phi(E) = W(E) \sum_{k=1}^{n} \sum_{i=1}^{n} A_{ki}\ K_i \sum_{j=1}^{n} A_{kj}\ \sigma_j\ (E) \qquad C.2.17$$

The result may be evaluated as we know the σ_j (E), measured the K_i, and calculated the spectrum.

C.2.1. Sample Problem Using Fuse-3

An example of a Fuse-3 fortran listing, a basic library of input cards and an example of the input-output calculation appears in this Appendix. The activation data and weighing function were taken from the ISPRA-1 Reactor.

Fuse-3: Weighted Orthonormal Method

The code Fuse-3 performs the Weighted Orthonormal Method calculation, which is described in Appendix C.2.

(a) It contains a library of cross-section curves in the range 0 to 15 Mev, for 5 threshold detectors. The foils are in two sets in the following sequence:

Set I $In^{115}(n,n')$ $Fe^{56}(n,p)$, $P^{31}(n,p)$

Set II $Ni^{56}(n,p)$ $Al^{27}(n,\alpha)$, $Al^{27}(n,p)$

(b) It allows the calculation to be done for any number of materials in the library set.

(c) It contains a smoothing feature which permits the calculation to be performed several times on the same set of data with statiscally deviated input values. It linearly averages the results to provide a smoothed flux curve.

(d) It calculates the expected activation for each material in the library for comparison to the input data.

A schematic flow diagram of the code Fuse-3 is shown in the Figure 5.2. The sequence of operations is the following:

(1) The subroutine INPUT reads in the cross-section data, control data, input activations, and weighting function.

(2) The weighted cross-section integrals (Eq. C.2.5) are computed by the subroutine CRSINT, using Simpson Integration subroutine AVGE.

(3) The appropriate number of orthonormal coefficients, Aij, corresponding to the materials used, are computed in ACALC, using the method outlined in Appendix C.2.

(4) The results of the above calculation are printed in OUTPUT.

(5) The differential spectrum is computed at each energy point by the subroutine FLUX, using a discretized form of the expression in Appendix C.2, Equation C.1.17.

(6) A loop is set up to recalculate the differential flux for an arbitrary number (0 to 5) of statistically deviated values of the input activations. Random numbers are produced in the library routine RANDNF and are used in STAT with an expression fit to the integral probability distribution, to calculate the deviated activations.

(7) The results of set of flux calculations are linearly averaged point by point, in FLUXAV. Justification for inclusion of this feature is that the experimental values are not expected to be exact and the calculation should reflect this fact.

(8) The expected activation of each material in the library and the integral flux above a given energy are computed in INTG, using the computed differential flux and the library of cross sections. The Simpson integration subroutine AVGE is used.

(9) The differential flux, integral flux, and expected activation are printed out in the subroutine TYPE. Differential flux values that are normalized are produced by interpolation using LININT.

(10) Control is returned to INPUT for additional sets of calculations.

The code is provided with a basic library of cards for each set and the dara are:

CARD 1, Format (214, E12.6)

MAXU - Number of foils in library, dimensioned (5), provided (3).

MAX - Number of equally spaced energy points in the library, dimensioned (61), provided (60).

WIDTH - Maximum energy corresponding to MAX, 15.0 Mev, used

CARD 2, Format (15I4)

NMIN - Energy point corresponding to first non-zero value for each cross section in the library, dimensioned (61), provided (60).

CARDS 3, etc. Format (12A6)

LABEL - Identification for each reaction in the library, dimensioned (5), provided (3).

CARDS 4, etc. Format (8E9.4)

SIGMA - Cross section data in millibarms, starting at energy point NMIN, dimensioned (5, 60), provided (5, 60).

The control cards for the remainder of the deck for the weighting function, activations etc., are:

CARD 1. Format (15I4)

NEW - Foil ordering parameter, > 0 read order, = 0 use same order as before.

NEWA - Activation data parameter, > 0 read activations, = 0 use previous activations

NMAX - Number of foils in set (5 MAX)

NST - Number of statistical deviations (5 MAX)

NIT - Provision for interation (Use 1)

NWY - Weighting function parameter, > 0 read weighting function < 0 use unit weights.

NOR - Orthonormal function check (Use 0, 1 for function check)

CARD 2, Format (15I4) (Used if NEW > 0)

IN - Foil order (See ordering sequence) dimensioned (15).

CARDS 3, etc. Format (8E9.4) (Used if NWY > 0)

W - Weighting function dimensioned (61), used (60), equally spaced points in the range 0 to 15 Mev.

CARDS 4, etc. Format (6E12.6) (Used if NEWA > 0)

ACT - Foil activation integral data, Ki, in order given by ordering sequency (Use blanks where foil is not used).

CARDS 5, etc. Format (6E12.6) (Used if NEWA > 0)

SIG - Estimated accuracy of activation values for foils given above in %.

```
*LIST PRINTER
*ALL STATEMENT MAP
C      FUSE-3 FITTING UNKOWN SPECTRA EXPERIMENTALLY K.L. CAGE
C      FUSE-3 CALCULATES FAST NEUTRON SPECTRUM FROM FOIL ACTIVATION DATA
C      FUSE-3 USES WIEGHTED ORTHONORMAL METHOD
C      THE DATA DECK CONTAINS THE FOLLOWING CROSS SECTIONS
C      1) NP-237 (N,F), 2) U-238(N,F), 3) S-32(N,P), 4) AL-27(N,P),
C      5) AL-27(N,A)
       DIMENSION PHIS(5,61),S(5,5),A(5,5),NMIN(5),IN(5),
      1LABEL(5),LABM(5),PHI(61),CR(5),SIGMA(5,61),ESIGMA(5,61),
      2ACT(5),CRD(5),W(61),F(61),X(61),SIG(5),ER(61),FLINT(61),
      3CALACT(5),T(5,5),CRSIG(5)
       COMMON PHIS,S,A,NMAX,MAX,MAXU,NST,NWY,NEW,NEWA,NIT,NOR,NMIN,IN,
      1LABEL,LABM,PHI,CR,SIGMA,ESIGMA,ACT,CRD,WIDTH,W,CRSIG,F,X,SIG,ER,
      2FLINT,CALAC,T
C      READ CONTROL INFORMATION
       RIT=0
   10  CALL INPUT(RIT)
       I=I+1
       DO 20 L=1,MAX
   20  F(L)=W(L)
       NI=NIT
C      CALCULATE CROSS SECTION INTEGRALS
   30  CALL CRSINT
C      CALCULATE COEFFICIENTS OF MATRIX
       CALL ACALC
C      PRINT COEFFICIENTS
       CALL OUTPUT(NI)
       DO 70 K=1,NST
C      STATISTICALLY  DEVIATE  ACTIVATIONS
       IF(NST-1)50,50,40
   40  CALL STAT(K,CRD,CR,CRSIG,NMAX)
C      CALCUALTE FLUXES AND AVERAGED FLUX
   50  CALL FLUX(K)
       IF(NST-K)60,60,70
   60  CALL FLUXAV
C      CALCULATE INTEGRAL FLUX,EXPECTED ACTIVATIONS
       CALL INTG
C      PRINT AND PLOT
       NI=1
       CALL TYPE(NI,I)
       NI=NI-1
       IF(NI)70,70,30
   70  CONTINUE
       RIT=0
       GO TO 10
       END
```

```
*LIST PRINTER
      SUBROUTINE INPUT(RIT)
      DIMENSION PHIS(5,61),S(5,5),A(5,5),NMIN(5),IN(5),
     1LABEL(5),LABM(5),PHI(61),CR(5),SIGMA(5,61),ESIGMA(5,61),
     2ACT(5),CRD(5),W(61),F(61),X(61),SIG(5),ER(61),FLINT(61),
     3CALACT(5),T(5,5),CRSIG(5),ACF(5)
      COMMON PHIS,S,A,NMAX,MAX,MAXU,NST,NWY,NEW,NEWA,NIT,NOR,NMIN,IN,
     1LABEL,LABM,PHI,CR,SIGMA,ESIGMA,ACT,CRD,WIDTH,W,CRSIG,F,X,SIG,ER,
     2FLINT,CALACT,T
    1 FORMAT(2I4,E12.6)
    2 FORMAT(18I4)
    3 FORMAT( 5A2)
    4 FORMAT(8E9.4)
    5 FORMAT(6E12.6)
      IF(RIT)30,10,30
C     READ CROSS SECTIONS
   10 READ 1,MAXU,MAX,WIDTH
      RIT=1.0
      READ 2,(NMIN(I),I=1,MAXU)
      READ 3,(LABEL(I),I=1,MAXU)
      DO 20 I=1,MAXU
      N=NMIN(I)
      JAB=N-1
      IF (JAB) 20,20,14
   14 DO 15 MNOP=1,JAB
   15 ESIGMA(I,MNOP)=0.
   20 READ 4,(ESIGMA(I,J),J=N,MAX)
C     READ CONTROL INFORMATION,FOIL ORDER,WEIGHTING FUNCTION
   30 READ 2,NEW,NEWA,NMAX,NST,NIT,NWY,NOR
      IF(NEW)50,50,40
   40 READ 2,(IN(I),I=1,NMAX)
   50 IF(NWY)70,90,60
C     READ WEIGHTING FUNCTION
   60 READ 4,(W(I),I=1,MAX)
      GO TO 90
   70 DO 80 I=1,MAX
   80 W(I)=1.0
   90 IF(NEWA)120,120,100
C     READ ACTIVATIONS
  100 READ 5,(ACT(J),J=1,MAXU)
C     ALPHA CORRECTION FACTOR
      READ 5,(ACF(J),J=1,MAXU)
      READ 5,(  SIG(J),J=1,MAXU)
      DO 110 J=1,MAXU
      ACT(J)=ACT(J)*ACF(J)
  110 SIG(J)=SIG(J)*ACT(J)*.01
  120 IF(NEW)130,130,140
  130 IF(NEWA)170,170,140
C     RECORDER DATA
  140 DO 160 I=1,NMAX
      ID=IN(I)
      DO 150 J=1,MAX
  150 SIGMA(I,J)=ESIGMA(ID,J)*1.0E-3
      LABM(I)=LABEL(ID)
      CRSIG(I)=SIG(ID)
```

```
     CR(I)=ACT(ID)
160  CRD(I)=ACT(ID)
170  RETURN
     END
```

```
*LIST PRINTER
      SUBROUTINE CRSINT
      DIMENSION PHIS(5,61),S(5,5),A(5,5),NMIN(5),IN(5),
     1LABEL(5),LABM(5),PHI(61),CR(5),SIGMA(5,61),ESIGMA(5,61),
     2ACT(5),CRD(5),W(61),F(61),X(61),SIG(5),ER(61),FLINT(61),
     3CALACT(5),T(5,5),CRSIG(5)
      COMMON PHIS,S,A,NMAX,MAX,MAXU,NST,NWY,NEW,NEWA,NIT,NOR,NMIN,IN,
     1LABEL,LABM,PHI,CR,SIGMA,ESIGMA,ACT,CRD,WIDTH,W,CRSIG,F,X,SIG,ER
     2FLINT,CALACT,T
C     CALCULATE CROSS SECTIONS INTEGRALS
      X(1)=0
      NPO=MAX+1
      DO 20 L=1,NMAX
      DO 20 M=1,L
      DO 10 I=1,MAX
   10 X(I+1)=SIGMA(L,I)*SIGMA(M,I)*F(I)
      CALL AVGE(X,XBAR,NPO)
      S(L,M)=XBAR*WIDTH
   20 S(M,L)=S(L,M)
      RETURN
      END
```

```
*LIST PRINTER
      SUBROUTINE ACALC
      DIMENSION S(5,5),A(5,5),C(5,5),PHIS(5,61)
      COMMON PHIS,S,A,NMAX
C     CALCUALTE FIRST THREE COEFFICIENTS
      DO 2 I=1,NMAX
      DO 2 J=1,NMAX
    2 A(I,J)=0.
      SJ=S(2,2)-S(1,2)*S(1,2)/S(1,1)
      A(1,1)=1.0/SQRTF(S(1,1))
      A(2,2)=1.0/SQRTF(SJ)
      A(2,1)=-A(2,2)*S(1,2)/S(1,1)
C     SET UP COMPUTATION OF OTHER,A,COEFFICIENTS
      NA=NMAX-1
      DO 60 I=2,NA
C     CALCULATE COEFFICIENTS,C,OF LINEAR MATRIX
      KA=I+1
      DO 10 N=1,KA
      DO 10 L=1,I
      SUM=0
      DO 10 M=1,L
      SUM=SUM+A(L,M)*S(M,N)
   10 C(L,N)=SUM
C     SET LOWER TRIANGULAR PART TO ZERO
      DO 20 L=2,I
      MA=L-1
      DO 20 N=1,MA
   20 C(L,N)=0
C     CALCULATE SCALED,A,COEFFICIENTS FROM THE BOTTOM UP
      A(KA,I)=-C(I,KA)/C(I,I)
      DO 40 J=2,I
      K=KA-J
      N=J-1
      SUM=-C(K,KA)
      DO 30 M=1,N
      KB=KA-M
   30 SUM=SUM-A(KA,KB)*C(K,KB)
   40 A(KA,K)=SUM/C(K,K)
C     SET UP NONLINEAR EQUATION AND SOLVE FOR DIAGONAL,A,TERM
      A(KA,KA)=1.0
      SUM=0
      DO 50 J=1,KA
   50 SUM=SUM+A(KA,J)*S(J,KA)
      IF(SUM)53,56,56
   53 SUM=-SUM
      PRINT 1,KA
    1 FORMAT(////25X12H ACALC ERROR,5XI2)
   56 A(KA,KA)=1.0/SQRTF(SUM)
C     SCALE,A,COEFFICIENTS FOR ANSWERS
      DO 60 J=1,I
   60 A(KA,J)=A(KA,J)*A(KA,KA)
      RETURN
      END
```

```
*LIST PRINTER
      SUBROUTINE AVGE(X,XBAR,NP)
      DIMENSION X(61),C(61)
C     SIMPSON INTEGRATION
   10 N=NP
      C(1)=1.
      C(N-1)=4.
      NM3=N-3
      DO 20 I=2,NM3,2
      C(I)=4.
   20 C(I+1)=2.
      C(N)=1.
   30 SUMN=0.
      SUMD=0.
      DO 40 I=1,N
      SUMN=SUMN+C(I)*X(I)
   40 SUMD=SUMD+C(I)
      XBAR=SUMN/SUMD
      RETURN
      END
```

```
*LIST PRINTER
      SUBROUTINE OUTPUT(NI)
      DIMENSION PHIS(5,61),S(5,5),A(5,5),NMIN(5),IN(5),
     1LABEL(5),LABM(5),PHI(61),CR(5),SIGMA(5,61),ESIGMA(5,61),
     2ACT(5),CRD(5),W(61),F(61),X(61),SIG(5),ER(61),FLINT(61),
     3CALACT(5),T(5,5),CRSIG(5)
      COMMON PHIS,S,A,NMAX,MAX,MAXU,NST,NWY,NEW,NEWA,NIT,NOR,NMIN,IN,
     1LABEL,LABM,PHI,CR,SIGMA,ESIGMA,ACT,CRD,WIDTH,W,CRSIG,F,X,SIG,ER,
     2FLINT,CALACT,T
    1 FORMAT(1H121X47H  FUSE-3  FITTING UNKOWN SPECTRA EXPERIMENTALLY//
     1/12X12H FOILS USED=I2,5X13H POINTS USED=I3,5X17H FOILS AVAILABLE=I
     22///30X20HMAXIMUM ENERGY(MEV)=F5.1)
    2 FORMAT (///38X14H FOIL ORDER(I)///22X5(I4,4X))
    3 FORMAT(21X5(A6,2X))
    4 FORMAT(1H138X10H ITERATIONI3)
    5 FORMAT(///23X38H WEIGHTED CROSS SECTION INTEGRALS(I,J)///(11X 5E12
     1.4/))
    6 FORMAT(///34X22H WEIGHTING FUNCTION(I)///(11X5E12.4/))
    7 FORMAT (///16X51H ORTHONORMAL COEFFICIENTS ((A(J,K),K=1,J),J=1,NMA
     1X)///(11X5E12.4/))
C      PRINT HEADING,CROSS SECTION INTEGRALS, WEIGHTING FUNCTION
C                    AND ORTHONORMAL COEFFICIENTS
      N=NIT-NI+1
      IF(NI-NIT)20,10,10
   10 PRINT 1,NMAX,MAX,MAXU,WIDTH
      PRINT 2,(IN(J),J=1,NMAX)
      PRINT 3,(LABM(J),J=1,NMAX)
      GO TO 30
   20 PRINT 4,N
   30 PRINT 5,((S(I,J),I=1,NMAX),J=1,NMAX)
      PRINT 6,(F(I),I=1,MAX)
      PRINT 7,((A(J,K),K=1,J),J=1,NMAX)
      RETURN
      END
```

```
*LIST PRINTER
      SUBROUTINE STAT(K,CRD,CR,CRSIG,NMAX)
      DIMENSION CRD(15),CR(15),CRSIG(15),A(200)
      IF(K-1)80,80,10
C     GENERATE RANDOM NUMBERS
   10 J=50
      DO 20 I=1,200
   20 A(I)=RANDNF(345.)
C     RANDOMLY DEVIATE ACTIVATIONS
      DO 70 I=1,NMAX
   30 DM=1.0
      DX=0
      IF(A(J)-0.5)40,40,50
   40 A(J)=1.0-A(J)
      DM=-1.0
   50 EX=0.61856322E1-0.1809236E2*A(J)-0.32870045E2*A(J)**2
     1+0.94119547E2*A(J)**3+0.99371956E2*A(J)**4-0.16113353E3*A(J)**5
     2-0.29833326E3*A(J)**6+0.39234567E3*A(J)**7-0.19193073E3*A(J)**8
     3+0.21389827E3*A(J)**9+0.35347469E3*A(J)**10-0.56288499E3*A(J)**11
     4-0.30324340E3*A(J)**12+0.76804136E3*A(J)**13-0.56425717E3*A(J)**14
      EY=+0.20819745E3*A(J)**15
      DX=EX+EY
      J=J+1
      IF(DX-2.0)60,60,30
   60 CR(I)=CRD(I)+CRSIG(I)*DM*DX
   70 CONTINUE
   80 RETURN
      END
```

```
*LIST PRINTER
      SUBROUTINE FLUX(J)
      DIMENSION DCR(5),DSIGMA(5)
      DIMENSION PHIS(5,61),S(5,5),A(5,5),NMIN(5),IN(5),
     1LABEL(5),LABM(5),PHI(61),CR(5),SIGMA(5,61),ESIGMA(5,61),
     2ACT(5),CRD(5),W(61),F(61),X(61),SIG(5),ER(61),FLINT(61),
     3CALACT(5),T(5,5),CRSIG(5)
      COMMON PHIS,S,A,NMAX,MAX,MAXU,NST,NWY,NEW,NEWA,NIT,NOR,NMIN,IN,
     1LABEL,LABM,PHI,CR,SIGMA,ESIGMA,ACT,CRD,WIDTH,W,CRSIG,F,X,SIG,ER,
     2FLINT,CALACT,T
C     CALCULATE FLUXES
      DO 30 M=1,MAX
      PHIS(J,M)=0.
      DO 20 K=1,NMAX
      DCR(K)=0.
      DSIGMA(K)=0.
      DO 10 I=1,NMAX
      DCR(K)=DCR(K)+A(K,I)*CR(I)
   10 DSIGMA(K)=DSIGMA(K)+A(K,I)*SIGMA(I,M)
   20 PHIS(J,M)=PHIS(J,M)+DCR(K)*DSIGMA(K)
   30 PHIS(J,M)=F(M)*PHIS(J,M)
      RETURN
      END
```

```
*LIST PRINTER
      SUBROUTINE FLUXAV
      DIMENSION PHIS(5,61),S(5,5),A(5,5),NMIN(5),IN(5),
     1LABEL(5),LABM(5),PHI(61),CR(5),SIGMA(5,61),ESIGMA(5,61),
     2ACT(5),CRD(5),W(61),F(61),X(61),SIG(5),ER(61),FLINT(61),
     3CALACT(5),T(5,5),CRSIG(5)
      COMMON PHIS,S,A,NMAX,MAX,MAXU,NST,NWY,NEW,NEWA,NIT,NOR,NMIN,IN,
     1LABEL,LABM,PHI,CR,SIGMA,ESIGMA,ACT,CRD,WIDTH,W,CRSIG,F,X,SIG,ER,
     2FLINT,CALACT,T
C     AVERAGE FLUXES POINT BY POINT
      DO 100 I=1,MAX
      IF(NST-1)70,70,10
   10 N=NST
      SUM=0
      DO 40 J=1,NST
      IF(PHIS(J,I))20,20,30
   20 N=N-1
      GO TO 40
   30 SUM=SUM+PHIS(J,I)
   40 CONTINUE
      SA=N
      IF(N)50,50,60
   50 PHI(I)=-PHIS(1,I)
      GO TO 100
   60 PHI(I)=SUM/SA
      GO TO 100
   70 IF(PHIS(1,I))80,90,90
   80 PHIS(1,I)=-PHIS(1,I)
   90 PHI(I)=PHIS(1,I)
  100 CONTINUE
      RETURN
      END
```

```
*LIST PRINTER
      SUBROUTINE INTG
      DIMENSION FLI(61),EN(61)
      DIMENSION PHIS(5,61),S(5,5),A(5,5),NMIN(5),IN(5),
     1LABEL(5),LABM(5),PHI(61),CR(5),SIGMA(5,61),ESIGMA(5,61),
     2ACT(5),CRD(5),W(61),F(61),X(61),SIG(5),ER(61),FLINT(61),
     3CALACT(5),T(5,5),CRSIG(5)
      COMMON PHIS,S,A,NMAX,MAX,MAXU,NST,NWY,NEW,NEWA,NIT,NOR,NMIN,IN,
     1LABEL,LABM,PHI,CR,SIGMA,ESIGMA,ACT,CRD,WIDTH,W,CRSIG,F,X,SIG,ER,
     2FLINT,CALACT,T
C     COMPUTE INTEGRAL FLUX,AND EXPECTED ACTIVATIONS
      DO 10 I=1,MAX
      MAO=MAX+1-I
   10 X(I)=PHI(MAO)
      K=0
      MA=MAX+1
      X(MA)=0
      XM=MAX
      FLI(1)=X(1)*WIDTH/XM
      EN(1)=WIDTH+.000001
      DO 20 I=3,MA,2
      CALL AVGE(X,XBAR,I)
      J=I-1-K
      XI=I-1
      XMI=XM-XI
      FLI(J)=XBAR*WIDTH*XI/XM
      EN(J)=WIDTH*XMI/XM
   20 K=K+1
      DO 30 I=1,MAX
      XX=I
      E=WIDTH*XX/XM
      ER(I)=E
      CALL LININT(J,EN,FLI,E,Q)
   30 FLINT(I)=Q
      DO 50 I=1,MAXU
      DO 40 J=1,MAX
   40 X(J)=ESIGMA(I,J)*PHI(J)
      CALL AVGE(X,XBAR,MA)
   50 CALACT(I)=XBAR*WIDTH
      IF(NOR)110,110,60
   60 DO 70 I=1,NMAX
      DO 70 J=1,MAX
   70 PHIS(I,J)=0
      DO 80 I=1,NMAX
      DO 80 J=1,I
      DO 80 K=1,MAX
   80 PHIS(I,K)=PHIS(I,K)+A(I,J)*SIGMA(J,K)
      DO 100 I=1,NMAX
      DO 100 J=1,I
      DO 90 K=1,MAX
   90 X(K)=PHIS(I,K)*PHIS(J,K)*F(K)
      CALL AVGE(X,XBAR,MA)
  100 T(I,J)=XBAR*WIDTH
  110 RETURN
      END
```

```
*LIST PRINTER
      SUBROUTINE LININT(MA,E,V,ES,Q)
      DIMENSION E(301),V(301)
    1 FORMAT (1H1,27H EXTRAPOLATION NOT POSSIBLE)
C     LINEAR INTERPOLATION
      J=0
      K=0
      NL=0
      NH=0
C     SORT FOR ADJACENT VALUES
      DO 90 I=1,MA
      Q=V(I)
      IF(E(I)-ES)10,130,50
   10 IF(J)20,20,30
   20 EL=E(I)
      NL=I
      J=I
      GO TO 90
   30 IF(EL-E(I))40,40,90
   40 EL=E(I)
      NL=I
      GO TO 90
   50 IF(K)60,60,70
   60 EH=E(I)
      NH=I
      K=I
      GO TO 90
   70 IF(E(I)-EH)80,90,90
   80 EH=E(I)
      NH=I
   90 CONTINUE
      IF(NL)110,110,100
  100 IF(NH)110,110,120
  110 PRINT 1
      CALL EXIT
C     INTERPOLATE
  120 Q=((ES-EH)*V(NL)+(EL-ES)*V(NH))/(EL-EH)
  130 RETURN
      END
```

```
*LIST PRINTER
      SUBROUTINE TYPE(NI,I)
      DIMENSION V1(61),V2(61),V3(61),V4(61),E(61),CO(6)
      DIMENSION PHIS(5,61),S(5,5),A(5,5),NMIN(5),IN(5),
     1LABEL(5),LABM(5),PHI(61),CR(5),SIGMA(5,61),ESIGMA(5,61),
I    2ACT(5),CRD(5),W(61),F(61),X(61),SIG(5),ER(61),FLINT(61),
     3CALACT(5),T(5,5),CRSIG(5)
      COMMON PHIS,S,A,NMAX,MAX,MAXU,NST,NWY,NEW,NEWA,NIT,NOR,NMIN,IN,
     1LABEL,LABM,PHI,CR,SIGMA,ESIGMA,ACT,CRD,WIDTH,W,CRSIG,F,X,SIG,ER
     2FLINT,CALACT,T
    1 FORMAT(1H138X13H CASE NUMBER I3///)
    2 FORMAT(///38X14H ACTIVATION(I)///(7X3(2X,A6,E12.5)/))
    3 FORMAT(///34X22H STANDARD DEVIATION(I)///(7X3(2X,A6,E12.5)/))
    5 FORMAT(///27X36H ORTHONORMAL FUNCTION CHECK,CHI(I,J)///(5F12.6/
    6 FORMAT(///29X32H CALCULATED ACTIVATION INTEGRALS///(7X3( 2X,A2,E
     1.5)/))
    7 FORMAT(///11X12H ENERGY(MEV)15X,5H FLUX10X16H INTEGRATED FLUX//
     10X,F6.2,18X,E12.5,10X,E12.5/))
C     PRINT FLUX
      PRINT 1,I
      IF(NI-NIT)40,10,10
   10 PRINT 2,(LABM(L),CRD(L),L=1,NMAX)
      PRINT 3,(LABM(L),CRSIG(L),L=1,NMAX)
      DO 15 L=1,MAXU
   15 CALACT(L)=.001*CALACT(L)
      IF(NOR)30,30,20
   20 PRINT 5,((T(L,J),J=1,L),L=1,NMAX)
   30 PRINT 6,(LABEL(L),CALACT(L),L=1,MAXU)
   40 PRINT 7,(ER(L),PHI(L),FLINT(L),L=1,MAX)
      RETURN
      END
```

FUSE-3 FITTING UNKOWN SPECTRA EXPERIMENTALLY

FOILS USED= 5 POINTS USED= 60 FOILS AVAILABLE= 5

MAXIMUM ENERGY(MEV)= 15.0

FOIL ORDER(I)

1	2	3	4	5
P	U	S	A	A

WEIGHTED CROSS SECTION INTEGRALS(I,J)

70.2258E+02	85.5004E+01	97.2948E+00	63.9071E-01	21.0881E-01
85.5004E+01	21.8817E+01	33.7300E+00	25.2350E-01	88.6161E-02
97.2948E+00	33.7300E+00	12.8201E+00	10.3806E-01	29.7090E-02
63.9071E-01	25.2350E-01	10.3806E-01	16.3331E-02	74.3598E-03
21.0881E-01	88.6161E-02	29.7090E-02	74.3598E-03	57.2388E-03

WEIGHTING FUNCTION(I)

70.0000E+02	48.0000E+02	31.0000E+02	21.0000E+02	14.0000E+02
10.0000E+02	64.0000E+01	43.0000E+01	30.0000E+01	20.0000E+01
16.0000E+01	12.0000E+01	92.0000E+00	74.0000E+00	60.0000E+00
51.0000E+00	44.0000E+00	38.0000E+00	33.0000E+00	28.0000E+00
24.0000E+00	21.0000E+00	18.0000E+00	15.5000E+00	13.2000E+00
11.5000E+00	10.0000E+00	85.0000E-01	73.0000E-01	64.0000E-01
54.0000E-01	47.0000E-01	40.0000E-01	35.0000E-01	30.0000E-01
26.0000E-01	22.0000E-01	19.0000E-01	16.5000E-01	14.0000E-01
12.0000E-01	10.0000E-01	90.0000E-02	80.0000E-02	70.0000E-02

62.0000E-02 55.0000E-02 48.0000E-02 42.0000E-02 37.0000E-02

33.0000E-02 29.0000E-02 25.0000E-02 22.5000E-02 20.0000E-02

17.5000E-02 15.0000E-02 13.5000E-02 11.8000E-02 10.0000E-02

ORTHONORMAL COEFFICIENTS ((A(J,K),K=1,J),J=1,NMAX)

11.9330E-03-11.3671E-03 93.3640E-03 34.6893E-04-70.6166E-03

37.0181E-02 53.6315E-05 32.1555E-04-30.0860E-02 35.6087E-01

60.9188E-05-16.4034E-03 25.1435E-02-47.6367E-01 74.5766E-01

CASE NUMBER 1

ACTIVATION(I)

P 4.17000E+11 U 3.39000E+10 S 4.07000E+09
A 2.54000E+08 A 5.28000E+07

STANDARD DEVIATION(I)

P 2.08500E+10 U 1.69500E+09 S 2.03500E+08
A 1.27000E+07 A 2.64000E+06

CALCULATED ACTIVATION INTEGRALS

P 3.91920E+11 U 3.23117E+10 S 4.01802E+09
A 2.55849E+08 A 5.30233E+07

ENERGY(MEV)	FLUX	INTEGRATED FLUX
.25	3.12318E+10	2.79608E+11
.50	1.15326E+11	2.69598E+11
.75	3.19680E+11	2.00053E+11
1.00	2.75022E+11	1.30508E+11
1.25	1.67703E+11	8.78904E+10
1.50	7.70050E+10	4.52720E+10
1.75	3.91707E+10	3.47582E+10
2.00	1.86433E+10	2.42444E+10
2.25	1.36425E+10	2.07700E+10

2.50	1.01720E+10	1.72956E+10
2.75	9.25757E+09	1.50087E+10
3.00	7.68303E+09	1.27218E+10
3.25	6.34376E+09	1.11176E+10
3.50	5.44211E+09	9.51349E+09
3.75	4.73132E+09	8.32453E+09
4.00	4.16779E+09	7.13556E+09
4.25	3.63576E+09	6.22452E+09
4.50	3.15406E+09	5.31348E+09
4.75	2.74845E+09	4.62408E+09
5.00	2.39773E+09	3.93468E+09
5.25	2.14781E+09	3.39204E+09
5.50	2.03450E+09	2.84939E+09
5.75	1.82775E+09	2.39150E+09
6.00	1.64384E+09	1.93361E+09
6.25	1.32158E+09	1.60571E+09
6.50	9.39460E+08	1.27781E+09
6.75	7.49691E+08	1.08933E+09
7.00	5.85176E+08	9.00864E+08
7.25	4.76278E+08	7.78377E+08
7.50	4.49390E+08	6.55890E+08
7.75	3.87589E+08	5.58190E+08
8.00	3.45049E+08	4.60490E+08
8.25	3.15863E+08	3.83121E+08
8.50	2.48351E+08	3.05752E+08
8.75	1.99473E+08	2.55274E+08
9.00	1.65236E+08	2.04795E+08

9.25	1.35830E+08	1.70567E+08
9.50	1.12928E+08	1.36338E+08
9.75	9.39636E+07	1.12824E+08
10.00	7.55616E+07	8.93099E+07
10.25	6.14499E+07	7.39190E+07
10.50	4.80202E+07	5.85281E+07
10.75	4.01017E+07	4.84703E+07
11.00	3.29586E+07	3.84126E+07
11.25	2.70516E+07	3.15998E+07
11.50	2.23416E+07	2.47870E+07
11.75	1.90473E+07	2.00265E+07
12.00	1.57218E+07	1.52660E+07
12.25	1.26795E+07	1.20887E+07
12.50	9.81360E+06	8.91153E+06
12.75	7.28339E+06	7.07914E+06
13.00	5.03026E+06	5.24674E+06
13.25	3.29436E+06	4.33377E+06
13.50	3.70358E+06	3.42080E+06
13.75	1.71483E+06	2.96414E+06
14.00	3.96900E+05	2.50748E+06
14.25	2.26320E+06	1.99240E+06
14.50	2.91234E+06	1.47731E+06
14.75	3.00324E+06	1.08896E+06
15.00	2.80245E+06	7.00615E+05

BIBLIOGRAPHY

1. RYDIN, R., RASMUSSEN, N. and BROWNELL, G., Fast Neutron Spectroscopy and Dosimetry of the MIT Reactor Medical Therapy Facility Beam. AFCRL-64-404.

2. RINGLE, J., A Technique for Measuring Neutron Spectra in the Range 2.5 to 30 Mev Using Threshold Detectors. UCRL-10732

3. GERKAN, W., (1963), Measurements of Neutron Energy Effects Using Multiple Threshold Detectors. Thesis, University of Maryland.

4. BRESESTI, M., DEL TURCO, A., OSTIDICH, A., ROTE, A. and SERGREE, G., (1963), Fast Neutron Measurements by Threshold Detectors in ISPA (CP-5-type) and Avogadro RS-1 (Swimming Pool) Reactors. Neutron Dosimetry. Vol. I, IAEA, Vienna, p. 27.

5. DIERCKX, R., (1963), In-Pile Fast Neutron Spectrum Measurements by Threshold Detectors. Neutron Dosimetry, Vol. I, IAEA, Vienna, p. 325.

6. GLASSTONE, S., (1955), Principles of Nuclear Engineering, D. Van Nostrand Company.

7. HOLKENBRINK, M. H., (1966) The Construction of a Multi-Threshold Foil for Fast Flux Measurements. Thesis, University of Missouri at Rolla (unpublished).

8. GUNDL, J., USNER, A., (1960) Spectral Comparison with High Energy Activation Detectors. Nuclear Science and Engineering 8, p. 598-607.

9. HUGHES, D. J., (1953), Pile Neutron Research, p. 5, Addision Wesley Publishing Company, Inc., Cambridge, Mass.

10. HUGHES, D. J. and SCHWARTZ, R.B., (1956), Neutron Cross Spectrons, BNL-325, Second Edition.

11. HUGHES, D. J., MAGURNO, B. Z., and BRUSSEL, M. K., (1960), Supplement Number 1, Neutron Cross-Sections, BNL-325, Second Edition.

12. PASSELL, T. O. and HEATH, R. L., (1961), Cross Sections of Threshold Reactions for Fission Neutrons, Nickel as a Fast Flux Monitor, Nuc. Sci. Eng., Vol. 10,308-315.

13. MAGURNO, B. A., GOLDBERG, M. D., STEHN, J. R. and WIENER-CHASMAN, R., (1964), Supplement Number 2, Neutron Cross-Sections, BNL-325, Second Edition.

14. GLASSTONE, S. and SEBUNSIVE A., Nuclear Reactor Engineering, D. Van Nostrand Company Inc.

15. DI COLA and ROTA, A., (1965), Calculation of Differential Fast Neutron Spectra from Threshold-Foil Activation, CETIS and Nuclear Chemistry Laboratory, C.C.R. Euratom, Ispra, Italy.

16. SCHOUPELD, E., (1965), Alpha-A Computer Program for the Determination of Radioisotopes by Least-Squares Resolution of the Gamma-Ray Spectra. ORNL-3810, VC-4-Chemistry TID-4500 (41st ed.)

17. CROUTHAMEL, C. E., (1960), Applied Gamma-Ray Spectrometry. McMillian Company, New York.

18. REACTOR EXPERIMENTS INC., Instruction Manual on Neutron Activation Foils. 140 Harbor Blvd., Belmont, Calif.

19. GOLDMAN, D. T., STEHN, J. R., (1961), Chart of the Nuclides General Electric Company, Sixth Edition.

20. CULP, A. W., BARAFF, G. A., PAGE, R. M., PELLETICUR, LENCE, J. T., and MALLON, R. G., The Activation and Residual Dose from the J-79 Engine Astra, Inc., Milford, Conn.

21. MOTEFF, J., BEEVER, E. J., McDULE, C. J., (1959), The Use of Threshold Detectors for Measuring Fast Neutron Flux, General Electric Company, U.S. Steel Corporation.

22. CROSS, W. G., (1963), The Use of Magnesium, Titanium, Iron, Nickel and Zinc in Fast Neutron Dosimetry, Neutron Dosimetry, Vol. I., IAEA, Vienna, p. 325.

23. PASSELL, T. O., (1963), The Use of Nickel-58 and Iron-54 as Integrators of Fast Neutron Flux, Neutron Dosimetry, Vol. I., IAEA, Vienna, p. 325.

24. KOHLER, A. Jr., (1964), An Improved Method of Neutron Spectroscopy Using Threshold Detectors, UCRL-11750.

25. HOWERTON, R. J., (1959), Tabulated Neutron Cross-Section, University of California Radiation Laboratory Report, UCRL-5226.

26. MURPHY, H. M. Jr., (1966), PPA, A Computer Program for Photopeak Analysis, AFWL-TR-65-111.

VITA

The author was born on October 9, 1940 in St. Louis, Missouri. He received his primary and secondary education in Crystal City, Missouri.

He has received his college education from the University of Missouri School of Mines and Metallurgy, where he received a Bachelor of Science Degree in Mechanical Engineering in June 1963.

He has been enrolled in the Graduate School of the University of Missouri at Rolla since January 1965. He has received the Monsanto Scholarship Mechanical Engineering for the period January 1965 to June 1965. In September 1965 he transferred to Nuclear Engineering where he served as a research assistant in the University of Missouri at Rolla Reactor.